

# Modelling plastic deformation of metals using irreversible thermodynamics

Ph.D. thesis

Nov. 2008

**Mingxin Huang**



ArcelorMittal

The research in this thesis has been financially supported by ArcelorMittal.

# Modelling plastic deformation of metals using irreversible thermodynamics

Proefschrift

ter verkrijging van de graad van doctor  
aan de Technische Universiteit Delft,  
op gezag van de Rector Magnificus prof.dr.ir. J.T. Fokkema,  
voorzitter van het College voor Promoties,  
in het openbaar te verdedigen op maandag 17 november 2008 om 10:00 uur

door

**Mingxin Huang**

Master of Science in Solid Mechanics  
Shanghai Jiao Tong University, China  
geboren te Lingshui, Provincie Hainan, China

Dit proefschrift is goedgekeurd door de promotor:

Prof.dr.ir. S. van der Zwaag

Copromotor:

Dr. P.E.J. Rivera Díaz del Castillo

Samenstelling promotiecommissie:

Rector Magnificus, voorzitter

Prof.dr.ir. S. van der Zwaag, Technische Universiteit Delft, promotor

Dr. P.E.J. Rivera Díaz del Castillo, Technische Universiteit Delft, copromotor

Prof.dr. Y. Bréchet, Grenoble Institute of Technology, France

Prof.dr. E.H. Brück, Technische Universiteit Delft

Prof.dr. J.Th.M. de Hosson, University of Groningen, The Netherlands

Prof.dr.ir. L.A.I. Kestens, Technische Universiteit Delft

Dr. O. Bouaziz, AreclorMittal, France, adviseur

Keywords: Dislocation Density, Irreversible Thermodynamics, Work Hardening, Modelling, Metals

Cover designed by Han Feng and Mingxin Huang

EBSD image of the cover provided by Dr. David San Martin

Copyright ©2008 by Mingxin Huang

mingxinhuang@hotmail.com

All rights reserved. No part of the material protected by this copyright notice may be reproduced or utilized in any form or by any means, electronic or mechanical, including photocopying, recording or by any information storage and retrieval system, without permission from the author.

Printed in The Netherlands by PrintPartners Ipskamp

ISBN: 978-90-9023542-4

To my parents and wife



# Contents

<b>1</b>	<b>Introduction</b>	<b>1</b>
1.1	Modelling of plastic deformation: an active research field in the metals industry . . . . .	1
1.2	Mechanisms of plastic deformation in metals . . . . .	2
1.3	Evolution of dislocation density . . . . .	3
1.4	State-of-the-art dislocation-based models . . . . .	4
1.5	Scope and outline of the thesis . . . . .	5
<b>2</b>	<b>Irreversible Thermodynamics Applied to Plastic Deformation</b>	<b>7</b>
2.1	General concepts . . . . .	7
2.1.1	Equilibrium and irreversible thermodynamics: a comparison	7
2.1.2	Entropy production: a core concept in irreversible thermodynamics . . . . .	8
2.1.3	Stationary non-equilibrium state . . . . .	9
2.2	Applications of irreversible thermodynamics . . . . .	10
2.3	Existing dislocation-based continuum models for plastic deformation in one dimension . . . . .	11
2.3.1	One-variable model . . . . .	11
2.3.2	Two-variables model . . . . .	13
2.3.3	Three-variables model . . . . .	15
2.4	Irreversible thermodynamics and plastic deformation . . . . .	17

<b>3</b>	<b>Modelling Stress Levels at Steady State Deformation Conditions</b>	<b>21</b>
3.1	Introduction . . . . .	21
3.2	Model . . . . .	25
3.2.1	Entropic analysis . . . . .	25
3.2.2	Dislocation annihilation due to dynamic recovery . . . . .	28
3.2.3	Dislocation annihilation due to dynamic recrystallization . . . . .	29
3.2.4	Dislocation density at the steady state . . . . .	30
3.3	Application and discussion . . . . .	31
3.3.1	Constant strain rate deformation with DRV only . . . . .	31
3.3.2	Steady state creep with DRV only . . . . .	34
3.3.3	Constant strain rate deformation with DRV and DRX . . . . .	35
3.4	Conclusions . . . . .	38
<b>4</b>	<b>Modelling the Stress-strain Behaviour of Single Crystals and (Ultra)fine Polycrystals</b>	<b>39</b>
4.1	Introduction . . . . .	39
4.2	Single crystals . . . . .	40
4.2.1	Model . . . . .	40
4.2.2	Application . . . . .	44
4.2.3	Discussion . . . . .	48
4.3	(Ultra)fine polycrystals . . . . .	50
4.3.1	Model . . . . .	50
4.3.2	Application . . . . .	53
4.3.3	Parametric analysis and discussion . . . . .	56
4.4	Conclusions . . . . .	60
<b>5</b>	<b>Modelling the Flow Stress under Quasi-static and Adiabatic Deformation Conditions</b>	<b>61</b>
5.1	Introduction . . . . .	61
5.2	Model . . . . .	62
5.2.1	Entropic analysis . . . . .	62
5.2.2	Dislocation annihilation . . . . .	64
5.2.3	Stress-strain behaviour . . . . .	67
5.3	Application . . . . .	68
5.4	Discussion . . . . .	70
5.5	Conclusions . . . . .	72
<b>6</b>	<b>Validation of the Irreversible Thermodynamics Model for Steels under Hot Rolling Conditions</b>	<b>73</b>
6.1	Introduction . . . . .	73

6.2	Model . . . . .	74
6.3	Calibration of parameters . . . . .	75
6.4	Comparison of the current model to experimental data and industrial model . . . . .	80
6.4.1	Comparison with experimental data . . . . .	80
6.4.2	Comparison with the industrial model . . . . .	85
6.5	Discussion . . . . .	87
6.6	Conclusions . . . . .	88
	<b>Summary</b>	<b>89</b>
	<b>Samenvatting</b>	<b>93</b>
	<b>Appendix A A Statistical Mechanics Model for Grain Deformation</b>	<b>97</b>
	<b>Bibliography</b>	<b>107</b>
	<b>Acknowledgements</b>	<b>119</b>
	<b>Curriculum Vitae and List of Publications</b>	<b>123</b>



# 1

## Introduction

### 1.1 Modelling of plastic deformation: an active research field in the metals industry

This plastic deformation involves the displacement of existing dislocations as well as the evolution of new dislocations. The dislocation density in turn not only determines the deformation forces but also two important metallurgical processes, recovery and recrystallization, which have a large effect on many physical and mechanical properties of the deformed metal. Therefore, understanding the evolution of the dislocation structure during the forming process is crucial to quantitatively predict the properties of the metal products. Furthermore, such understanding can provide essential information to understand the work hardening phenomena and therefore to predict the stress-strain curves, which in turn can predict the forces involved in the metal-forming process. This understanding can be achieved by developing physical dislocation-based models, which are more flexibly applied to different products than the empirical models, which can not predict the situation beyond the limits within which the test was performed. Consequently, physically-based dislocation models are currently strongly demanded by the metal industry for optimizing their forming process so as to control and improve the properties of their final products. Moreover, such modes may explain and predict the high strength but poor ductility of ultrafine grained alloys [65], which are currently under intensive investigation [7][124][127].

## 1.2 Mechanisms of plastic deformation in metals

When a stress applied on a metal sample exceeds a critical value, it undergoes plastic (irreversible) deformation: the shape of the metal changes permanently. In the most common cases, such deformation results from the motion of dislocations (linear defects in crystals) on the crystallographic planes through a shearing process schematically shown in figure 1.1 [60]. If a dislocation with a Burgers vector  $b$  moves to the surface of the metal, a surface step occurs, which results in a small shear strain  $b/l$  where  $l$  is the thickness of the metal (figure 1.1). The macroscopic shear strain is induced by the collective motion of many dislocations [42].

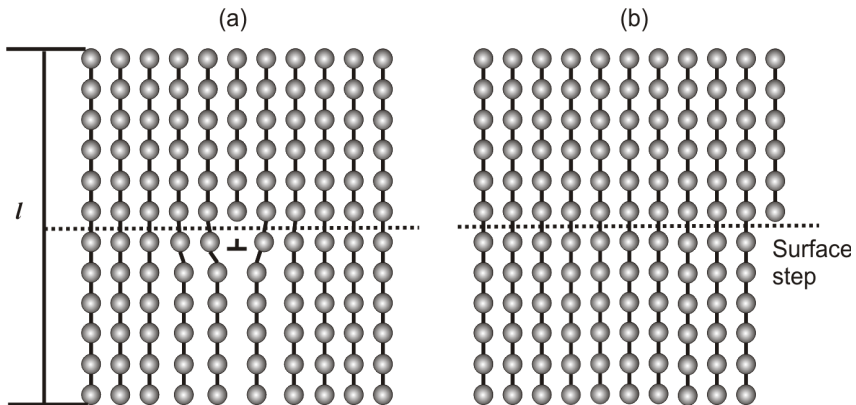


FIGURE 1.1. Illustration of plastic deformation: (a) a dislocation present in the metal which (b) glides to the surface under an applied stress resulting in the formation of a surface step and plastic deformation (shape change).

Besides the dislocation motion mechanism, there are other mechanisms which accompany plastic deformation. For instance, twinning is one additional deformation mechanism in face-centred cubic (FCC) metals and alloys with low stacking fault energy (e.g. silver, copper-rich alloys, high Mn austenitic steels such as TWIP steels [7] and in all close-packed hexagonal metals [68]. It may also occur in FCC metals with high stacking fault energy and in body-centred cubic (BCC) metals if deformation takes place at low temperature or high strain rates [68]. Grain boundary sliding is an important deformation mechanism in nanocrystalline metals [125] and in high temperature creep conditions for polycrystalline metals [121]. For transformation-induced plasticity (TRIP) steels, plastic deformation can be induced by displacive phase transformations (austenite transformed into martensite) [7]. This thesis focuses on plastic deformation induced by the glide of dislocations only.

### 1.3 Evolution of dislocation density

For most metals, during plastic deformation the dislocation population evolves towards a maximum, which is present at the steady state (large strains) at which it remains constant with further straining [67][96]. The dislocation population is commonly described in terms of the “dislocation density” (the total length of dislocations per unit volume). The evolution includes two mechanisms: dislocation generation and annihilation. These two mechanisms are competing against each other: the generation increases the dislocation density while the annihilation reduces it [60][64][73][76].

The generation of dislocations can result from several kinds of dislocation sources. The best known source is the Frank-Read source (figure 1.2) [60]. A segment of dislocation  $AB$  is pinned at points  $A$  and  $B$  by obstacles, which could be precipitates or forest dislocations in other slip planes (figure 1.2a). Under an applied stress the segment bows out by glide. When the applied stress is less than a critical value, a metastable equilibrium configuration is obtained (figure 1.2b), in which the line-tension force is in balance with the applied stress. When the applied stress exceeds a critical value, the segment will displace to the successive positions shown in figure 1.2b-e and form a dislocation closed loop, and the configuration of the source comes back to its original shape. The newly generated loop exerts a back stress on the source, which opposes the applied stress. If the back stress is high enough, the source ceases to provide dislocation loops. Another dislocation source could be the grain boundaries in polycrystalline metals. Li [80] suggested that edge grain-boundary dislocations could be emitted into the grain interiors, thereby acting as a dislocation source. High-velocity dislocations could also be possible dislocation sources [60]. Molecular dynamics simulations confirmed that new dislocations can be generated around a moving dislocation when its velocity approaches 70% of the velocity of sound [74].

When a dislocation moves out of its slip plane, it may eventually meet with an antiparallel dislocation on the new glide plane so that both dislocations are annihilated [42]. At low temperatures, annihilation occurs mainly by the cross-slip of screw dislocations. A screw dislocation does not have a defined glide plane and thus, can change its glide plane. A screw dislocation will glide on that plane where it experiences largest shear stress. At high temperatures, edge dislocation climb, which is accompanied by vacancy diffusion, plays a dominant role in the annihilation process due to a large amount of vacancies presented [98].

The generation rate is usually larger than the annihilation rate so that the dislocation density increases with straining up to the steady state. This causes the increase of the resistance to the motion of dislocations due to the overlap of the stress field of individual dislocations, causing the metal to be less deformable.

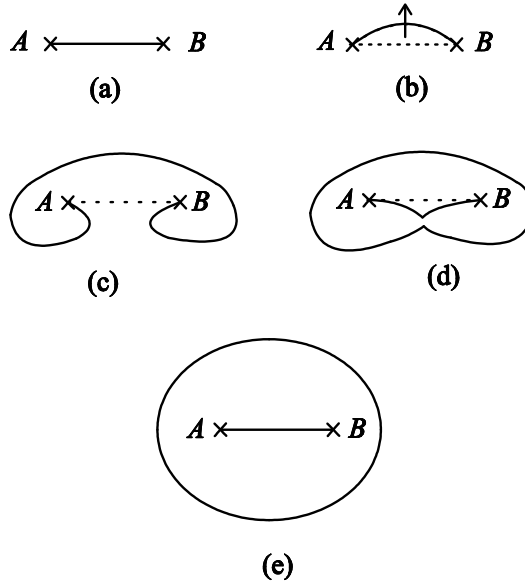


FIGURE 1.2. Frank-Read source: (a) a segment of dislocation  $AB$  in a slip plane; (b) a metastable equilibrium configuration of the dislocation under an applied stress; (c)-(e) successive procedures of generation of a dislocation loop.

This effect is known as work hardening (also “strain hardening”): when metals are deformed they become harder [42][68][73][76].

## 1.4 State-of-the-art dislocation-based models

In the literature, three groups of physically-based models can be distinguished. The first one is based on the concept of modelling the evolution of the average dislocation density. These models are not able to describe the spatial distribution of dislocations and are rather simple and easily utilized. They are able to predict and explain the stress-strain curves and the work hardening phenomena. Three types of models in this group can be distinguished: (1) average dislocation density approaches by Kocks and Mecking [73] and Estrin and Mecking [31]; (2) average dislocation densities at the cell walls and cell interiors by Nix and co-workers [98], Bréchet and co-workers [32] and Nes [96]; (3) and models accounting for the evolution of three types of average dislocation densities (the average mobile dislocation density, the average immobile dislocation densities in the cell interiors and in the cell walls) by Gottstein and co-workers [113].

The second group of models describes the spatiotemporal distribution of dislocations by assuming the dislocation density to be a continuum variable in the space. The formation of dislocation patterns such as cells, deformation bands, and persistent slip bands can be described. This group of models, inspired by Holt [62], usually contain nonlinear differential equations and are more complex than the first group. For instance, Walgraef [130] and Walgraef and Aifantis [131][132][133] developed models where different dislocation populations evolve according to reaction-diffusion equations. Hähner [50] and Zaiser and co-workers [134] proposed a stochastic approach for describing the fractal geometry of cellular dislocation structures in terms of nonlinear stochastic processes. Groma [47] derived a continuum description of the evolution of parallel straight edge dislocations accounting for the interactions between dislocations. El-Azab [29] formulated the evolution of distributions of curved dislocations in three dimensions.

The third group of models is the discrete dislocation dynamics including two-dimensional simulations by Van der Giessen and Needleman [41] and by Groma and Pawley [48]; and three dimensional simulations by Bréchet and co-workers [14] and by Kubin and co-workers [26][75], with which the behaviour of individual dislocation is described. The stress-strain curves and the dislocation patterns can be investigated by such simulations. However, due to the complexity of the long range interaction of dislocations, such simulations require long computational time.

## 1.5 Scope and outline of the thesis

This thesis is an attempt to develop a new physical model to understand and predict the evolution of the average dislocation density in metals undergoing plastic deformation. Inspired by a statistical mechanics model for grain deformation (Appendix A), this thesis proposes models to describe the plastic deformation of metals following the principles of irreversible thermodynamics. Such approach has widely been followed in physics and chemistry but is not commonly employed in metallurgy. The existing models for describing the evolution of the dislocation density are based on a phenomenological building block: the dislocation generation rate is related to the mean distance travelled by dislocations [30][31][73]. In this thesis, irreversible thermodynamics is referred to linear irreversible thermodynamics which deals with states not far from equilibrium.

The outline of this thesis is given as follows. **Chapter 2** gives a general introduction to irreversible thermodynamics and some of its applications in metallurgy, physics, chemistry and biology. How irreversible thermodynamics can be employed for plastic deformation is also briefly discussed. Furthermore, the details of state-

of-the-art models for the evolution of the average dislocation densities (the first group of models introduced above) are given in this chapter.

Considering the steady state of plastic deformation being a stationary non-equilibrium state in the context of irreversible thermodynamics, **Chapter 3** derives a model to predict the average dislocation density at the steady state of plastic deformation in FCC metals. The temperature and strain rate effects are taken into account. By combining the predicted dislocation density with the well known Taylor's relation [126], the capability of the model for predicting the stress levels at the steady state is demonstrated.

**Chapter 4** extends the model developed in Chapter 3 to describe the evolution of the average dislocation density during the plastic deformation. The work hardening behaviour and stress-strain curves of single crystals and (ultra)fine polycrystals are discussed. Especially, the origin of the low ductility of ultrafine grained alloys is explained, and methods for increasing their ductility are suggested.

In **Chapter 5** the model is generalised to describe the evolution of the average dislocation density under quasi-static (low strain rate) and adiabatic (high strain rate) deformation conditions. The stress-strain curves at both conditions are predicted by the model, and are in good agreement with experiment.

The model developed in Chapter 5 is modified to incorporate grain size and alloying effects in **Chapter 6**. Then, the model is applied to predict the stress-strain curves of 13 steel grades at hot working conditions.

# 2

## Irreversible Thermodynamics Applied to Plastic Deformation

### 2.1 General concepts

#### *2.1.1 Equilibrium and irreversible thermodynamics: a comparison*

A system placed in a given environment changes spontaneously until it has exhausted its capacity for change. When the system attains a final state, it is said to have reached an equilibrium state [24]. Classical equilibrium thermodynamics aims at describing such an equilibrium state for any given system. That description can be expressed in different forms depending on the external environment which the system is subjected to. For instance, for an isolated system, equilibrium is reached when the entropy approaches a maximum value. In a system constrained to constant temperature and pressure, equilibrium is approached when the Helmholtz free energy becomes minimum; similarly, for constant temperature and volume, equilibrium appears when the Gibbs free energy becomes minimum [24][40].

Equilibrium thermodynamics has successfully been applied in many fields of science such as physics and chemistry. For materials science, one greatly successful application is the prediction of phase diagrams, which indicates which phases and their relative amounts at a given temperature. For instance, in a binary system (iron and carbon), the amount of austenite (FCC) and/or ferrite (BCC) at the equilibrium state can be predicted for different temperatures and compositions [24]. Another example is the description of adiabatic elastic deformation, which is

a reversible process. At any instant strain of elastic deformation the metal is at the thermodynamic equilibrium state. The temperature decrease due to the elastic loading (i.e. thermoelastic effect) can be predicted. For instance, for pure iron and nickel deformed in the elastic regime, the temperature decrease is in the range between 0.1 and 0.3 °C [112].

However, many systems subjected to certain external conditions are out of equilibrium and equilibrium thermodynamics is not applicable for their description. These include the transport of heat, electricity or matter across the borders of a system. A very relevant example of a non-equilibrium system is the plastic deformation of metals. At any plastic strain level, the metal is in the non-equilibrium state. Irreversible thermodynamics, as developed by Onsager [99][100], Prigogine [107] and many others, is able to describe systems out of equilibrium. Onsager and Prigogine won Nobel prices in chemistry in 1968 and 1977, respectively, for their work on irreversible thermodynamics.

Summarizing: the objective of equilibrium thermodynamics is to describe the equilibrium states, while irreversible thermodynamics focuses on non-equilibrium states.

### 2.1.2 Entropy production: a core concept in irreversible thermodynamics

In contrast to equilibrium thermodynamics calculations, the second law of thermodynamics in irreversible thermodynamics is reformulated in terms of the entropy production in the system using the assumption of local equilibrium [72][107]. The entropy is an extensive property, which is additive. Therefore, for a system undergoing multiple irreversible processes, the entropy generation  $d_i S$  of the system is the sum of the entropy generation of all irreversible processes [107]. It is expressed mathematically as

$$d_i S = \sum_{K=1}^N d_i S^K > 0 \quad (2.1)$$

where  $N$  is the number of irreversible processes taking place in the system and  $d_i S^K$  is the entropy generation due to the process  $K$ .  $d_i S^K$  is determined by the dissipative energy  $dW_{dis}^K$  consumed by the process  $K$  [106]:

$$d_i S^K = \frac{dW_{dis}^K}{T} \quad (2.2)$$

Inserting equation 2.2 into equation 2.1,  $d_i S$  is rewritten as

$$d_i S = \sum_{K=1}^N \frac{dW_{dis}^K}{T} \quad (2.3)$$

Besides equation 2.3, there is an alternative approach to calculate  $d_i S$ . The entropy production is expressed as the sum of the products of generalised forces and their corresponding fluxes in the system [107]:

$$\frac{d_i S}{dt} = \sum_{K=1}^N J_K X_K \quad (2.4)$$

where  $t$  is time.  $J_K$  is the rate of the generalised flux of process  $K$ .  $X_K$  is the generalised force of process  $K$ . As an example, the entropy generation due to a chemical reaction can be expressed as [107]

$$\frac{d_i S}{dt} = J_{ch} X_{ch} \quad (2.5)$$

where  $J_{ch} = v_{ch}$  is the chemical reaction rate and  $X_{ch} = A_{ch}/T$  where  $A_{ch}$  is the affinity of the chemical reaction related to the chemical potentials.

Each flux in equation 2.4 is a linear combination of all forces: [107]:

$$J_K = \sum L_{KI} X_I \quad (2.6)$$

where  $L_{KI}$  is the phenomenological coefficient. This relation can be derived from the Onsager's extremum principle (maximisation of dissipative energy) [57]. To illustrate this relation further, the case of two simultaneous irreversible processes is considered. The rates of the two generalised fluxes can be expressed as

$$J_1 = L_{11} X_1 + L_{12} X_2 \quad (2.7)$$

and

$$J_2 = L_{21} X_1 + L_{22} X_2. \quad (2.8)$$

The coefficient  $L_{KK}$  may stand for the heat conductivity, the electrical conductivity or the chemical drag coefficient, while the coefficients  $L_{KI}$  ( $K \neq I$ ) describes the "interference" of the two irreversible processes  $K$  and  $I$  [107].  $L_{KI} = L_{IK}$  is proved by Onsager [72][99][100]. If the two irreversible processes represent thermal conductivity and diffusion, the coefficient  $L_{KI}$  connects the thermodiffusion, i.e., a concentration gradient can be introduced by a temperature gradient [107].

### 2.1.3 Stationary non-equilibrium state

Analogous to the equilibrium state, a stationary non-equilibrium state abbreviated to stationary state can be defined in the context of irreversible thermodynamics. The evolution of irreversible processes in the system tends to decrease the entropy generation rate ( $d_i S/dt$ ) under certain external constrains. When the entropy generation rate reaches a minimum value, the system reaches its stationary state [107].

In order to present a qualitative picture of a stationary state relevant to irreversible thermodynamics, an example illustrated by Prigogine [107] is introduced: a system receives a component  $P$  from the outside environment and transforms it, through a certain number of intermediate compounds, into a final product  $F$ , which is released into the external environment. A stationary state is reached when the concentrations of the intermediate components no longer vary with time. For such system, thermodynamic equilibrium state can never be reached due to the presence of the external constrains (flux of components between the system and the environment,  $d_i S > 0$ ). Nevertheless, the interest on such a system is to determine the properties of the stationary state not those of the equilibrium state.

One important property of the stationary state is that all thermodynamic state variables including entropy are independent with time [107]:

$$\frac{dS}{dt} = \frac{d_e S}{dt} + \frac{d_i S}{dt} = 0. \quad (2.9)$$

Therefore, it is clear that a negative flow of entropy at the stationary state is required as  $d_i S/dt > 0$ :

$$\frac{d_e S}{dt} = \frac{1}{T} \frac{dQ}{dt} < 0. \quad (2.10)$$

This implies that a heat flow from the system into the outside environment ( $dQ < 0$ ) is required at the stationary state. For an isolated system, a stationary state can not occur since there is no flow of entropy between the system and the environment.

## 2.2 Applications of irreversible thermodynamics

Since Onsager, irreversible thermodynamics has been applied extensively to many diverse fields of science. For example, the transport processes in electrolytic systems can be well described [37]. Kuiken [77] introduced the most general treatment of multicomponent diffusion and rheology of colloidal and other systems. The growth of living organisms can be understood better by analyzing the entropy production which is decreasing during evolution up to the stationary state [107]. The origin of life on earth can be discussed in terms of energy and entropy in the context of irreversible thermodynamics [101].

Moreover, irreversible thermodynamics has been employed successfully to model several metallurgical processes occurring at a non-equilibrium state. Rios [110], Rios *et al.* [111] and Fischer *et al.* [34] modelled the rate of grain growth. Fischer and Svoboda [33] derived equations of void growth. Sintering and coarsening of rows of spherical particles were modelled by Parhami and co-workers [103]. Poliak and Jonas [106] predicted the critical conditions for the initiation of dynamic

recrystallization. These successful applications offer some confidence to employ irreversible thermodynamics for modelling the kinetics of plastic deformation. This is performed via describing the evolution of the dislocation microstructure, which undergoes a series of non-equilibrium states.

## 2.3 Existing dislocation-based continuum models for plastic deformation in one dimension

Before introducing irreversible thermodynamics to model plastic deformation via employing the average dislocation as the only variable, it is interesting to discuss the existing dislocation-based models for work hardening. These continuum approaches consider average dislocation densities without taking into account the spatial distribution of dislocations, and are therefore referred as one dimensional here.

### 2.3.1 One-variable model

Employing the total dislocation density as the single variable, Kocks and Mecking [73] and Estrin and Mecking [31] developed a work hardening model for single phase metals. The shear stress  $\tau$  is related to the total dislocation density  $\rho$  via

$$\tau = \tau_0 + \alpha\mu b\sqrt{\rho}, \quad (2.11)$$

where  $\mu$  is the shear modulus and  $b$  is the magnitude of the Burgers vector.  $\tau_0$  is caused by the lattice resistance and solid solution.  $\alpha$  is a constant depending on temperature  $T$  and shear strain rate  $\dot{\gamma}$ . It can be split into two parts:

$$\alpha = s(\dot{\gamma}, T)\alpha_0, \quad (2.12)$$

where  $\alpha_0$  is a constant at  $T = 0$ .  $s$  is a function of strain rate and temperature, which decreases with increasing temperature and decreasing strain rate. The actual value of  $\alpha_0$  is determined by the geometrical arrangement of the dislocations and is assumed to decrease continuously with deformation when the dislocation structure is gradually converted from a random into a cellular arrangement. But the variations are within a 10% range.

The core of the Kocks-Mecking model is the evolution equation for the total dislocation density with the shear strain  $\gamma$ , which is expressed as

$$\frac{d\rho}{d\gamma} = \frac{1}{b\Lambda} - \Theta\rho \quad (2.13)$$

where  $\Lambda$  is the mean distance travelled by the dislocation before being stopped. The variation of  $\Lambda$  with deformation can be measured by nuclear magnetic resonance (NRM) as demonstrated by De Hosson *et al.* [21][23] and for Al alloys was shown to decrease with deformation. Term  $1/(b\Lambda)$  describes the dislocation generation rate during plastic deformation.  $\Theta\rho$  accounts for the dislocation annihilation rate due to dynamic recovery (DRV). For single crystals,  $1/(b\Lambda)$  is expressed as

$$\frac{1}{b\Lambda} = \frac{\sqrt{\rho}}{b}. \quad (2.14)$$

For polycrystals, it takes into account the grain size effect and is written as

$$\frac{1}{b\Lambda} = \frac{1}{bD} + \frac{\sqrt{\rho}}{b} \quad (2.15)$$

where  $D$  is the grain size.

Since DRV is thermally activated,  $\Theta$  is a function of temperature and the shear strain rate:

$$\Theta = \left( \frac{\dot{\gamma}_0}{\dot{\gamma}} \right)^{1/m}. \quad (2.16)$$

In the low temperature range,  $m$  is temperature dependent following the predictions of the cross-slip theory while  $\dot{\gamma}_0$  is constant. In the high temperature range  $m$  is constant (typically  $m = 4$ ) while  $\dot{\gamma}_0$  bears an Arrhenius type temperature dependence and is proportional to  $\exp(-Q_{ac}/kT)$  where  $Q_{ac}$  is the activation energy for self-diffusion.

The Kocks-Mecking model is widely used and has been developed further by many researchers. For instance, by considering twins as impenetrable obstacles for dislocations, Bouaziz and Guelton [12] extended the Kocks-Mecking model to describe the TWIP effect on work hardening of austenitic steels.  $1/(b\Lambda)$  in equation 2.13 is rewritten as

$$\frac{1}{b\Lambda} = \frac{1}{bD} + \frac{k_0\sqrt{\rho}}{b} + \frac{1}{d_{twin}} \quad (2.17)$$

where  $d_{twin}$  is the average spacing of twins and  $k_0$  is a constant.

The Kocks-Mecking model can be modified for two phase alloys by introducing the geometrically-necessary dislocation (GND) density  $\rho_g$ . The origin of GND is due to the two phases not being equally easy to deform. One phase deforms plastically more than the other such that deformation gradients build up [4]. The total dislocation density is the sum of the statistically stored dislocation (SSD) density  $\rho_s$  and GND density. The evolution of SSD density follows equation 2.13:

$$\frac{d\rho_s}{d\gamma} = \frac{1}{b\Lambda} - \Theta\rho_s \quad (2.18)$$

The evolution of GND density for non-deformable cube-shaped particles of length  $d_p$  is derived by Ashby [4]:

$$\frac{d\rho_g}{d\gamma} = \frac{8f}{bd_p} \quad (2.19)$$

where  $f$  is the volume fraction of non-deformation particles. The shear stress in equation 2.11 can be rewritten as

$$\tau = \tau_0 + \alpha\mu b\sqrt{\rho_s + \rho_g} \quad (2.20)$$

The application of such modified Kocks-Mecking model for dual-phase steels has been demonstrated by Bouaziz and co-workers [13].

### 2.3.2 Two-variables model

In contrast to the Kocks-Mecking model, Nix and co-workers [98] proposed a two-variables model to describe the work hardening of single phase metals. The two variables of the model are the dislocation density in the cell walls  $\rho_W$  and that in the cell interiors  $\rho_C$ . It is assumed that the cell walls contain only edge dislocations while screw dislocations are present in the cell interiors. DRV mechanisms in the cell walls and cell interiors are assumed to be diffusion controlled climb of edge dislocations and cross-slip of screw dislocations, respectively. Cell walls and cell interiors are treated as two different phases. The cell walls represent the “hard” phase while the cell interiors are the “soft” one. The shear flow stress can be expressed by the mixtures rule:

$$\tau = \frac{L_C}{L_C + L_W}\tau_C + \frac{L_W}{L_C + L_W}\tau_W \quad (2.21)$$

where  $L_C$  is the diameter of the cell interiors;  $L_W$  is the thickness of cell walls;  $\tau_C$  and  $\tau_W$  are the shear stresses acting in the cell interiors and cell walls, respectively.  $L_C$  is assumed to be 10 times the average dislocation spacing in the cell interiors ( $L_C = 10/\sqrt{\rho_C}$ ).  $L_W$  is assumed to be a constant.  $\tau_C$  and  $\tau_W$  are related to their corresponding dislocation densities:

$$\tau_C = \mu b\sqrt{\rho_C} \quad (2.22)$$

$$\tau_W = \mu b\sqrt{\rho_W}. \quad (2.23)$$

The evolution of  $\rho_C$  is expressed as

$$\frac{d\rho_C}{d\gamma} = \frac{1}{b\Lambda_C} - \Theta_C\rho_C \quad (2.24)$$

where  $\Lambda_C$  is the mean distance travelled by the screw dislocation in the cell interiors before it is stopped. It is assumed that  $\Lambda_C = 100\rho_C^{-1/2}$ .  $\Theta_C\rho_C$  describes the screw dislocation annihilation rate which is caused by the cross-slip. Following the theory of cross-slip [9],  $\Theta_C\rho_C$  is expressed as

$$\Theta_C\rho_C = \frac{\sqrt{\rho_C} v_0}{50b \dot{\gamma}} \exp\left(-\frac{W_{cs}}{kT}\right) \left[ \exp\left(\frac{\tau_C k_C W_{cs}}{\mu kT}\right) - 1 \right] \quad (2.25)$$

where an attempt frequency  $v_0 = 10^9 \text{ s}^{-1}$  is assumed,  $k$  is the Boltzmann constant,  $W_{cs}$  is the activation energy for cross-slip and  $k_C$  is a constant. Both  $W_{cs}$  and  $k_C$  are fitting parameters.

The evolution of  $\rho_W$  is expressed as

$$\frac{d\rho_W}{d\gamma} = \frac{2}{bL_W} - \Theta_W\rho_W \quad (2.26)$$

where  $2/(bL_W)$  represents the edge dislocation generation rate in the cell walls.  $\Theta_W\rho_W$  represents the DRV rate in the cell walls and is written as

$$\Theta_W\rho_W = \rho_W^2 \frac{D_L}{\dot{\gamma}} \frac{\mu b^3}{kT} \quad (2.27)$$

where  $D_L$  is the lattice diffusivity. Combining equations 2.21 to 2.27, the stress-strain curves and the dislocation densities in the cell walls and cell interiors can be predicted.

Another two-variables model has been proposed by Bréchet and co-workers [32] for single phase metals. Similar to the model described above, the two variables in the model are the dislocation densities in the cell walls and cell interiors. The deformed metals are also considered as a two phase mixture: cell walls being one phase and cell interiors being the other one. The shear stress  $\tau$  is obtained with the help of the mixture rule:

$$\tau = f_W \tau_W \left( \frac{\dot{\gamma}}{\dot{\gamma}_0^*} \right)^{1/m^*} + (1 - f_W) \tau_C \left( \frac{\dot{\gamma}}{\dot{\gamma}_0^*} \right)^{1/m^*} \quad (2.28)$$

where  $f_W$  is the volume fraction of the cell walls.  $1/m^*$  is the strain rate sensitivity index.  $\dot{\gamma}_0^*$  is a reference shear rate (constant).  $\tau_W$  and  $\tau_C$  are respectively determined by the dislocation density in the walls and interiors:

$$\tau_W = \alpha_1 \mu b \sqrt{\rho_W}. \quad (2.29)$$

$$\tau_C = \alpha_1 \mu b \sqrt{\rho_C}. \quad (2.30)$$

where  $\alpha_1$  is a constant.

The evolution of the dislocation density in the cell interior is expressed as

$$\frac{d\rho_C}{d\gamma} = \underbrace{\alpha^* \frac{2}{3\sqrt{3}} \frac{\sqrt{\rho_W}}{b}}_i - \underbrace{\frac{4\beta^*}{bd\sqrt{1-f_W}}}_{ii} - \underbrace{k^* \left( \frac{\dot{\gamma}}{\dot{\gamma}_0^*} \right)^{\frac{-1}{r^*}}}_{iii} \rho_C \quad (2.31)$$

where  $i$  stands for the dislocation generation rate introduced by the dislocation sources on the wall surface in contact with the cell interior.  $\alpha^*$  is a constant denoting the fraction of operative dislocation sources.  $ii$  accounts for the dislocation loss rate in the cell interiors, which is due to cell interior dislocations moving into the walls and becoming part of the wall dislocations.  $\beta^*$  is a constant describing the fraction of interior dislocations moving into the cell walls. Term  $iii$  describes the dislocation loss rate due to the cross-slip of dislocations.  $k^*$  is a constant and  $r^*$ , similar to  $m^*$ , is inversely proportional to the absolute temperature.

For the dislocation density in the cell walls, its evolution equation is written as

$$\frac{d\rho_W}{d\gamma} = \underbrace{\beta^* \frac{4\sqrt{1-f_W}}{bdf_W}}_{iv} + \underbrace{\frac{2\beta^*(1-f_W)\sqrt{\rho_W}}{f_W b\sqrt{3}}}_v - \underbrace{k^* \left( \frac{\dot{\gamma}}{\dot{\gamma}_0^*} \right)^{\frac{-1}{r^*}}}_{vi} \rho_W \quad (2.32)$$

where  $iv$  accounts for the dislocation emigrating from the cell interior into the wall ( $ii$ ); it takes into account the fact that dislocations lost to the cell interior and embedded into the walls are spread over four wall elements. Term  $v$  is the dislocation generation rate in the cell walls due to Frank-Read sources. Term  $vi$  is the dislocation loss rate, identical to  $iii$ . Cross-slip processes are assumed to occur both in the cell walls as well as in the cell interiors.

### 2.3.3 Three-variables model

For alloys containing second phase precipitates as well as single phase alloys, Gottstein and co-workers [113] proposed a three-variables model. These variables are the mobile dislocation density  $\rho_M$ , immobile dislocation density in the cell interior  $\rho_C^{im}$  and immobile dislocation density in the cell walls  $\rho_W^{im}$ . Similar to the two-variables model, in this approach the deformed alloy is divided into two phases: dislocation cell interiors and dislocation walls. The mobile dislocations are assumed to be able to glide through cell interiors and cell walls. The shear stress is expressed by using the rule of mixtures:

$$\tau = f_C \tau_C + f_W \tau_W \quad (2.33)$$

where  $f_C$  and  $f_W$  are the volume fractions of cell interiors and cell walls, respectively.  $\tau_C$  and  $\tau_W$  are the contribution of the shear stress from the cell interiors

and cell walls, respectively.  $\tau_C$  is given by

$$\tau_C = \tau_C^{th} + \alpha_2 \mu b \sqrt{\rho_C^{im}} \quad (2.34)$$

where  $\tau_C^{th}$  is the thermal stress in the cell interiors and  $\alpha_2$  is a constant weakly depending on the temperature.  $\tau_W$  is written as

$$\tau_W = \tau_W^{th} + \alpha_2 \mu b \sqrt{\rho_W^{im}} \quad (2.35)$$

where  $\tau_W^{th}$  is the thermal stress in the cell walls. Both  $\tau_C^{th}$  and  $\tau_W^{th}$  depend on temperature and strain rate.

The core of the model is the evolution kinetics of different types of dislocation populations. The evolution of mobile dislocation density is written as

$$\frac{d\rho_M}{d\gamma} = \underbrace{\frac{1}{bL_{eff}}}_{vii} - \underbrace{\frac{2d_{annihil-c}}{bn_a}}_{viii} \rho_M - \underbrace{4d_{lock} \frac{n_a - 1}{bn_a}}_{ix} \rho_M - \underbrace{2(d_{dipol} - d_{annihil-c})}_{x} \frac{\rho_M}{bn_a} \quad (2.36)$$

where *vii* stands for the generation rate of mobile dislocations.  $L_{eff}$  is the effective distance travelled by the mobile dislocation before it is trapped.  $L_{eff}$  is determined by the effective grain size  $K$  and three obstacle spacings: the forest dislocation spacing in the cell interiors  $L_C$ , the forest dislocation spacing in the cell walls  $L_W$ , and the spacing of the precipitates  $L_P$ .

$$\frac{1}{L_{eff}} = \frac{\beta_C}{L_C} + \frac{\beta_W}{L_W} + \frac{1}{K} + \frac{1}{L_P} \quad (2.37)$$

where  $\beta_C$  and  $\beta_W$  are constants. *viii* is the loss rate of the mobile dislocations due to the annihilation of dislocations with opposite Burgers vector.  $d_{annihil-c}$  is a constant determining the critical distance for annihilation.  $n_a$  is the number of activated glide systems. Term *ix* is the loss rate due to the formation of dislocation locks.  $d_{lock}$  is the critical distance for the spontaneous formation of locks and is a constant. Term *x* takes into account the formation of dislocation dipoles.  $d_{dipol}$  is the critical distance for the formation of dislocation dipoles and is also a constant.

The evolution kinetics of the immobile dislocation density in the cell interior is expressed as

$$\frac{d\rho_C^{im}}{d\gamma} = \underbrace{4d_{lock} \frac{n_a - 1}{bn_a}}_{xi} \rho_M - \underbrace{2v_{climb} d_{climb}}_{xii} \frac{(\rho_C^{im})^2}{\dot{\gamma} n_a} \quad (2.38)$$

where term *xi* is the rate of increase of the dislocation density in the cell interiors, which is equal to the decrease of mobile dislocation density due to the formation of

locks (term ix). Term *xii* describes the annihilation rate due to dislocation climb, which is a diffusion controlled process.  $d_{climb}$  is the climb distance (constant).  $v_{climb}$  is the dislocation climb velocity and is expressed as

$$v_{climb} = \frac{D_{climb}}{kT} \tau A_{climb}$$

where  $D_{climb}$  is the self-diffusion coefficient and  $A_{climb}$  is the activation area.

For the immobile dislocations in the cell walls, the evolution equation reads

$$\frac{d\rho_W^{im}}{d\gamma} = \frac{2}{f_W} \underbrace{(d_{dipol} - d_{annihil-c})}_{xiii} \frac{\rho_M}{bn_a} - \underbrace{2v_{climb} d_{climb}}_{xiv} \frac{(\rho_W^{im})^2}{\dot{\gamma} n_a} \quad (2.39)$$

where term *xiii* is the increase rate of the immobile dislocation density in the cell walls. This is calculated by assuming all dipoles formed by the mobile dislocations (related to term *x*) are stored in the cell walls. Term *xiv* is the annihilation rate due to the climb of dislocations.

## 2.4 Irreversible thermodynamics and plastic deformation

In the existing dislocation-based models, the equations of the dislocation density evolution are derived from a phenomenological building-block approach as mentioned by El-Azab [30] who asserts that the proportionality relationship between the dislocation generation rate and the mean free distance travelled by dislocations lacks a thermodynamic and physical foundation. Furthermore, many fitting parameters are involved in those models. Some of the parameters are not physically rooted so that the flexibility of those models is limited. Based on the principles of thermodynamics, the present work is an attempt to produce dislocation-based models with solid physical foundations. Only a few but physically-rooted parameters are involved. The total dislocation density can be treated as a thermodynamic state variable as suggested by Bridgman [15], which is related to the other thermodynamic state variables such as energy and entropy.

As demonstrated in the existing dislocation-based models described above, during the plastic deformation of metals, three irreversible processes related to dislocations are in general taking place: (1) dislocation generation, (2) dislocation glide and (3) dislocation annihilation. [60][64][65][67][68]. Grain boundary sliding, which is an important mechanism for plastic deformation in nanocrystalline metals [118][125] and in high temperature creep conditions for polycrystalline metals

[121], is not considered in the present work. The entropy generation during plastic deformation can be calculated by using equations 2.3 or 2.4 [64][67]:

$$d_i S = \frac{dW_{ge}}{T} + \frac{dW_{gl}}{T} + \frac{dW_{an}}{T} \quad (2.40)$$

or

$$\frac{d_i S}{dt} = J_{ge} X_{ge} + J_{gl} X_{gl} + J_{an} X_{an} \quad (2.41)$$

where  $dW_{ge}$ ,  $dW_{gl}$  and  $dW_{an}$  are the dissipative energies due to the irreversible processes of dislocation generation, glide and annihilation, respectively.  $J_{ge}$ ,  $J_{gl}$  and  $J_{an}$  are the dislocation generation rate, the average dislocation glide velocity and dislocation annihilation rate, respectively.  $X_{ge}$ ,  $X_{gl}$  and  $X_{an}$  are the generalised forces for dislocation generation, glide and annihilation, respectively. Explicit expressions are shown in the following chapters. Equations 2.40 and 2.41 are core equations employed in this thesis for describing the evolution of the total dislocation density.

The stationary state of plastic deformation can be reached when the dislocation density and their microstructures (e.g. size and orientation of dislocation cells) are independent of time [67]. The internal energy and entropy are independent of time at the stationary state. For isothermal deformation, all mechanical work done into the metal is transformed into heat and is released into the environment, which implies that  $dQ/dt < 0$ . As a result, a negative entropy flow is ensured (equation 2.10) to maintain the stationary state. Invoking the law of energy conservation ( $dU = dQ + dW$ , where  $U$  is the internal energy of the deformed metal and  $W$  is the mechanical work done into the metal) and equation 2.10, the entropy flow between the deformed metal and the environment can be expressed as

$$d_e S = \frac{dQ}{T} = \frac{-dW}{T} = \frac{-\sigma d\epsilon}{T} \quad (2.42)$$

where  $\sigma$  is the applied stress and  $\epsilon$  is the corresponding strain. Equations 2.42 and 2.9 will be employed in Chapter 3 to quantitatively predict the stress level at the stationary state of plastic deformation.

It is interesting to analyse the evolution of the entropy before the deformation reaches the stationary state. Since the entropy generation rate evolves towards the minimum value and the occurrence of a negative entropy flow from the metal into the system, the entropy of metals deformed at isothermal conditions could decrease with straining [64]. The orientation of the grains in the deformed polycrystalline metals will follow a certain direction during the deformation (the formation of texture). Moreover, the dislocations will form a certain pattern (e.g. cells and persistent slip bands) instead of a homogeneous distribution. These two phenomena could bring the deformed metal to a state being more ordered than its initial form.

Furthermore, the entropy of a system in an ordered state is lower than the one in a random state [17]. As a result, the entropy of the deformed metal shows a decrease during straining. This argument will be explored further in Chapter 4 in order to model the entire stress-strain behaviour of plastic deformation. Both equations 2.40 and 2.41 will be employed in Chapters 5 and 6 to describe the evolution of the average dislocation density under adiabatic and quasi-static deformation conditions.

In summary, the current thesis aims at deriving equations for the evolution of the average dislocation density during industrially relevant deformation conditions for single phase of FCC and BCC metals using the principles of irreversible thermodynamics.



# 3

## Modelling Stress Levels at Steady State Deformation Conditions

### 3.1 Introduction

Based on the theory of irreversible thermodynamics introduced in Chapter 2, a model to describe the steady state of plastic deformation in FCC metals is presented. The steady state is characterised by a constant flow stress during straining, which implies that the work hardening rate vanishes, i.e.  $\theta = 0$  where  $\theta \equiv d\tau/d\gamma$ ,  $\tau$  is the shear stress and  $\gamma$  is the shear strain.

A steady state can be achieved in three different situations: (1) constant strain rate deformation under conditions of DRV only, (2) creep under the conditions of DRV only and (3) constant strain rate deformation under conditions of both DRV and dynamic recrystallization (DRX). The details of each metallurgical process and the corresponding steady state will be discussed shortly.

Firstly, a schematic plot of the stress-strain curve at intermediate and high temperatures and a typical testing strain rate is shown in figure 3.1. The stress-strain curve can be divided into three stages (Assuming multi-slip of dislocations takes place at all strain levels, work hardening stage I can be ignored [96]). These stages are easier to distinguish by plotting the work hardening rate versus the flow stress schematically illustrated in figure 3.2 [96]. At low temperatures, a fourth work hardening stage (IV) can appear between stage III and the steady state [136]. This deformation condition is not considered here. At stage II, the flow stress increases linearly with strain and the work hardening rate is constant with increasing

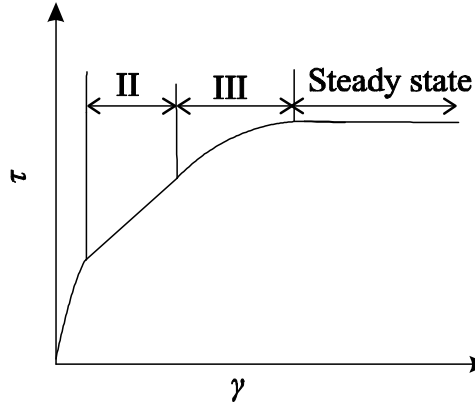


FIGURE 3.1. Schematic representation of three stages of stress-strain curves under constant-strain-rate tests with DRV only.

stress. Stage III begins when the stress-strain curve deviates from linearity. The flow stress still increases with strain but at a lower pace as DRV appears at the beginning of this stage [96]. Consequently, the work hardening rate decreases with flow stress.

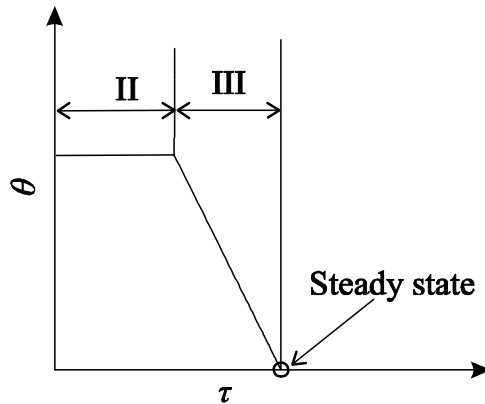


FIGURE 3.2. Schematic representation of work hardening rate vs flow stress for three stages.

The steady state is reached as the flow stress saturates ( $\theta = 0$ ). It is worth to note that the steady state is usually difficult to achieve under conventional tensile testing conditions since the sample will fail by cracking or necking before it reaches this stage, but it can generally be achieved under hot rolling or torsion conditions.

The second condition under which a steady state can be achieved is the creep schematically described in figure 3.3. As opposed to plastic deformation described in figure 3.1, which displays a constant strain rate, creep is usually associated with time-dependent plasticity under a fixed stress at an elevated temperature, often higher than  $0.5T_m$ , where  $T_m$  is the absolute melting temperature [71]. Creep of pure FCC metals is in general divided into three stages (figure 3.3): (1) primary creep, in which the strain rate (or creep rate) is changing with increasing strain or time; (2) secondary creep where strain rate is constant over a range of strain; (3) tertiary creep, where the strain rate increases due to cavitation and/or cracking [71]. The secondary creep is the steady state (constant stress and strain rate) which is dealt with in the current model.

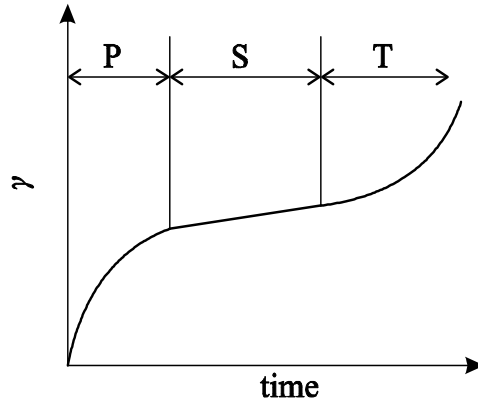


FIGURE 3.3. Schematic representation of three stages of creep: primary creep (P), secondary creep (steady state, S) and tertiary creep (T). At steady state, strain increases linearly with time (constant strain rate).

It is worth to note that, besides the dislocation controlled mechanism, steady state creep may also be induced by a diffusion controlled mechanism (e.g. Nabarro-Herring creep and Coble creep) [71]. Nabarro-Herring creep is caused by the mass transport of vacancies through the grains from one grain boundary to another [56][71]. The strain in Coble creep is controlled by the diffusion of vacancies along grain boundaries [20]. These diffusional controlled steady state creep mechanisms are not considered in the current model. Only dislocation controlled deformation processes will be considered.

Finally, a third metallurgical process is described schematically in figure 3.4. For low stacking fault energy metals, dislocations extend into relatively large stacking faults, which hinders the climb and/or cross-slip of dislocations, so that a sufficient dislocation density can be accumulated to trigger DRX for such metals deformed at

elevated temperatures [28]. When DRX occurs, both nucleation as well as growth (grain boundary migration) take place while the strain is being applied [28]. The flow curves associated with DRX can be single or cyclic peak [28] followed by the steady state as demonstrated in figure 3.4.

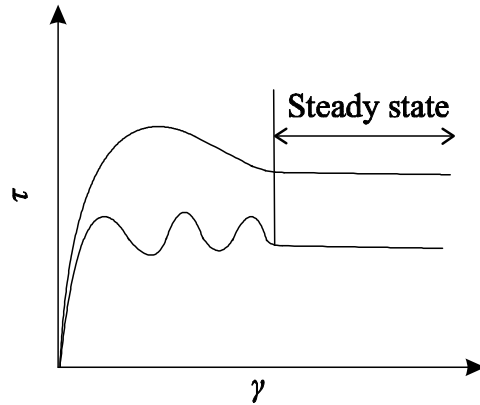


FIGURE 3.4. Schematic representation of stress-strain curves with DRX.

It is often observed that the average dislocation density and subgrain size are constant with straining at the steady state [68]. In order to understand the development of microstructures at the steady state introduced via various metallurgical process, a number of physical models have been proposed in the literature.

The steady state achieved via the first two metallurgical processes (DRV only, figures 3.1 and 3.3) are in general described by the same model. For instance, the model proposed by Mecking and Kocks [83] and the one developed by Gottstein and Argon [43] predict the average dislocation density and the flow stress at the steady state of constant strain rate test and creep test. More recently, a three parameter approach proposed by Nes [96] and Marthinsen and Nes [82] describes the steady state of constant strain rate test and creep test in terms of the subgrain size, the dislocation density inside the subgrains, and the subgrain boundary dislocation density or the subgrain boundary misorientation.

However, for the third metallurgical process (DRV+DRX, figure 3.4), a different physical model is required as the material microstructure is no longer homogeneous but contains regions with a high dislocation density (un-recrystallized regions) and regions of a low dislocation density (recrystallized region). For instance, incorporating DRX, the average dislocation density and the flow stress at the steady state can be described by the models proposed by Sandstrom and Lagneborg [117] and

Hodgson and co-workers [114]. These models employ the dislocation density as a key parameter which is assumed to progress following kinetic approaches.

As discussed in Chapter 2, irreversible thermodynamics is frequently employed for describing irreversible processes in mechanical and chemical engineering [107]. It constitutes an alternative approach to model the steady state of plastic deformation which can be achieved via different metallurgical process as described above. The differences in metallurgical processes are not relevant to an irreversible thermodynamics model (which only compares states and is not interested in routes). Therefore, based on the theory of irreversible thermodynamics, a succinct unified model is proposed to describe the steady states introduced via different metallurgical process. The model predictions are compared to experimental data for a wide range of deformation strain rates and temperatures.

## 3.2 Model

### 3.2.1 Entropic analysis

There are three irreversible processes related to dislocations occurring at the steady state: (1) dislocation generation, (2) dislocation glide and (3) dislocation annihilation. They are illustrated highly schematically in figure 3.5: during a shear strain interval  $d\gamma$ ,  $d\rho^+$  dislocations are generated at the subgrain boundary in the form of Frank-Read sources; then, the generated dislocations glide through the subgrain; finally, they are trapped at the opposite side of the subgrain boundary. In the meantime,  $d\rho^-$  dislocations are annihilated due to DRV and/or DRX. These three dislocation activities are irreversible processes which, according to the theory of irreversible thermodynamics, produce entropy  $d_iS$ . This is mathematically expressed as [67][107]

$$d_iS = \frac{dW_{ge}}{T} + \frac{dW_{gl}}{T} + \frac{dW_{an}}{T} \quad (3.1)$$

where  $dW_{ge}$ ,  $dW_{gl}$  and  $dW_{an}$  are the dissipative energies due to the processes of dislocation generation, glide, and annihilation, respectively;  $T$  is the absolute temperature.  $dW_{ge}$  is assumed to be proportional to  $d\rho^+$ :

$$dW_{ge} = Ed\rho^+ \quad (3.2)$$

where  $E$  is the elastic energy of the dislocation per unit length.

The energy dissipated due to dislocation glide,  $dW_{gl}$ , is expressed as

$$dW_{gl} = \tau_f b l d\rho^+ \quad (3.3)$$

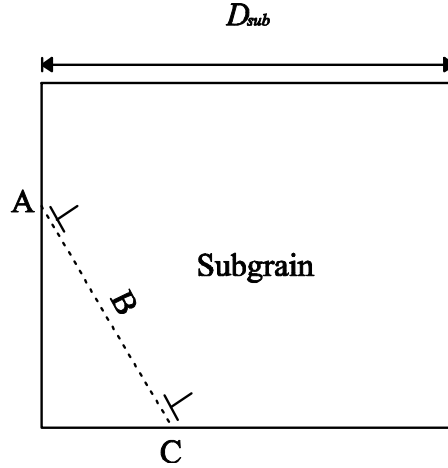


FIGURE 3.5. Dislocations are generated at A, then glide through the subgrain following path B and finally trapped at C.

where  $\tau_f$  is the shear friction stress for dislocation gliding. It is assumed that  $\tau_f = \tau$ , where  $\tau$  is the applied shear stress which is expressed as [5][83]

$$\tau = \tau_0 + \alpha\mu b\sqrt{\rho} \quad (3.4)$$

where  $\tau_0$  is the contribution of the lattice resistance and elements in solid solution; the term  $\alpha\mu b\sqrt{\rho}$  incorporates the contribution of existing dislocations. For pure FCC metals deformed at the steady state,  $\tau_0$  can be neglected [5][81]. Referring to equation 3.3,  $l$  is the mean gliding distance during  $d\gamma$  assumed to be equal to the average distance between dislocations:

$$l = \frac{1}{\sqrt{\rho}}. \quad (3.5)$$

When dislocations are annihilated, their elastic energies will be dissipated and released into the surroundings. Therefore,  $dW_{an}$  is expressed as

$$dW_{an} = E d\rho^- \quad (3.6)$$

and  $E$  is approximated by [68]:

$$E = \frac{1}{2}\mu b^2. \quad (3.7)$$

Combining equations 3.1-3.7, equation 3.1 can be rewritten as

$$d_i S = (1 + 2\alpha) \frac{\mu b^2}{2T} d\rho^+ + \frac{\mu b^2}{2T} d\rho^-. \quad (3.8)$$

At the steady state, the average dislocation density  $\rho$  remains constant with straining due to the balance between dislocation generation and annihilation [68][96][136], which is mathematically expressed as

$$d\rho = d\rho^+ - d\rho^- = 0. \quad (3.9)$$

Inserting equation 3.9 into equation 3.8,  $d_i S$  is rewritten as

$$d_i S = (1 + \alpha) \frac{\mu b^2}{T} d\rho^-. \quad (3.10)$$

The entropy flux  $d_e S$  for a shear strain increment  $d\gamma$  is related to the heat flux  $dQ$  between the deformed metal and the environment [107]:

$$d_e S = \frac{dQ}{T}. \quad (3.11)$$

At the steady state, the overall dislocation density does not change with increasing strain [68][96][136], causing the stored energy to remain constant ( $dU = 0$ ), being  $U$  is the stored energy of the deformed metal. According to the energy conservation law,  $dQ$  is expressed as

$$dQ = dU - dW = -dW \quad (3.12)$$

where  $dW$  is the mechanical work done into the metal by external loading:

$$dW = \tau d\gamma. \quad (3.13)$$

Inserting equations 3.4, 3.12 and 3.13 into equation 3.11,  $d_e S$  is rewritten as

$$d_e S = \frac{-\alpha \mu b \sqrt{\rho}}{T} d\gamma. \quad (3.14)$$

The total entropy change  $dS$  of the deformed metals during a strain interval  $d\gamma$  is the sum of the entropy production and flux [107]:

$$dS = d_i S + d_e S. \quad (3.15)$$

Assuming that the steady state of the plastic deformation is a stationary state in the context of irreversible thermodynamics,  $dS = 0$  since all state variables (including entropy) are time independent. This can be rewritten as [107]

$$d_i S = -d_e S. \quad (3.16)$$

Inserting equations 3.10 and 3.14 into equation 3.16, the average dislocation density  $\rho$  at the steady state can be derived:

$$\rho = \left[ \frac{b(1 + \alpha)}{\alpha} \frac{d\rho^-}{d\gamma} \right]^2. \quad (3.17)$$

The dislocation annihilation can be due to DRV and/or DRX depending on the deformation conditions (temperature and strain rate) and the stacking fault energy of metals. Therefore,  $d\rho^-/d\gamma$  can be expressed as the sum of annihilation rate due to DRV and DRX:

$$\frac{d\rho^-}{d\gamma} = \frac{d\rho_{DRV}^-}{d\gamma} + \frac{d\rho_{DRX}^-}{d\gamma} \quad (3.18)$$

where  $d\rho_{DRV}^-/d\gamma$  and  $d\rho_{DRX}^-/d\gamma$  represent the dislocation annihilation rates due to DRV and DRX, respectively.

### 3.2.2 Dislocation annihilation due to dynamic recovery

DRV could be induced by dislocation climb and/or cross-slip. At the steady state, most dislocations are stored in the subgrain boundaries [68][76][96] in which DRV is mainly due to the climb of edge dislocations [98]. In the current model, it is reasonable to assume that DRV is only caused by the climb of edge dislocations, which is a process controlled by the diffusion of vacancies [2][123]. As a result,  $d\rho_{DRV}^-/d\gamma$  can be expressed as [2]

$$\frac{d\rho_{DRV}^-}{d\gamma} = \frac{2c_j v_c}{\dot{\gamma}} \rho \quad (3.19)$$

where  $\dot{\gamma}$  is the shear strain rate.  $c_j$  is the number of dislocation jogs per unit length and is proportional to the dislocation density [96]:

$$c_j = \sqrt{\rho}. \quad (3.20)$$

Based on the hard ball model, the dislocation climb velocity  $v_c$  along the dislocation line is expressed as [2][96]

$$v_c = 2bv_D n_c (b/d)^2 \exp\left(-\frac{U_{SD}}{RT}\right) \left[ \exp\left(\frac{F\Omega}{kT}\right) - 1 \right] \quad (3.21)$$

where  $v_D$  ( $10^{13} \text{ s}^{-1}$ ) is the Debye frequency.  $n_c$  is the number of nearest neighbours for diffusion ( $n_c = 11$  for FCC).  $d$  is the stacking fault width.  $U_{SD}$  is the activation energy for self-diffusion.  $F$  is the assistant stress to enhance the dislocation climb, and is originated from the combination of the applied stress and the stress of existing dislocations [2][96].  $\Omega$  is the atomic volume (assumed to be  $b^3$ ).  $k$  is the Boltzmann constant and  $R$  is the universal gas constant. The ratio  $(b/d)$  is given by the equilibrium extension of an edge dislocation [2]:

$$\frac{b}{d} = \frac{24\pi(1-\nu)\chi}{(2+\nu)\mu b} \quad (3.22)$$

where  $\nu$  is the Poisson's ratio and  $\chi$  is the stacking fault energy. The assistant stress  $F$  is related to the dislocation density as [96]

$$F = \xi \mu b \sqrt{\rho} \quad (3.23)$$

where  $\xi$  is the stress intensity factor, a constant value between 70 and 90 [96] for FCC metals. In the present work,  $\xi = 70$  is taken.

The factor 2 in equation 3.19 accounts for the fact that the dislocation annihilation is due to a positive and a negative dislocation segment converge at the same place. In other words, two dislocation segments of opposite Burgers vector will disappear simultaneously in one annihilation step.

Inserting equation 3.20 into equation 3.19, the dislocation annihilation rate due to DRV is rewritten as

$$\frac{d\rho_{DRV}^-}{d\gamma} = \frac{2v_c}{\dot{\gamma}} \rho^{3/2}. \quad (3.24)$$

### 3.2.3 Dislocation annihilation due to dynamic recrystallization

DRX can be described by the nucleation and growth of new grains in deformed metals. At the steady state, the grain size is constant due to the balance between nucleation and growth of new grains [39]. The dislocation annihilation rate due to DRX is related to the movement of grain boundaries. This is mathematically expressed as [68]

$$\frac{d\rho_{DRX}^-}{dt} = Av_{gb}\rho \quad (3.25)$$

where  $t$  is time.  $A$  is the area (per unit volume) of moving grain boundaries at the steady state.  $v_{gb}$  is the average grain boundary velocity. Equation 3.25 can be rewritten as

$$\frac{d\rho_{DRX}^-}{d\gamma} = \frac{Av_{gb}}{\dot{\gamma}} \rho. \quad (3.26)$$

Assuming the nuclei of DRX are the subgrains located at the grain boundaries,  $A$  can be expressed as

$$A = K_1 S_{sub} \quad (3.27)$$

where  $S_{sub}$  is the total area of subgrains per unit volume and  $K_1$  is a constant ( $0 < K_1 < 1$ ) representing the fraction of subgrains located at the grain boundaries.  $K_1 = 0.1$  is assumed. For simplicity, the geometry of subgrains is assumed to be cubic (figure 3.5), which leads to

$$S_{sub} = \frac{1}{2} \times \frac{6D_{sub}^2}{D_{sub}^3} = \frac{3}{D_{sub}}. \quad (3.28)$$

where  $D_{sub}$  is the subgrain size.  $6D_{sub}^2$  represents the area of one subgrain and  $D_{sub}^3$  is its volume. The factor  $1/2$  takes into account that the surface of one subgrain is shared by two adjacent subgrains.  $D_{sub}$  is found experimentally [62] and theoretically to be proportional to the average dislocation density:

$$D_{sub} = \frac{K_2}{\sqrt{\rho}} \quad (3.29)$$

where  $K_2 = 10$  is a constant taken from the literature by Holt [62].

The grain boundary velocity  $v_{gb}$  is determined by the grain boundary mobility  $M_{gb}$  and the driving force  $P$  via the relationship [68]:

$$v_{gb} = M_{gb}P. \quad (3.30)$$

The driving force is given by [68][116]

$$P = \frac{1}{2}\mu b^2\rho. \quad (3.31)$$

The grain boundary mobility can be expressed as [138]

$$M_{gb} = \frac{\delta D_{gb} V_m}{b^2 RT} \quad (3.32)$$

where  $\delta$  is the grain boundary thickness.  $V_m$  is the molar volume.  $D_{gb}$  is the grain boundary self diffusion coefficient which can be expressed by an Arrhenius relationship [138]:

$$D_{gb} = D_{gb0} \exp\left(-\frac{U_{gb}}{RT}\right) \quad (3.33)$$

where  $D_{gb0}$  is the pre-exponential factor and  $U_{gb}$  is the activation energy for grain boundary diffusion.

Inserting equations 3.27, 3.28 and 3.29 into equation 3.26, the dislocation annihilation rate due to DRX is rewritten as

$$\frac{d\rho_{DRX}^-}{d\gamma} = \frac{3K_1 v_{gb}}{K_2 \dot{\gamma}} \rho^{3/2}. \quad (3.34)$$

### 3.2.4 Dislocation density at the steady state

In section 3.2.1, the average dislocation density at the steady state is found to be related to the dislocation annihilation rate due to DRV and DRX (equation 3.17). Moreover, the dislocation annihilation rate is derived in sections 3.2.2 and 3.2.3 (equations 3.24 and 3.34). As a result, the average dislocation density at the steady state is now obtained by inserting equations 3.18, 3.24 and 3.34 into equation 3.17:

$$\rho = \frac{\dot{\gamma}}{bv_{an}} \quad (3.35)$$

where  $v_{an}$  is the pertinent velocity related term combining the dislocation climb velocity and grain boundary velocity and is expressed as

$$v_{an} = \frac{1 + \alpha}{\alpha} \left[ \underbrace{2v_c}_I + \underbrace{(3K_1/K_2)v_{gb}}_{II} \right] \quad (3.36)$$

where terms  $I$  and  $II$  account for the effects of DRV and DRX, respectively.

### 3.3 Application and discussion

#### 3.3.1 Constant strain rate deformation with DRV only

For the case with DRV only, the term  $II$  in equation 3.36 vanishes. Therefore, by rewriting equation 3.35, the dislocation density at the steady state for the constant strain rate test with DRV only is expressed as

$$\rho = \frac{\alpha \dot{\gamma}}{2(1 + \alpha)bv_c}. \quad (3.37)$$

Inserting equation 3.37 into equation 3.4 (Taylor relation), the shear flow stress  $\tau$  for pure FCC metals at the steady state with DRV can be expressed as

$$\tau = \alpha \mu b \left[ \frac{\alpha \dot{\gamma}}{2(1 + \alpha)bv_c} \right]^{1/2}. \quad (3.38)$$

By solving equation 3.38, the flow stress at the steady state under the constant strain rate test condition is obtained. This prediction is compared to the temperature dependent flow stress  $\langle 111 \rangle$  single crystals.

Single crystals are chosen as a first assessment because of the absence of grain boundary sliding at high temperatures and the considerable delay in DRX compared to polycrystals [84]. In compression tests on Cu and Ni single crystals of  $\langle 111 \rangle$  orientation conducted by Gottstein and Kocks [45], it is shown that the critical stress and strain for the initiation of DRX are much higher than those in polycrystals. Furthermore, the  $\langle 111 \rangle$  orientation is stable in both tension and compression, and deforms in multi-slip like polycrystals. The texture does not change much during deformation [84]. All these effects allow for a good assessment of the DRV model presented here.

Critical material dependent constants employed in the model are obtained from the literature [84][96], and are listed in table 3.1. The Poisson's ratio  $\nu = 0.3$  and  $\alpha = 0.4$  [64][67] are assumed for all metals. The temperature effects are incorporated in the term  $v_c$  (equation 3.21). Figure 3.6 shows that the model prediction is

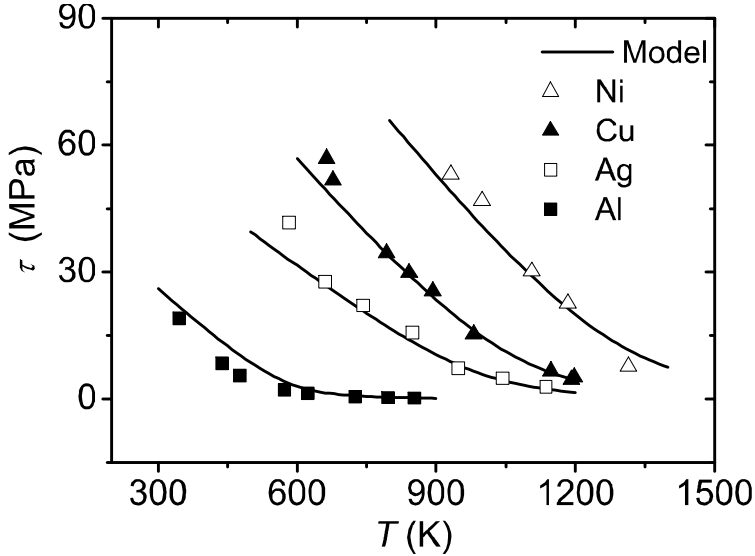


FIGURE 3.6. Temperature dependence of steady shear stresses for Ni, Cu, Ag and Al pure single crystals of  $\langle 111 \rangle$  orientation. Dots are experimental data.

	$b$ (nm)	$\mu$ (MPa)	$\chi$ ( $\times 10^{-3} \text{ J}\cdot\text{m}^{-2}$ )	$T_m$ (K)	$U_{SD}$ ( $\times 10^3 \text{ J}\cdot\text{mol}^{-1}$ )	
					M	E
Ni	0.249	$87416.4 - 32.73T$ $+ 2.95 \times 10^{-3}T^2$	125	1728	290	280
Cu	0.256	47400 $\times \exp(-3.97 \times 10^{-4}T)$	47	1358	236	210-236
Ag	0.289	$29997.5 - 12T$ $- 7.96 \times 10^{-5}T^2$	16	1235	208	179-208
Al	0.286	$29438.4 - 15.052T$	166	933	138	136-142

TABLE 3.1. Material constants employed in the model are obtained from the literature [84][96]. Two sets of values of  $U_{SD}$  are included. Column M represents the values used in the model. Column E contains the values measured from experiments reported in the literature [96].

in good agreement with the experimental data for Ni, Cu, Ag and Al single crystals reported by Mecking and co-workers [84]. The steady shear stress decreases with temperature.

By solving equation 3.37, the temperature dependence of the average dislocation densities at the steady state for Cu, Ag, Ni and Al single crystals are calculated

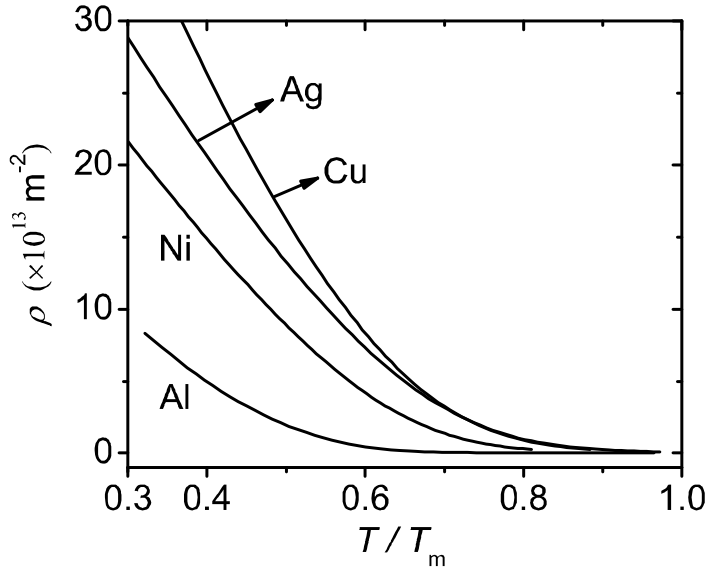


FIGURE 3.7. The average dislocation density vs normalised temperature at the steady state. The shear strain rate is  $4 \times 10^{-4} \text{ s}^{-1}$ .

and the results are plotted in figure 3.7. The figure shows that Al and Cu display, respectively, the lowest and the highest dislocation density, both of which decrease monotonically with temperature. The reason is that the dislocation climb velocity increases with temperature as faster diffusion of vacancies takes place. At temperatures higher than approximate  $0.8T_m$ , all four single crystals approach the same dislocation density because the dislocation climb velocity is almost equal for these four metals due to vacancy diffusion reaching a limiting value.

It is generally accepted in the literature that the stacking fault energy plays an important role in DRV [2][60][84]. Higher stacking fault energy (corresponding to smaller stacking fault width (equation 3.22) can increase the DRV rate resulting a lower dislocation density. Moreover, in addition to stacking fault energy, the self diffusion energy is a key parameter. This is related to the melting temperature; higher melting temperatures correspond to higher self diffusion energies, which make dislocation climb more difficult, resulting in higher dislocation densities in the deformed metals. Referring to figure 3.7, Al has the highest stacking fault energy and the lowest self diffusion energy (lowest melting point) (table 3.1), leading to fastest DRV and lowest dislocation density. For Ni, although its stacking fault energy is higher than that of Ag and Cu, its dislocation density is still lower due to its highest self diffusion energy. On the other hand, Ag display the lowest stacking

fault energy and a relatively high self diffusion energy, resulting in a dislocation density higher than Ni and Al. In summary, stacking fault energy and self diffusion energy are competitive parameters: the dislocation density decreases with stacking fault energy but increases with self diffusion energy.

In the current calculation, the stacking fault energy of each metal is assumed to be constant with temperature. One may argue that the stacking fault energy could increase with temperature. For instance, the stacking fault energy of austenitic steels with high Mn content is found to increase with temperature at the relative low temperature regime ( $T < 0.3T_m$ ) [1]. However, for pure FCC metals, the increase of stacking fault energy with temperature within the temperature regime considered here ( $T > 0.3T_m$ ) may be small enough such that the stacking fault energy may be assumed to be constant.

### 3.3.2 Steady state creep with DRV only

Another application of the model is the steady state creep of high purity coarse grained polycrystalline Al. Combining Taylor relation (equation 3.4) and equation 3.35 and assuming no DRX taking place (the term  $II$  in equation 3.36 vanishes), the creep rate (strain rate) can be expressed as

$$\dot{\gamma} = \kappa \frac{v_c}{b} \left( \frac{\tau}{\mu} \right)^2 \quad (3.39)$$

where  $\kappa = 2(1 + \alpha)/\alpha^3$ . Equation 3.39 indicates that the creep rate is determined by the stress and the dislocation climb velocity.

By solving equation 3.39, the relationship between creep rate and stress is obtained as shown in figure 3.8 for pure polycrystalline Al. Figure 3.8 shows that the model recovers the experimental data obtained by Sherby and Burke [121] over a wide range of temperatures from near the melting temperature to as low as  $0.57T_m$ . It is noted that, in figure 3.8, the stress is uniaxial stress ( $\sigma = M\tau$ , where  $M$  is the Taylor factor) as strain rate does ( $\dot{\epsilon} = \dot{\gamma}/M$ ). The Taylor factor is taken as 3.06 [83]. At such creep conditions, DRX does not occur [71] and equation 3.39 can be applied.

Figure 3.8 shows that the creep rate increases with stress. For the same stress level, the creep rate increases with temperature. Another interesting feature in this figure is that, at low temperatures (533 and 644 K), the slope of the curves increases with stress, while at high temperatures (755 and 866 K), they remain constant. This phenomenon is described as the power-law breakdown in the classical semi-empirical power-law descriptions of creep [71], and is due to the change in creep mechanism from dislocation climb to dislocation pipe diffusion [71].

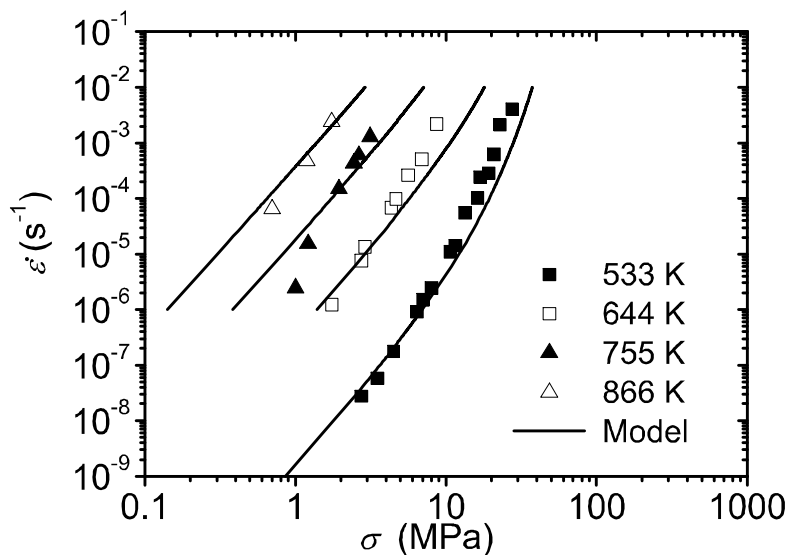


FIGURE 3.8. Uniaxial stress ( $\sigma$ ) vs uniaxial strain rate ( $\dot{\epsilon}$ ) for steady state creep of high purity polycrystalline Al at various temperatures. Dots are experimental values.

In contrast, in the current model, it is not necessary to postulate a change of dislocation related mechanism in order to explain the change of the slopes in figure 3.8. In the current model, the increase of the slopes is due to the introduction of the assistant force  $F$  for the formation of vacancies (equation 3.21). Moreover, the influence of  $F$  is only relevant at the high stress level (low temperature regime). In other words, vacancies can only experience the presence of the assistant force when it is larger than a certain value. As a result, the slopes start to increase when the influence of  $F$  becomes relevant.

In summary, employing only one single dislocation mechanism, the current model can describe the creep of pure Al over a wide range of temperatures, while the classical semi-empirical power-law model needs to introduce different mechanisms for different temperature regimes.

### 3.3.3 Constant strain rate deformation with DRV and DRX

For polycrystalline metals with low stacking fault energy and relative high self diffusion energy (relative high melting temperature) such as Cu, the dislocation density stored in the deformed metal is relatively high as discussed in previous section (figure 3.7). For such circumstance, DRX takes place at the steady state under hot deformation conditions as schematically shown in figure 3.4. The steady

flow stress for this case can be obtained by inserting equation 3.35 into equation 3.4:

$$\tau = \alpha\mu \left( \frac{b\dot{\gamma}}{v_{an}} \right)^{1/2} \quad (3.40)$$

In order to apply the model to the situation of DRV+DRX (solving equation 3.40), 3 more terms ( $\delta \cdot D_{gb0}$ ,  $U_{gb}$ ,  $V_m$ , see equations 3.32 and 3.33), which are related to the grain boundary mobility, need to be known. In the current calculations, the values for  $\delta \cdot D_{gb0} = 9.44 \times 10^{-15} \text{ m}^3 \cdot \text{s}^{-1}$  and  $V_m = 7.11 \times 10^{-6} \text{ m}^3 \cdot \text{mol}^{-1}$  are obtained from literature [16][88].  $U_{gb}$  ( $\text{J} \cdot \text{mol}^{-1}$ ) in the current calculations is determined by adjusting to experimental data and is assumed to take the form as

$$U_{gb} = U_{gb0} \ln \frac{\dot{\gamma}_0}{\dot{\gamma}} \quad (3.41)$$

where  $U_{gb0} = 3.4 \times 10^3 \text{ J} \cdot \text{mol}^{-1}$  and  $\dot{\gamma}_0 = 4 \times 10^8 \text{ s}^{-1}$  are taken. For instance, when the shear strain rate increases from  $10^{-4}$  to  $10^{-1} \text{ s}^{-1}$ ,  $U_{gb}$  decreases from  $98.7 \times 10^3$  to  $75.2 \times 10^3 \text{ J} \cdot \text{mol}^{-1}$ . These activation energy values are similar to those reported in the literature [88].

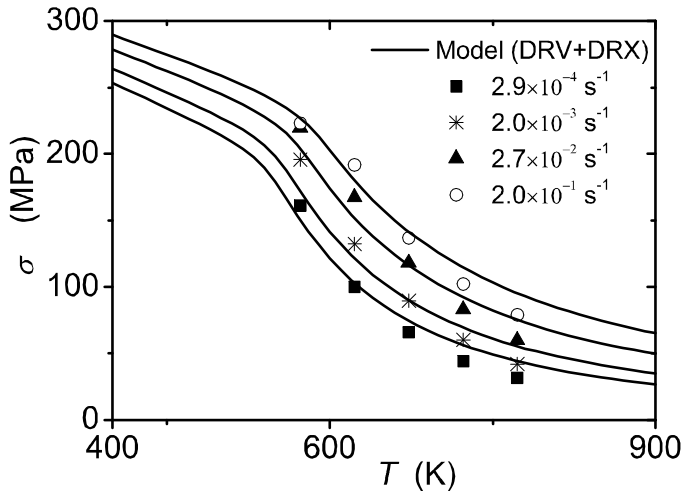


FIGURE 3.9. Steady uniaxial stress vs temperature for pure polycrystalline Cu at four different strain rates.

By solving equation 3.40, the steady flow stresses of high purity (99.99999%) polycrystalline Cu under hot compression are predicted as shown in figure 3.9. The model predictions are in good agreement with compression tests performed by Gao and co-workers [39]. Figure 3.9 shows that the steady state stress increases

with strain rate and decreases with temperature. The stress and strain rate in this figure are uniaxial stresses and uniaxial strain rate. The Taylor factor  $M$  for these compression tests is assumed to be 3.06 [83].

In order to identify the relative contributions of DRV and DRX at the steady state, three different calculations are made for  $\dot{\epsilon} = 0.2 \text{ s}^{-1}$  as shown in figure 3.10: (1) DRV only (i.e. term  $II$  vanishes in equation 3.36); (2) DRX only (i.e. term  $I$  vanishes in equation 3.36); (3) DRV+DRX. It is shown that the curve of DRX merges with the curve of DRV+DRX when the temperature is higher than about 600 K. This implies that DRX is the dominant softening mechanism at this temperature regime. In contrast, the curve of DRV joins the curve of DRV+DRX when the temperature is lower than about 450 K, which indicates that DRV plays a dominant role. At such low temperature, it is too difficult to initiate DRX. In the range between 450 and 600 K, both DRV and DRX are important. This is the transitional regime.

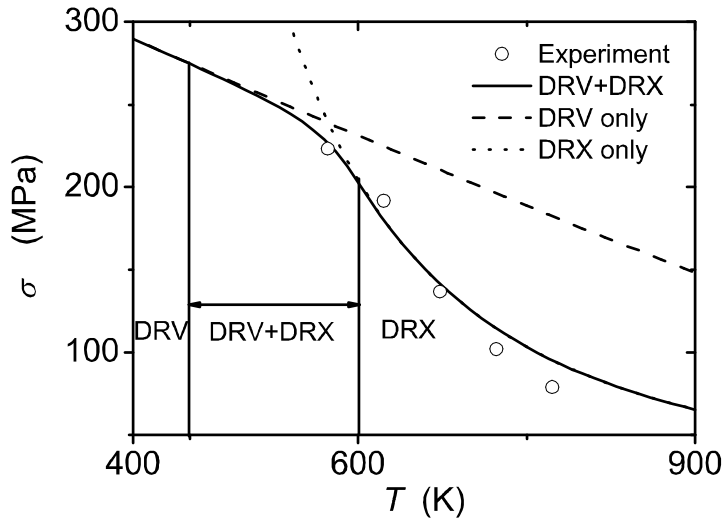


FIGURE 3.10. Steady uniaxial stress vs temperature for pure polycrystalline Cu. Lines are model predictions. Three regions are indicated: (1) DRV, (2) DRV+DRX and (3) DRX. The experimental data are the same in figure 3.9 for  $\dot{\epsilon} = 0.2 \text{ s}^{-1}$ .

It is interesting to note that the above observations are in full agreement with the Zener-Hollomon criterion for the occurrence of DRX. The Zener-Hollomon criterion combines the deformation temperature and strain rate into one Zener-Hollomon parameter  $Z$  :

$$Z = \dot{\gamma} \exp\left(\frac{Q_z}{RT}\right) \quad (3.42)$$

where  $Q_Z$  is the activation energy [68]. DRX mainly occurs under conditions of low  $Z$  value, which corresponds to low strain rates or high temperatures [68]. For a given strain rate, increasing the deformation temperature decreases the value of  $Z$ . Therefore, for a given strain rate, the temperature needs to be high enough to obtain a low  $Z$  value such that DRX can occur. Finally, for a given strain rate, it is easier to initiate DRX at higher deformation temperature, which is in agreement with the predictions of the current model (figure 3.10).

### 3.4 Conclusions

A novel succinct physical model based on the theory of irreversible thermodynamics is developed in this chapter to predict the average dislocation density and then the flow stress at the steady state of plastic deformation for pure FCC metals. The dislocation density is found to be a function of shear strain rate and a velocity term combining the climb velocity of dislocations and the grain boundary velocity, i.e.  $\rho = \dot{\gamma}/(bv_{an})$ .

The effects of DRV and DRX are naturally incorporated into one single formula. At low temperatures, the model predicts that the DRV is the dominant softening mechanism, while at high temperatures, DRX plays the major role.

In contrast to the classical semi-empirical power-law model, the current model can describe the creep of pure Al over a wide range of temperatures without the need to introduce different creep mechanisms for different temperature regimes.

# 4

## Modelling the Stress-strain Behaviour of Single Crystals and (Ultra)fine Polycrystals

### 4.1 Introduction

As discussed in Chapter 3, the stress-strain curve of metals at a constant strain rate and temperature can be divided into several work hardening stages. The steady state has been described in Chapter 3 by an irreversible thermodynamics model. This chapter is to extend this model to describe other work hardening stages (entire stress-strain curve) in terms of the evolution of dislocation microstructures.

A large amount of experimental evidence (e.g. TEM [6][19][59] and x-ray diffraction [69]) shows that the density and arrangement of dislocations change with the progress of deformation. For instance, dislocation density increases with increasing deformation in metals at a constant strain rate and temperature [52][92]. Concerning the arrangement of dislocations, it is often observed that, with increasing deformation, dislocations are organized into high and low density regions (dislocation cell/subgrain boundaries and interiors, respectively). [38][51][68].

A number of models have been developed to describe (or explain) the work hardening of metals based on several types of dislocation densities. Nix and co-workers [98] proposed a composite model with which the dislocation densities in cell boundaries and interiors can be predicted. More recently, Nes and co-workers [95][96][97] proposed a three parameter approach to model work hardening in terms of the dislocation densities in the cell/subgrain boundary and interior, as well as the cell/subgrain size. A similar three parameter model has been developed to

describe the work hardening of metals and alloys by Gottstein and co-workers [113]. It distinguishes three types of dislocations: mobile dislocations, immobile dislocations in the cell interior and immobile dislocations at the cell boundary. All these models have in common that some additional parameters to the dislocation density are involved.

Besides the multiple parameter models, Kocks and Mecking [73] and Estrin and Mecking [31] proposed a one parameter approach based on an average dislocation density. This model successfully predicts the stress-strain curves by utilizing the Taylor relationship between the flow stress and the average dislocation density. One of the advantages of the one parameter model is that the number of free parameters is reduced, though it sacrifices the heterogenic nature of the dislocation structures.

Despite the success of the parametric approaches, they lack a firm thermodynamic foundation. Adopting the one parameter concept (average dislocation density), this chapter proposes models based on the theory of irreversible thermodynamics to describe the entire plastic region of the stress-strain curves deformed at a constant strain rate and temperature. Firstly, section 4.2 develops a model for FCC single crystals deformed at a wide range of temperatures. Secondly, incorporating the grain size effects on the development of dislocation microstructures, section 4.3 extends the single crystal model to (ultra)fine grained FCC and BCC alloys. The predictions on ductility emphasize that the engineering applications of ultrafine grained (UFG) alloys are intrinsically limited by their low ductility.

## 4.2 Single crystals

### 4.2.1 Model

It is generally accepted that there are three irreversible processes taking place during plastic deformation of metals [60][64][67]: (1) dislocation generation from Frank-Read sources, (2) dislocation glide along their slip systems and (3) dislocation annihilation due to edge dislocation climb and/or screw dislocation cross-slip, depending on the loading conditions (temperature and strain rate) [98]. In the present work, the dislocation annihilation due to the motion of subgrain boundaries or due to DRX is omitted from the analysis as the deformation conditions considered (low deformation temperature and small strain) are not sufficient to trigger those processes.

According to the theory of irreversible thermodynamics, all irreversible processes produce entropy, which is related to the energy dissipation [107]. Therefore, during a shear strain increment  $d\gamma$ , the entropy production in the metal bulk is expressed

as [60][67][107]

$$d_i S = \frac{dW_{ge}}{T} + \frac{dW_{gl}}{T} + \frac{dW_{an}}{T} \quad (4.1)$$

where  $dW_{ge}$ ,  $dW_{gl}$  and  $dW_{an}$  are the dissipative energies due to processes of dislocation generation, glide, and annihilation, respectively;  $T$  is the absolute temperature.  $dW_{ge}$  is assumed to be proportional to  $d\rho^+$  [64][67]:

$$dW_{ge} = E d\rho^+ \quad (4.2)$$

where  $d\rho^+$  is the length of dislocations per unit volume generated during  $d\gamma$  and  $E$  is the elastic energy of the dislocations per unit length.

$dW_{gl}$  is expressed as [64][67]

$$dW_{gl} = \tau_f b l d\rho^+ \quad (4.3)$$

where  $\tau_f$  is the shear friction stress for dislocation gliding. It is assumed that  $\tau_f = \tau$  where  $\tau$  is the shear flow stress which is expressed as [5][83]

$$\tau = \tau_0 + \alpha \mu b \sqrt{\rho} \quad (4.4)$$

where  $\tau_0$  is the contribution of the lattice resistance and elements in solid solution; the term  $\alpha \mu b \sqrt{\rho}$  accounts for the contribution due to existing dislocations.  $\alpha$  is a constant accounting for the interaction between dislocations,  $\mu$  is the shear modulus, and  $b$  is the magnitude of Burgers vector. For pure FCC single crystals,  $\tau_0$  can be neglected [5][81]. Referring to equation 4.3,  $l$  is the mean glide distance of dislocations during  $d\gamma$  assumed to be equal to the average distance between dislocations [64][67]:

$$l = \frac{1}{\sqrt{\rho}}. \quad (4.5)$$

Concerning the annihilation process during  $d\gamma$ ,  $d\rho^-$  dislocations are annihilated due to edge dislocation climb and/or screw dislocation cross-slip depending on the loading conditions, their elastic energies will be dissipated and released into the surroundings. Therefore,  $dW_{an}$  is expressed as [64]

$$dW_{an} = E d\rho^- \quad (4.6)$$

and  $E$  is approximated by [68]:

$$E = \frac{1}{2} \mu b^2. \quad (4.7)$$

Combining equations 4.1-4.7,  $d_i S$  is rewritten as

$$d_i S = (1 + 2\alpha) \frac{\mu b^2}{2T} d\rho^+ + \frac{\mu b^2}{2T} d\rho^-. \quad (4.8)$$

The change of the average dislocation density during  $d\gamma$  is expressed as

$$d\rho = d\rho^+ - d\rho^-. \quad (4.9)$$

Inserting equation 4.9 into 4.8, the entropy generation takes the form:

$$d_i S = (1 + 2\alpha) \frac{\mu b^2}{2T} d\rho + (2 + 2\alpha) \frac{\mu b^2}{2T} d\rho^-. \quad (4.10)$$

The entropy flux  $d_e S$  during  $d\gamma$  is related to the heat flux between the deformed metal and the environment [107]:

$$d_e S = \frac{dQ}{T}. \quad (4.11)$$

According to the energy conservation law ( $dQ = dU - dW$ ), equation 4.11 can be modified as

$$d_e S = \frac{dU - dW}{T} \quad (4.12)$$

where  $dU$  is the increase of the stored energy due to the dislocation density increase during  $d\gamma$  and is expressed as [68]

$$dU = \frac{1}{2} \mu b^2 d\rho. \quad (4.13)$$

$dW$  is the mechanical work done into the metal by the external loading:

$$dW = \tau d\gamma \quad (4.14)$$

Inserting equations 4.4, 4.13 and 4.14 into equation 4.12,  $d_e S$  is rewritten as

$$d_e S = \frac{\mu b^2}{2T} d\rho - \frac{\alpha \mu b \sqrt{\rho}}{T} d\gamma \quad (4.15)$$

The total entropy change  $dS$  of the deformed metal during  $d\gamma$  is the sum of the entropy generation and entropy flux [107]:

$$dS = d_i S + d_e S \quad (4.16)$$

Inserting equations 4.10 and 4.15 into 4.16,  $dS$  is rewritten as

$$dS = (1 + \alpha) \frac{\mu b^2}{T} d\rho + (1 + \alpha) \frac{\mu b^2}{T} d\rho^- - \frac{\alpha \mu b \sqrt{\rho}}{T} d\gamma \quad (4.17)$$

Rewriting equation 4.17 provides

$$\frac{dS}{d\gamma} = (1 + \alpha) \frac{\mu b^2}{T} \frac{d\rho}{d\gamma} + (1 + \alpha) \frac{\mu b^2}{T} \frac{d\rho^-}{d\gamma} - \frac{\alpha \mu b \sqrt{\rho}}{T} \quad (4.18)$$

$dS/d\gamma$  describes the rate of total entropy change in the deformed metal during plastic deformation. Equation 4.18 relates the entropy to plastic deformation via the development of the dislocation structure. Another way to link entropy to plastic deformation may be made via the relation between the entropy and the “hardness parameter  $\sigma^*(\tau, \dot{\gamma})$ ” due to Hart [55], which is a function of stress and strain rate and has the dimensions of stress. Nabarro [91] argued that the hardness parameter and the entropy both measure the internal disorder of the deformed metal, and shall therefore be related. Moreover, as discussed in Chapter 3, both work hardening rate and entropy changing rate vanish at the steady state ( $d\tau/d\gamma = 0$  and  $dS/d\gamma = 0$ ). Therefore, inspired by Nabarro’s concept and the properties at the steady state, and taking the hardness parameter to be the work hardening rate ( $d\tau/d\gamma$ ), it is postulated that

$$\frac{dS}{d\gamma} = \frac{C b}{T l} \frac{d\tau}{d\gamma} \quad (4.19)$$

where  $C$  is a temperature dependent proportionality constant.

Employing equation 4.4, the work hardening rate can now be expressed as

$$\frac{d\tau}{d\gamma} = \frac{\alpha \mu b}{2\sqrt{\rho}} \frac{d\rho}{d\gamma} \quad (4.20)$$

Inserting equations 4.20 and 4.5 into equation 4.19,  $dS/d\gamma$  is rewritten as

$$\frac{dS}{d\gamma} = \frac{C\alpha\mu b^2}{2T} \frac{d\rho}{d\gamma} \quad (4.21)$$

Equating the right hand sides of equations 4.18 and 4.21 offers

$$\frac{d\rho}{d\gamma} = \frac{2\alpha}{(2 + 2\alpha - C\alpha) b} \sqrt{\rho} - \frac{2 + 2\alpha}{2 + 2\alpha - C\alpha} \frac{d\rho^-}{d\gamma} \quad (4.22)$$

The annihilation of individual dislocations in FCC metals is a thermally activated process which can quantitatively be expressed as [64][73]

$$\frac{d\rho^-}{dt} = v_0 \exp\left(\frac{\Delta G}{kT}\right) \rho \quad (4.23)$$

where  $t$  stands for time,  $v_0$  is the atomic vibration frequency ( $v_0 = 10^{12} \text{ s}^{-1}$ [98]),  $k$  is the Boltzmann constant and  $\Delta G$  is the effective activation energy. The present work does not distinguish edge and screw dislocations due to the one parameter approach. Therefore, dislocation annihilation in the present work is treated as the combination of edge dislocation climb and screw dislocation cross-slip. The effective activation energy in equation 4.23 accounts for the average of the activation energies for both mechanisms. In order to obtain the precise value of  $\Delta G$  at different temperatures and strain rates, one needs to know the fraction of edge and screw

dislocations annihilated during the deformation. This is a rather complex task and not fully understood yet. Consequently,  $\Delta G$  is treated as a fitting parameter in the current model.

Equation 4.23 can be rewritten as

$$\frac{d\rho^-}{d\gamma} = \frac{v_0}{\dot{\gamma}} \exp\left(\frac{\Delta G}{kT}\right) \rho \quad (4.24)$$

where  $\dot{\gamma}$  is the shear strain rate. Inserting equation 4.24 into 4.22, the evolution of the average dislocation density during plastic deformation is obtained:

$$\frac{d\rho}{d\gamma} = (2 + 2\alpha - C\alpha)^{-1} \left[ \underbrace{\frac{2\alpha}{b} \sqrt{\rho}}_A - \underbrace{(2 + 2\alpha) \frac{v_0}{\dot{\gamma}} \exp\left(\frac{\Delta G}{kT}\right) \rho}_B \right] \quad (4.25)$$

Equation 4.25 describes the dislocation evolution during plastic deformation. Term  $A$  represents the generation of dislocations, whereas  $B$  stands for their annihilation. This equation is similar to the classical one parameter model proposed by Kocks and Mecking [73] and Estrin and Mecking [31]. By solving equation 4.25 the average dislocation density can be found for the entire work hardening stages for a given deformation temperature and strain rate. Then, employing the Taylor relation ( $\tau = \alpha\mu b\sqrt{\rho}$ ), the stress-strain curve in the plastic regime can be obtained.  $\alpha$  is reported to lie between 0.3 and 1.0 for FCC metals[54], and is taken to be 0.4 for FCC metals in the application of this model [64][67]. This same value was used in Chapter 3.

### 4.2.2 Application

The model is firstly applied to pure Cu  $\langle 111 \rangle$  single crystals under tension. The  $\langle 111 \rangle$  orientation is chosen as it undergoes multiple-slip during tensile and compression testing in FCC metals, similar to polycrystalline specimens. Furthermore, the  $\langle 111 \rangle$  orientation is stable in both tension and compression and the texture does not change much during deformation [84]. In equation 4.25 there are two parameters ( $C$  and  $\Delta G$ ) which need to be determined in order to predict the evolution of dislocation density with imposed strain, and then the stress-strain curve.  $\Delta G$  is temperature and strain rate dependent; and reference values for it may be found in the literature [135]. In the current model,  $C$  and  $\Delta G$  are fitted to the experimental stress-strain curves for several temperatures. Figure 4.1a shows the shear stress-strain curve for 78, 295, 673 and 1123 K. The experimental data are taken from Gottstein *et al.* [44][46]. The initial dislocation density ( $\gamma = 0$ ) is assumed to be  $10^{11} \text{ m}^{-2}$ . The magnitude of the Burgers vector for Cu is  $2.56 \times 10^{-10} \text{ m}$  [96].

The shear modulus of Cu is temperature dependent and has been experimentally determined as  $\mu = 4.74 \times \exp(-3.97 \times 10^{-4}T) \times 10^{-4}$  MPa [84]. The values of  $C$  and  $\Delta G$  employed in the model for different temperatures are displayed in figures 4.1b and 4.1c, respectively. It is interesting to note that  $C$  and  $\Delta G$  change with temperature linearly.

The model is also applied to pure Al  $\langle 111 \rangle$  single crystals under tension. The initial dislocation density before deformation is also assumed to be  $10^{11} \text{ m}^{-2}$ . The magnitude of the Burgers vector for Al is  $2.86 \times 10^{-10} \text{ m}$  [96]. The shear modulus of Al was experimentally found to be  $\mu = 29438.4 - 15.052T$  MPa [96]. Figure 4.2a shows the shear stress-strain curves for four temperatures (4.2, 77, 200 and 273 K) at a shear strain rate of  $2.3 \times 10^{-6} \text{ s}^{-1}$ . The experimental data are taken from the literature [63] and are well predicted by the model. Figures 4.2b and 4.2c illustrate the temperature dependence of  $C$  and  $\Delta G$ , respectively. Similar to the Cu case, they show linear dependence with temperature suggesting Cu and Al both have similar work hardening and softening mechanisms. The effect of stacking fault energy variations between Cu and Al is incorporated in the effective activation energy.

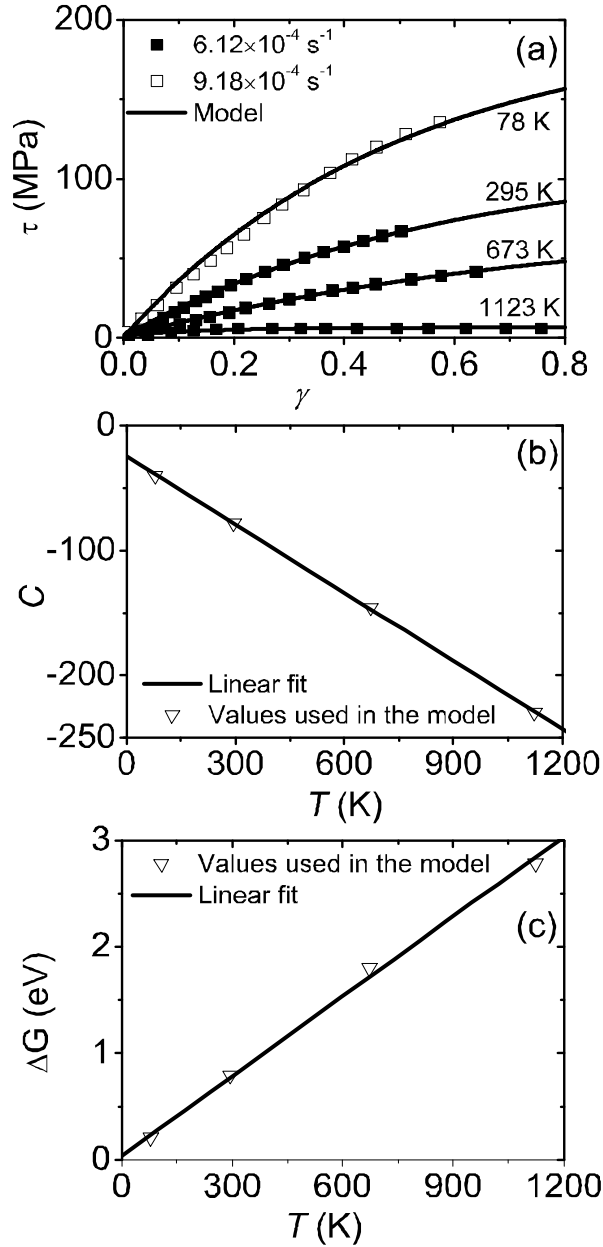


FIGURE 4.1. Cu <111> single crystal: (a) Shear stress versus shear strain at four temperatures, dots being experimental data; (b)  $C$  values at different temperatures; (c)  $\Delta G$  at different temperatures.

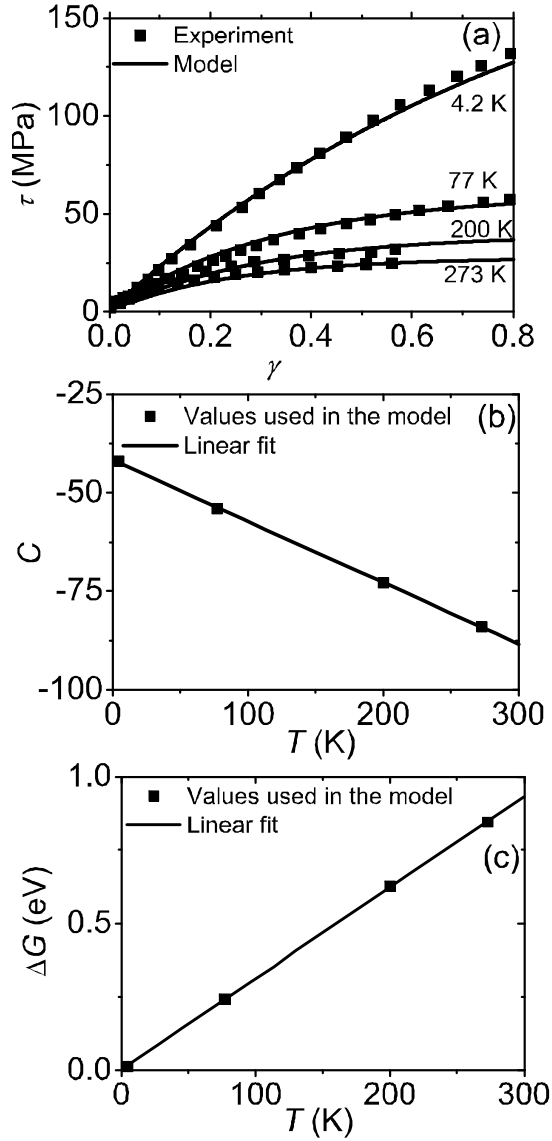


FIGURE 4.2. Al  $\langle 111 \rangle$  single crystal: (a) Shear stress versus shear strain at four temperatures; (b)  $C$  values at different temperatures; (c)  $\Delta G$  at different temperatures.

### 4.2.3 Discussion

It is interesting to explore the prediction of the present model for a limiting case (i.e. the steady state of plastic deformation as discussed in Chapter 3). Assuming the dislocation annihilation at the steady state of medium-high deformation temperature is dominated by edge dislocation climb, due to the fact that most of dislocations are stored in the subgrain boundaries, the dislocation annihilation term  $d\rho^-/d\gamma$  can for this special case be expressed as (different to equation 4.24) [2]

$$\frac{d\rho^-}{d\gamma} = \frac{2c_j v_c}{\dot{\gamma}} \rho \quad (4.26)$$

where  $c_j$  is the number of dislocation jogs per unit length along the dislocation lines and is proportional to the dislocation separation ( $c_j = \sqrt{\rho}$  [96]) and  $v_c$  is the edge dislocation climb velocity along the dislocation line. This is the same as equation 3.19 in Chapter 3. At the steady state, the dislocation density becomes constant with increasing strain, which implies that  $d\rho/d\gamma = 0$ . Inserting equation 4.26 into equation 4.25 and considering  $d\rho/d\gamma = 0$ , the dislocation density at the steady state predicted by the present model is reduced to the expression obtained in Chapter 3 for the case of DRV being the only softening mechanism (equation 3.37).

The core equation proposed in this chapter (equation 4.19) assumes that, as plastic deformation takes place, the system entropy changes proportionally to the work hardening rate ( $d\tau/d\gamma$ ). Such process may be expressed as  $dS \propto d\tau$ . An increase in the stress ( $d\tau$ ) required to produce plastic deformation is accompanied by the generation, glide and annihilation of dislocations; each of these mechanisms produces distortions in the crystal structure modifying its degree of order and changing the system entropy. Referring to equation (4.19), the term  $b/l$  is a scaling factor accounting for the average distance at which dislocation interactions take place. The proportionality constant  $C$  is negative as the entropy of the deformed metal decreases with imposed strain for constant temperature: while dislocation generation, glide and annihilation increase the entropy, the heat flux towards the surroundings decreases it, dominating the entropy development in such irreversible process. The linear relationship of  $C$  with temperature indicates that there is an athermal component of  $dS/d\gamma$  given by the slope of the  $C - T$  curves (figures 4.1b and 4.2b). Additionally, there is a thermal component determined by  $C$  ( $T = 0$ ). The relative values of those components depend on the metallic system under consideration (crystal structure and chemistry). The athermal entropy stems from the tendency to have dislocations even in the limit of 0 K which, on application of an external stress, undergo generation, glide and annihilation processes. The magnitude of the thermal entropy depends on the value of  $C$  at  $T = 0$ ; having

$C < 0$  ensures that this component plays a role in the entropy development. It is interesting to note that equation 4.25 displays a critical point at  $C = (2 + 2\alpha)/\alpha$ , this corresponds to increasing or decreasing the dislocation density change towards infinity. Such situation requires a value of  $C \approx 5$ , demanding heat dissipation to vanish ( $C > 0$ ).

The effective activation energy  $\Delta G$  in the current model represents the average contributions of edge dislocation climb and screw dislocation cross-slip, being the former usually larger than the later. At high temperature, edge dislocation climb dominates [98], hence,  $\Delta G$  increases with temperature (figures 4.1c and 4.2c). Similar linear variations in the activation energy for dislocation annihilation have been reported earlier [121][135].

It is interesting to compare the present model to the classical approach by Kocks and Mecking [73] and Estrin and Mecking [31]. Such model describes the dislocation density progress with strain as  $d\rho/d\gamma = k_1\sqrt{\rho} - k_2\rho$  where  $k_1$  was associated with the athermal storage of dislocations, and  $k_2$  was associated with the dynamic recovery, a thermally activated process which is a function of temperature and strain rate. The current model has developed a qualitatively similar expression (equation 4.25), but derived on a purely thermodynamics basis. It is worth noting that, for wide temperature ranges, the predictions of the model presented here (equation 4.25) describe the stress-strain curve more accurately than the approach by Kocks and Mecking and by Estrin and Mecking. In such classical approach, at low strains the temperature independent term becomes dominant, displaying similar deformation behaviour irrespective of temperature.

A sensitivity analysis was performed to assess the influence of varying the parameters  $C$ , the initial dislocation density and  $\Delta G$ . Variations of the order of  $\pm 10\%$  in the value of  $C$  produced shifts of approximately  $\pm 10\%$  in the shear stress values in figures 4.1a and 4.2a. Modifying the initial dislocation densities for one order of magnitude above or below the employed values altered slightly the onset of deformation, but the shear stress asymptotically approached the experimental values.  $\Delta G$  variations, however, produce sharp effects on the computed shear stresses; in the case of Al  $\langle 111 \rangle$  single crystals deformation at 273 K (figure 4.2a), a variation from 0.846 eV to 0.87 eV raises the shear stress value from 25 MPa to 42 MPa at  $\gamma = 0.5$ . In the current model the activation energy for dislocation annihilation plays therefore the strongest role in the work hardening behaviour, especially at large strains.

The model developed here for describing the work hardening behaviour of Al and Cu single crystals has shown important potential for further applications. Nevertheless, a major limitation is its inability to capture grain size effects. Dislocation-

grain boundary interactions have a crucial effect in the work hardening behaviour. This issue is addressed in the next section.

## 4.3 (Ultra)fine polycrystals

### 4.3.1 Model

In single phase polycrystalline metals, three factors determine the flow stress [25]: (1) the lattice friction stress ( $\tau_0$ ), (2) the dislocations in the grain interior ( $\tau_{in}$ , isotropic hardening) and (3) long range back stress due to dislocation pile-up at the grain boundary ( $\tau_b$ , kinematic hardening). This can be mathematically expressed as

$$\tau = \tau_0 + \tau_{in} + \tau_b \quad (4.27)$$

where  $\tau$  is the shear flow stress.  $\tau_0$  is the deformation independent contribution of the Peierls force and solid solution strengthening;  $\tau_{in}$  is the obstacle stress caused by short range dislocation-dislocation interactions when a mobile dislocation glides through the grain interior, and is generally described by the Taylor relation

$$\tau_{in} = \alpha\mu b\sqrt{\rho_{in}} \quad (4.28)$$

where  $\rho_{in}$  is the dislocation density in the grain interior.  $\tau_b$  is the long range back stress hampering the glide of mobile dislocations on a given slip plane. This back stress is due to dislocations on a given slip plane piling up at a grain boundary and may be expressed as [10][122]

$$\tau_b = \frac{\mu b}{D}n \quad (4.29)$$

where  $D$  is the (equiaxed) grain size and  $n$  is the number of dislocations that pile up at the grain boundary on a given slip plane. In this formulation, it is assumed that the long range back stress acting on the mobile dislocations active on a given slip plane is due to dislocations piled up at the same slip plane. The contributions of dislocations piled up at other slip planes are considered to be negligible.

In order to describe the evolution of shear flow stress with shear strain ( $\gamma$ ), the progress of  $\tau_{in}$  and  $\tau_b$  must be described in terms of  $\rho_{in}$  and  $n$ , respectively. Sinclair *et al.* [122] and Bouaziz and Dirras [10] have postulated the evolution of  $n$  to take the form

$$\frac{dn}{d\gamma} = \frac{\lambda}{b} \left(1 - \frac{n}{n^*}\right) \quad (4.30)$$

where  $\lambda$  is the mean spacing between slip planes at the grain boundaries, the ratio  $\lambda/b$  is the number of dislocations per slip plane geometrically necessary to provide

the deformation and  $n^*$  is the maximum number of dislocations which can pile up at the grain boundary on a given slip plane. When the number of dislocations in the pile up exceeds  $n^*$ , the stress acting on the head dislocation in the pile up is large enough for dislocations to climb or cross slip onto another slip plane. Integrating equation 4.30 and assuming  $n = 0$  when  $\gamma = 0$ , equation 4.29 can be rewritten as

$$\tau_b = \frac{\mu b}{D} n^* \left[ 1 - \exp\left(-\frac{\lambda}{bn^*}\gamma\right) \right]. \quad (4.31)$$

Equation 4.31 now describes the evolution of the back stress with shear strain for polycrystalline metals.

Similar to the single crystals, there are three irreversible processes occurring in the grain interior during plastic deformation: (1) dislocation generation from Frank-Read sources, (2) dislocation glide along their slip systems and (3) dislocation annihilation due to edge dislocation climb and/or screw dislocation cross-slip, depending on the loading conditions (temperature and strain rate) [64]. According to the theory of irreversible thermodynamics, all irreversible processes produce entropy [107], which itself is related to the energy dissipation. Therefore, during a shear strain increment  $d\gamma$ , the entropy production in the grain interior is expressed as [107]

$$d_i S = \frac{dw_{ge}}{T} + \frac{dw_{gl}}{T} + \frac{dw_{an}}{T}. \quad (4.32)$$

where  $dw_{ge}$ ,  $dw_{gl}$ , and  $dw_{an}$  are the dissipative energies due to dislocation generation, glide, and annihilation in the grain interior, respectively.  $T$  is the absolute temperature.  $dw_{ge} = (1/2)\mu b^2 d\rho_{in}^+$  is assumed, where  $d\rho_{in}^+$  is the length of dislocations per unit volume generated in the grain interior during a strain increase  $d\gamma$ .  $dw_{gl}$  is expressed as  $dw_{gl} = (\tau b l_{in}) d\rho_{in}^+$  where  $l_{in}$  is the mean glide distance assumed to be equal to the average distance between dislocations in the grain interior ( $l_{in} = (\rho_{in})^{-1/2}$ ).  $dw_{an}$  is the energy dissipated when  $d\rho_{in}^-$  dislocations are annihilated in the grain interior due to edge dislocation climb and/or screw dislocation cross-slip depending on the loading conditions, expressed as  $dw_{an} = (1/2)\mu b^2 d\rho_{in}^-$ . Therefore, equation 4.32 can be rewritten as

$$d_i S = \frac{1}{2T} \left( \mu b^2 + \frac{2\tau b}{\sqrt{\rho_{in}}} \right) d\rho_{in}^+ + \frac{\mu b^2}{2T} d\rho_{in}^-. \quad (4.33)$$

This formulation assumes that dislocations in the grain interior are the main contributor to the system energetics. The change of the dislocation density  $d\rho_{in}$  in the grain interior during straining is expressed as

$$d\rho_{in} = d\rho_{in}^+ - d\rho_{in}^-. \quad (4.34)$$

Inserting equation 4.34 into 4.33,  $d_i S$  can be rewritten as

$$d_i S = \frac{1}{T} \left( \frac{1}{2} \mu b^2 + \frac{\tau b}{\sqrt{\rho_{in}}} \right) d\rho_{in} + \frac{1}{T} \left( \mu b^2 + \frac{\tau b}{\sqrt{\rho_{in}}} \right) d\rho_{in}^-. \quad (4.35)$$

Dislocation annihilation (dynamic recovery) is a thermally activated process, so  $d\rho_{in}^-$  can be expressed as [73]

$$d\rho_{in}^- = \frac{v_0}{\dot{\gamma}} \exp\left(-\frac{\Delta G}{kT}\right) \rho_{in} d\gamma \quad (4.36)$$

where  $v_0$  is the atomic vibration frequency ( $v_0 = 10^{12} \text{ s}^{-1}$ [98]),  $k$  is the Boltzmann constant and  $\Delta G$  is the effective activation energy accounting for the average of the activation energies for edge dislocation climb and screw dislocation cross slip, and  $\dot{\gamma}$  is the shear strain rate.

The entropy flux  $d_e S_{in}$  in the grain interior during  $d\gamma$  is related to the heat flux  $dQ_{in}$  which is released into the surroundings. Here we assume that all heat generated during the deformation is absorbed immediately by the surrounding environment (i.e. isothermal deformation takes place).  $d_e S_{in}$  is expressed as [64][66][107]

$$d_e S_{in} = \frac{dQ_{in}}{T}. \quad (4.37)$$

According to the law of energy conservation ( $dQ_{in} = dU_{in} - dW_{in}$ ), equation 4.37 can be rewritten as

$$d_e S_{in} = \frac{dU_{in} - dW_{in}}{T} \quad (4.38)$$

where  $dU_{in}$  is the energy stored in the grain interior and  $dW_{in}$  is the external work done into the grain interior during  $d\gamma$ . They can be expressed as

$$dU_{in} = \frac{1}{2} \mu b^2 d\rho_{in} \quad (4.39)$$

and

$$dW_{in} = \tau_{in} d\gamma. \quad (4.40)$$

Inserting equations 4.28, 4.39 and 4.40 into equation 4.38,  $d_e S_{in}$  can be rewritten as

$$d_e S_{in} = \frac{1}{T} \left( \frac{1}{2} \mu b^2 d\rho_{in} - \alpha \mu b \sqrt{\rho_{in}} d\gamma \right). \quad (4.41)$$

The total entropy change of the grain interior ( $dS_{in}$ ) during  $d\gamma$  is the sum of the entropy generation and entropy flux [107]:

$$dS_{in} = d_i S_{in} + d_e S_{in}. \quad (4.42)$$

Inserting equations 4.35, 4.36 and 4.41 into equation 4.42,  $dS_{in}$  is rewritten as

$$dS_{in} = \frac{1}{T} \left( \mu b^2 + \frac{\tau b}{\sqrt{\rho_{in}}} \right) d\rho_{in} + \frac{1}{T} \left( \mu b^2 + \frac{\tau b}{\sqrt{\rho_{in}}} \right) \frac{v_0}{\dot{\gamma}} \exp \left( -\frac{\Delta G}{kT} \right) \rho_{in} d\gamma - \frac{1}{T} \alpha \mu b \sqrt{\rho_{in}}. \quad (4.43)$$

Equation 4.43 relates the entropy change to the plastic deformation via the development of the dislocation density. Similar to the case of single crystals (equation 4.19), entropy and plastic deformation are linked via a (material related) constant  $C$ :

$$dS_{in} = \frac{C}{T} \frac{b}{l_{in}} d\tau_{in} \quad (4.44)$$

Combing equations 4.28 and 4.44,

$$dS_{in} = \frac{C\alpha\mu b^2}{2T} d\rho_{in} \quad (4.45)$$

Inserting equation 4.27 into equation 4.43 and equating the right hand sides of equations 4.43 and 4.45, the evolution of the dislocation density in the grain interior can be obtained:

$$\frac{d\rho_{in}}{d\gamma} = k_1 \sqrt{\rho_{in}} - k_2 \rho_{in} \quad (4.46)$$

where

$$k_1 = \alpha \left[ b \left( 1 + \alpha + \frac{\tau_0}{\mu b \sqrt{\rho_{in}}} + \frac{n}{D \sqrt{\rho_{in}}} - \frac{1}{2} C \alpha \right) \right]^{-1} \quad (4.47)$$

and

$$k_2 = \frac{\left( 1 + \alpha + \frac{\tau_0}{\mu b \sqrt{\rho_{in}}} + \frac{n}{D \sqrt{\rho_{in}}} \right) v_0 \exp \left( -\frac{\Delta G}{kT} \right)}{\dot{\gamma} \left( 1 + \alpha + \frac{\tau_0}{\mu b \sqrt{\rho_{in}}} + \frac{n}{D \sqrt{\rho_{in}}} - \frac{1}{2} C \alpha \right)} \quad (4.48)$$

The grain size effect is incorporated in two ways: it influences the evolution of the dislocation density in the grain interior (equations 4.46-4.48) and it builds up the long range back stress, as demonstrated in equation 4.29. By solving the equation 4.46 with an assumption of an initial dislocation density  $\rho_0$  in the grain interior (dislocation density before loading), the evolution of  $\rho_{in}$  is obtained. Then, the evolution of  $\tau_{in}$  is obtained (equation 4.28).

### 4.3.2 Application

The present model is of a general nature derived from irreversible thermodynamics. Therefore, it is in principle applicable to different metal systems such as BCC

and FCC alloys. Two different alloys (ultrafine and fine grained interstitial free (IF) steels (BCC) and aluminium alloys (AA1100, FCC)) are employed to test the model predictions. The experimental data sets are obtained from the literature by Tsuji and co-workers [127]. The alloys were tested under tension at room temperature (295K) and a uniaxial strain rate of  $\dot{\epsilon} = 8.3 \times 10^{-4} \text{ s}^{-1}$  (i.e. shear strain rate  $\dot{\gamma} = M\dot{\epsilon} = 2.5 \times 10^{-3} \text{ s}^{-1}$ , where  $M = 3.06$  is the Taylor factor). The samples were fabricated by an accumulative roll-bonding (ARB) process to achieve ultrafine grain size. The chemical compositions are shown in table 4.1 and table 4.2 for the IF steel and the Al alloy, respectively. Table 4.3 presents the physical parameter values employed in the model. The parameters  $C$  and  $\Delta G$  are the only two fitting parameters, the rest of the values are obtained from the literature.

C	Si	Mn	P	S	Ti	B	Sol. Al	Fe
0.0031	<0.01	0.15	0.01	0.005	0.049	<0.0001	0.054	Bal.

TABLE 4.1. Chemical composition of the IF steel (wt %)

Si	Fe	Cu	Mg	Ti	B	V	Ni	Al
0.11	0.55	0.11	0.02	0.02	0.0007	0.011	0.003	Bal.

TABLE 4.2. Chemical composition of the AA1100 alloy (wt%)

	$\mu$ GPa	$b$ nm	$\tau_0$ MPa	$\rho_0$ $\text{m}^{-2}$	$\Delta G$ eV	$\lambda$ nm	$\alpha$	$M$	$C$	$n^*$
Steel	80 [13]	0.25 [13]	18 [129]	$10^{13}$ [68]	0.766	150 [10]	0.25 [25]	3.06 [25]	-100	4 [10]
Al	25.5 [102]	0.284 [102]	1 [64]	$10^{12}$ [68]	0.748	150 [122]	0.4 [64]	3.06 [25]	-88 [64]	5.5 [122]

TABLE 4.3. Parameter values used in the model

The true uniaxial stress ( $\sigma$ ) and strain ( $\epsilon$ ) measured in the tensile test are expressed in terms of the shear stress and strain as

$$\sigma = M\tau = M \left\{ \tau_0 + \alpha\mu b\sqrt{\rho_{in}} + \frac{\mu b}{D}n^* \left[ 1 - \exp\left(-\frac{\lambda}{bn^*}\gamma\right) \right] \right\} \quad (4.49)$$

and

$$\epsilon = \gamma/M. \quad (4.50)$$

Figure 4.3a shows the experimental and modelled true uniaxial stress-strain relation for IF steels of three different grain sizes tested in simple tension. The

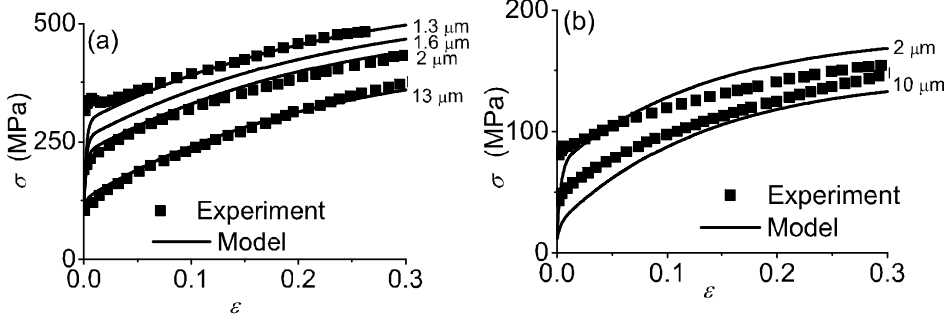


FIGURE 4.3. True uniaxial stress-strain curves with different grain sizes: a) IF steels and b) Al 1100.

model describes the data for samples with 2 and 13  $\mu\text{m}$  grain size rather accurately but underestimates the stress curve for a grain size of 1.6  $\mu\text{m}$ . The experimental data for a nominal grain size of 1.6  $\mu\text{m}$  are well fitted assuming a 1.3  $\mu\text{m}$  grain size. The slight discrepancy between both values may be attributed to uncertainties in the experimental grain size measurements as well as in the model parameters used. Furthermore, the morphology of ultrafine grains is often slightly elongated [127][128] while the model (equation 4.29) applies to equiaxed grains. Figure 4.3b describes the true uniaxial stress-strain curves for Al alloys with grain sizes of 2 and 10  $\mu\text{m}$ . The model predictions fit the experiments for Al alloys reasonably well.

For tensile tests, it is well accepted that necking begins when the work hardening rate approaches the flow stress (Considère's criterion) [27]:

$$\frac{d\sigma}{d\epsilon} = \sigma. \quad (4.51)$$

Combining the derivatives of equations 4.49 and 4.50,  $d\sigma/d\epsilon$  is expressed as

$$\frac{d\sigma}{d\epsilon} = M^2 \left[ \frac{\mu b}{2\sqrt{\rho_{in}}} (k_1\sqrt{\rho_{in}} - k_2\rho_{in}) + \frac{\mu\lambda}{D} \exp\left(-\frac{\lambda}{bn^*}\gamma\right) \right]. \quad (4.52)$$

Inserting equations 4.49 and 4.52 into equation 4.51 offers

$$\begin{aligned} M^2 \left[ \frac{\mu b}{2\sqrt{\rho_{in}}} (k_1\sqrt{\rho_{in}} - k_2\rho_{in}) + \frac{\mu\lambda}{D} \exp\left(-\frac{\lambda}{bn^*}\gamma\right) \right] \\ = M \left\{ \tau_0 + \alpha\mu b\sqrt{\rho_{in}} + \frac{\mu b}{D} n^* \left[ 1 - \exp\left(-\frac{\lambda}{bn^*}\gamma\right) \right] \right\} \end{aligned} \quad (4.53)$$

The only variable in equation 4.53 is the shear strain  $\gamma$ . By solving equation 4.53, the uniform shear strain at which the necking begins is obtained for different grain

sizes. The corresponding shear stress is then obtained via the shear stress-strain relation (equation 4.27). Then, the corresponding uniaxial strain (true uniform strain) and uniaxial stress (true tensile strength) are obtained via equations 4.50 and 4.49, respectively. The true uniaxial strain are shown in figure 4.4a and 4.4b for IF steels and Al alloys, respectively. The variation of the true tensile strength (the true uniaxial stress when necking occurs) with grain size is shown in figure 4.5a and 4.5b for IF steels and Al alloys, respectively.

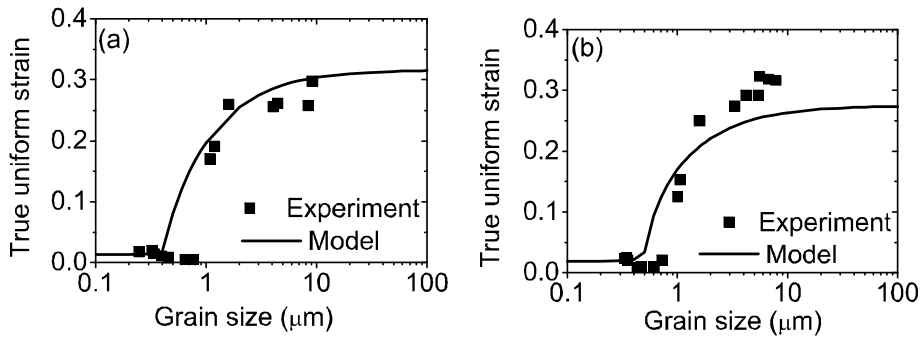


FIGURE 4.4. True uniform strain variation with grain size: a) IF steels and b) AA1100.

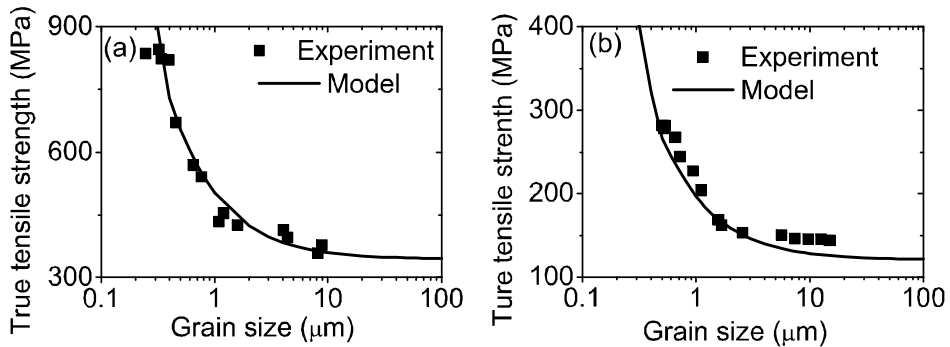


FIGURE 4.5. True tensile strength variation with grain size: a) IF steels and b) AA1100

### 4.3.3 Parametric analysis and discussion

Figures 4.3 to 4.5 show that for the parameter values selected the model describes the deformation behaviour of the ultra(fine) grained IF steel and the Al alloy

rather well over a range of grain sizes down to the submicron level. It is interesting to analyse the parameter values used in some more detail. Referring to table 4.3, the shear modulus and the magnitude of the Burgers vector have been obtained from the literature [13][102]; the Taylor constant  $\alpha$  in the range of 0.3 is found ubiquitously [25];  $\alpha = 0.25$  in the present case for IF steels and 0.4 for Al alloys [64]; the Taylor factor of 3.06 has also been employed earlier [25] by assuming a random grain orientation distribution; the friction stress value of 25 MPa has been reported for low carbon steels [129], in the present work  $\tau_0 = 18$  MPa for IF steels. For pure FCC metals,  $\tau_0$  is negligible [5][81] and here is assumed to be 1 MPa for commercial pure Al alloy AA1100. The parameters  $C$  and  $\Delta G$ , which have been introduced to describe plastic deformation in single crystals, deserve special attention. The values for  $C$  (-100) and  $\Delta G$  (0.766 eV) used for IF steels have been obtained by fitting the model to the stress-strain curve for the 13  $\mu\text{m}$  grain size sample of IF steels. The value of  $C$  (-88) used for the Al alloy has been employed for pure Al single crystals (figure 4.2b).  $\Delta G = 0.748$  eV is obtained from fitting the experimental data for the Al alloy. Similar to the single crystal case,  $C$  is a physical constant relating the increase in dislocation density due to the entropy development in a grain boundary free environment via equation 4.46. A value of  $C = -100$  for IF steels is to be compared to the  $C$  values for plastic deformation of pure Cu and Al single crystals deformed at room temperature, -78 and -88, respectively (section 4.2.2). The  $\Delta G$  values of 0.766 eV (IF steel) and 0.748 eV (AA1100) are to be compared to the  $\Delta G$  values for pure Cu and Al single crystals,  $\Delta G = 0.761$  and 0.781 eV respectively (section 4.2.2). Given the big behavioural differences between polycrystalline IF steels and the Al and Cu single crystals, the modest differences in  $C$  and  $\Delta G$  values are encouraging.

In the model presented here, the parameters  $\lambda$  and  $n^*$  have been introduced for the first time in the context of an irreversible thermodynamics model for describing plastic deformation.  $\lambda = 150$  nm and  $n^* = 4$  (IF steels) were fitted to the experimental data of figure 4.4a and 4.5a. Such a value for  $\lambda$  is larger than the 16 nm mean spacing between slip planes employed by Bouaziz and Dirras in IF steels [10]; and to those experimentally observed by Hansen (42 nm) [53]. However, the values of  $n^* = 4$  (IF steels) and  $n^* = 5.5$  (AA1100) employed here are close to those employed earlier for IF steels ( $n^* = 3$  [10]) and for pure Cu ( $n^* = 6.7$  [122]).

The extent to which the present model can be employed for optimising the engineering properties of UFG steels is best appreciated from figure 4.4. Four regimes are observed: for grain sizes lower than 0.4  $\mu\text{m}$ , the true uniform strain is nearly constant; however, it sharply increases for grain sizes in the range of 0.4 to 1  $\mu\text{m}$ . For grain sizes between 1 and 10  $\mu\text{m}$  it increases slowly with grain size, and approaches an asymptotic value at grain sizes larger than 10  $\mu\text{m}$ . This behaviour

results from the differences in dislocation storage with strain for different grain sizes. Employing the parameters used in figures 4.3 to 4.5, figure 4.6 shows the variation of dislocation density for IF steels and Al alloys in the grain interior with grain size. The figure indicates that the ability for storing dislocations in the grain interior is directly proportional to the true uniform strain behaviour, and inversely proportional to the grain size. The ability to modify this behaviour lies in the work hardening response of the material. This is illustrated in figure 4.7, where Considère's criterion is met at the intersection points on  $\sigma$  and  $d\sigma/d\epsilon$  curves in the strain domain.  $d\sigma/d\epsilon$  is calculated by equation 4.52 for any given value of  $\gamma$  which is related to  $\epsilon$  via equation 4.50. In other words, for any given value of  $\epsilon$ ,  $d\sigma/d\epsilon$

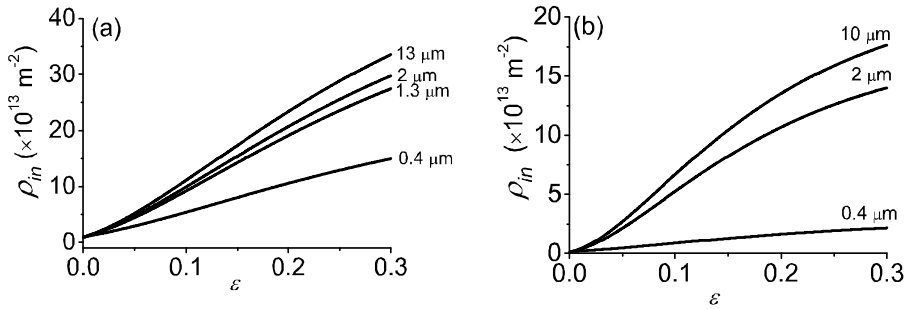


FIGURE 4.6. The evolution of the dislocation density in the grain interior: a) IF steels and b) AA1100.

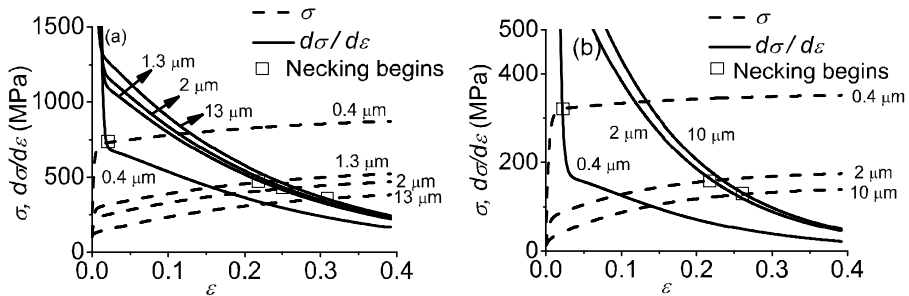


FIGURE 4.7. The evolution of the work hardening rate and flow stress for different grain sizes: a) IF steels and b) AA1100.

can be calculated by equations 4.52 and 4.50. As a result,  $d\sigma/d\epsilon - \epsilon$  curve can be plotted (figure 4.7). It is interesting to notice that smaller grain sizes display

a smaller work hardening capability at a given strain (figure 4.7), allowing only a very small uniform elongation at grain sizes lower than  $0.4 \mu\text{m}$ , and approaching a limiting value for it when grain sizes exceed  $10 \mu\text{m}$  (figure 4.4).

The low ductility limits the practical application of UFG alloys. Therefore, the ability to increase the elongation of UFG alloys is of great technological importance. Using the model just presented such an increase may be achieved by increasing the work hardening rate, which is determined by the rate at which new dislocations are stored for a given strain increment. This may be achieved via adding fine precipitates in the grain interior to increase the dislocation storage rate [104][124] or by finding suitable alloying elements to increase the activation energy ( $\Delta G$ ) for dislocation DRV so as to decrease the dislocation annihilation rate. Figure 4.8 illustrates the influence of the activation energy on the true uniform strain for a grain size of  $0.4 \mu\text{m}$ . According to the model prediction, the true uniform strain for IF steels can be increased from 4.3% to 28.2% when the activation energy increases from 0.766 eV to 0.8 eV (figure 4.8a). For AA1100 alloys, it increases from 2.2% to 26.3% when the activation energy increases from 0.748 eV to 0.78 eV (figure 4.8b).

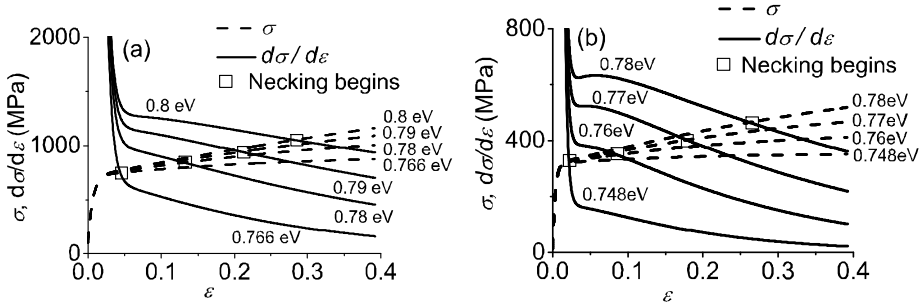


FIGURE 4.8. The evolution of the work hardening rate and flow stress for different activation energies: a) IF steels and b) AA1100. Grain size of  $0.4 \mu\text{m}$ .

It is worth noting that the current model is dealing with the grain size larger than  $100 \text{ nm}$  such that the volume fraction of grain interior is much larger than that of grain boundary. Grain boundary sliding, which is an important plastic deformation mechanism for nanocrystalline metals [118][125], is not considered in this model.

## 4.4 Conclusions

Assuming a proportionality relationship between the development of entropy and work hardening in a metallic system undergoing plastic deformation, expressions for describing the progress in average dislocation density were obtained for FCC single crystals. The model was successfully applied to Cu and Al  $\langle 111 \rangle$  single crystals, reproducing accurately experimental observations for large ranges of temperatures. The proportionality constant ( $C$ ) relating entropy and hardening was shown to be linearly dependent on temperature. The model predictions of dislocation density showed to be most sensitive to the activation energy for dislocation annihilation. At the steady state, the model is reduced to an expression obtained in Chapter 3 for predicting the saturation stress of Al, Ag, Cu and Ni single crystals.

Incorporating the grain size effects via the back stress, the single crystal model is extended to (ultra)fine grained FCC and BCC alloys. The model recovers the tensile strength and ductility patterns experimentally observed in (ultra)fine grained interstitial free steels and aluminium alloys over a wide range of grain sizes rather accurately. It is shown that small changes in the activation energy for dislocation DRV may produce dramatic improvements in the alloy ductility, especially at submicron grain sizes.

# 5

## Modelling the Flow Stress under Quasi-static and Adiabatic Deformation Conditions

### 5.1 Introduction

In Chapter 4, a model has been developed to describe the stress-strain behaviour of metals deformed at low strain rates (quasi-static deformation). This chapter is to extend the model to account for high strain rate (adiabatic) deformation.

There are many engineering applications of metals related to high strain rate deformation such as high speed machining, armour systems, high speed transportation vehicles and spacecraft. In order to optimize the performance of metals undergoing plastic deformation at such dynamic loading conditions, it is necessary to understand its physical mechanism, which is different from the counterpart at low strain rates. For instance, TEM micrographs show that the dislocation structures at a fixed imposed strain are substantially different between low strain rates and high strain rates [58]. Moreover, when the strain rate exceeds  $\sim 10^3 \text{ s}^{-1}$ , many investigators found experimentally that the flow stress increases dramatically in many metals and alloys such as copper [35], tantalum [70], aluminium [78][79] and stainless steels [93]. Viscous drag effects on dislocation movement are thought by some researchers [36][94] as the main origin of the increase of flow stress at such high strain rate regime. However, Armstrong and co-workers [3] proposed that such flow stress increase is caused by the dislocation generation at the shock front, not by a retarding effect of dislocation drag.

In order to understand the physical mechanism for such high strain rate deformation, a large number of physically based constitutive models involving dislocations have been proposed such as the Zerilli-Armstrong model [137], the mechanical threshold stress model [35], the model incorporating phonon drag effects [93][94] and the model proposed by Meyers and co-workers [86][87].

The present chapter is to understand and describe quantitatively the evolution of the average dislocation density for both low and high strain rate deformation in FCC metals. A unified physical formulation for the evolution of the average dislocation density is derived for both quasi-static and adiabatic deformation conditions. The model in the current chapter is an extension of the one developed in Chapter 4. The model in Chapter 4 only describes the dislocation evolution at low strain rate regime at which dislocation velocity is low enough to ignore the viscous effects on the glide and accumulation of dislocations. At high strain rate regimes, the dislocation evolution follows different patterns.

One of the fundamental assumptions in the model developed in Chapter 4 is that all the heat generated during deformation will be immediately released into the surroundings (i.e. isothermal deformation). However, for high strain rate conditions (say strain rate larger than  $10^2 \text{ s}^{-1}$ ), the deformation is adiabatic because there is not enough time to radiate heat into the environment. An extension of the model is, therefore, required.

## 5.2 Model

### 5.2.1 Entropic analysis

During plastic deformation in metals, three irreversible processes are in general taking place [60][64][67]: (1) dislocation generation, (2) dislocation annihilation (DRV and/or DRX depending on the deformation conditions) and (3) dislocation glide. In the current model, the conditions under which DRX occurs are not considered. According to the theory of irreversible thermodynamics, the entropy generation rate can be expressed as the sum of the products of generalised forces and their corresponding fluxes in the irreversible processes [107]. Therefore, the entropy generation rate due to the three irreversible processes is expressed as [107]

$$\frac{d_i S}{dt} = \underbrace{J_1 X_1}_{\substack{\text{dislocation} \\ \text{generation}}} + \underbrace{J_2 X_2}_{\substack{\text{dislocation} \\ \text{annihilation}}} + \underbrace{J_3 X_3}_{\substack{\text{dislocation} \\ \text{glide}}} . \quad (5.1)$$

The general flux  $J_1$  represents the dislocation generation rate expressed as

$$J_1 = \frac{d\rho^+}{dt} \quad (5.2)$$

where  $d\rho^+$  is the length of dislocations per unit volume generated during a time interval  $dt$ . The general force for dislocation generation or annihilation can be expressed as

$$X_i = \frac{E}{T} \quad (5.3)$$

where  $i = 1$  for generation and  $i = 2$  for annihilation.  $E$  is the potential energy of the dislocation per unit length.  $T$  is the absolute temperature.  $J_2$  corresponds to the dislocation annihilation rate expressed as

$$J_2 = \frac{d\rho^-}{dt} \quad (5.4)$$

where  $d\rho^-$  is the length of dislocations per unit volume annihilated during a time interval  $dt$ .  $J_3$  is the general flux corresponding to dislocation glide expressed as

$$J_3 = \rho_m v \quad (5.5)$$

where  $\rho_m$  is the mobile dislocation density and  $v$  is the average velocity of mobile dislocations. The relation between strain rate and mobile dislocation density is expressed by the well known Orowan relationship as [49]

$$\dot{\gamma} = \rho_m v b \quad (5.6)$$

where  $\dot{\gamma}$  is the shear strain rate and  $b$  is the magnitude of the Burgers vector.  $X_3$  is the general force for dislocation glide expressed as

$$X_3 = \frac{\tau_{eff} b}{T} \quad (5.7)$$

where  $\tau_{eff}$  is the effective shear stress acting on the moving dislocations.  $\tau_{eff} = \tau - \tau_f$  where  $\tau_f$  is the friction stress for dislocation glide. In the framework of classical mechanics, if the dislocation is moving at a constant velocity, i.e. no acceleration,  $\tau_{eff} = 0$  [61]. However, the dislocation will experience acceleration and deceleration during plastic deformation such that  $\tau_{eff} \neq 0$ . Inserting equations 5.2-5.7 into equation 5.1 the entropy generation rate can be rewritten as

$$\frac{d_i S}{dt} = \frac{1}{T} \left[ (\tau - \tau_f) \dot{\gamma} + E \frac{d\rho^+}{dt} + E \frac{d\rho^-}{dt} \right]. \quad (5.8)$$

An increase of the total dislocation density  $d\rho$  during the time interval  $dt$  is the sum of the dislocation generation and annihilation:

$$\frac{d\rho}{dt} = \frac{d\rho^+}{dt} - \frac{d\rho^-}{dt}. \quad (5.9)$$

Inserting equation 5.9 into equation 5.8, it can be rewritten as

$$\frac{d_i S}{dt} = \frac{1}{T} \left[ (\tau - \tau_f) \dot{\gamma} + E \frac{d\rho}{dt} + 2E \frac{d\rho^-}{dt} \right]. \quad (5.10)$$

The entropy generation rate is proportional to the energy dissipation rate and can therefore be expressed in another form [64][67][107]:

$$\frac{d_i S}{dt} = \frac{1}{T} \frac{dW_{diss}}{dt} \quad (5.11)$$

where  $W_{diss}$  is the dissipative energy transformed into heat during plastic deformation. According to the energy conservation law, the dissipative energy can be written as

$$\frac{dW_{diss}}{dt} = \frac{dW_{in}}{dt} - \frac{dU_s}{dt} \quad (5.12)$$

where  $dW_{in}$  is the input energy during the time interval  $dt$  by loading expressed as

$$dW_{in} = \tau d\gamma \quad (5.13)$$

where  $\gamma$  is the shear strain.  $dU_s$  is the increase of stored energy due to the dislocation density increase (the sum of generation and annihilation) during  $dt$  expressed as

$$dU_s = E d\rho. \quad (5.14)$$

Therefore, inserting equations 5.12-5.14 into equation 5.11, it can be rewritten as

$$\frac{d_i S}{dt} = \frac{1}{T} \left( \tau \dot{\gamma} - E \frac{d\rho}{dt} \right). \quad (5.15)$$

Equations 5.10 and 5.15 are two different expressions to describe the entropy generation. They should be equal. Therefore, equating the right hand side of equations 5.10 and 5.15 offers the evolution of the average dislocation density:

$$\frac{d\rho}{dt} = \frac{\tau_f \dot{\gamma}}{2E} - \frac{d\rho^-}{dt}. \quad (5.16)$$

### 5.2.2 Dislocation annihilation

At high temperatures, the dislocation annihilation mechanism is mainly due to dislocation climb caused by the diffusion of vacancies along the dislocation line [2]. However, at low temperatures, the dislocation annihilation mechanism is mainly due to the cross-slip of dislocations [109]. The current work deals with the deformation of FCC metals at room temperature such that the annihilation mechanism considered here is the cross-slip of dislocations. In FCC metals, the most common

cross-slip mechanism is compact cross slip (i.e. Friedel-Escaig mechanism [9] shown schematically in figure 5.1: the cross-slip segment  $L$  immediately re-dissociates in the cross-slip plane (e.g.  $(11\bar{1})$ ) which is also a compact plane. More details about the modelling of the cross-slip mechanism may be found in the review paper by Puschl [109]. The dislocation annihilation process due to the dislocation cross-slip can be expressed as [98]

$$\frac{d\rho^-}{dt} = N2Lv_{cs}P_{cs} \quad (5.17)$$

where where  $N$  is the number of sites per unit volume where such cross-slip events can occur and is approximately set as  $N = \rho/L$ . The factor 2 accounts for two screw dislocation segments with opposite sign of Burgers vector which annihilate simultaneously at one single annihilation event.  $v_{cs}$  is the attempt frequency for such cross-slip event and is taken to be  $v_{cs} = (b/L)v_D$  [98] where  $v_D$  ( $10^{13}\text{s}^{-1}$ ) is the Debye frequency. The cross-slip length  $L$  is related to its activation volume  $V$  (figure 5.1):

$$L \cong \frac{V}{db} \quad (5.18)$$

where  $d$  is the stacking fault width of screw dislocations, which is determined by the stacking fault energy  $\chi$  [109] :

$$d = \frac{\mu b^2}{16\pi\chi}. \quad (5.19)$$

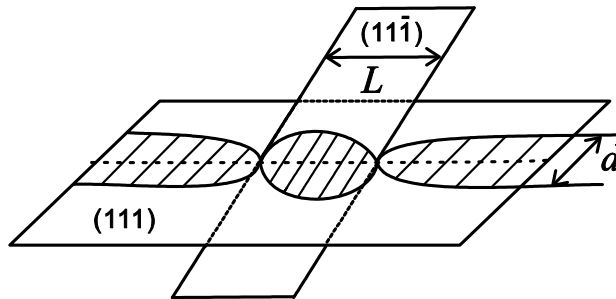


FIGURE 5.1. Schematic illustration of the cross-slip mechanism (Friedel-Escaig model): a segment  $L$  re-dissociates in the cross-slip plane (e.g.  $11\bar{1}$ ).  $L$  is the cross-slip length and  $d$  is the stacking fault width.

The cross-slip length  $L$  and its attempt frequency  $v_{cs}$  can respectively be rewritten as:

$$L = \frac{16\pi\chi V}{\mu b^3} \quad (5.20)$$

and

$$v_{cs} = \frac{\mu b^4}{16\pi\chi V} v_D. \quad (5.21)$$

$P_{cs}$  is the probability that the cross-slip attempt is successful and may be expressed as [98]

$$P_{cs} = \exp\left(-\frac{\Delta G}{kT}\right) \quad (5.22)$$

where  $k$  is the Boltzmann constant and  $\Delta G$  is the activation energy for the cross-slip. Therefore, the dislocation annihilation rate (equation 5.17) can be rewritten as

$$\frac{d\rho^-}{dt} = \frac{\mu b^4}{8\pi\chi V} v_D \exp\left(-\frac{\Delta G}{kT}\right) \rho \quad (5.23)$$

The activation energy for cross-slip effectively increases with temperature but decreases with strain rate [73]; it may be expressed as

$$\Delta G = AkT \ln \frac{c_1 v_D}{\dot{\gamma}} - \frac{kT}{\mu b^3} \tau V \quad (5.24)$$

where  $A$  is a material related constant of the order of 1 and  $c_1$  is constant for a given temperature. It is assumed here that  $c_1 v_D = v_{cs}$ . The temperature dependence of  $c_1$  is demonstrated in Chapter 6. The term  $(kT/\mu b^3) \tau V$  accounts for the reduction in activation energy due to the applied stress; this is consistent with the well known Friedel-Escaig model [9][109]. Incorporating  $c_1 v_D = v_{cs}$  and equation 5.21, equation 5.24 is rewritten as

$$\Delta G = AkT \ln \left( \frac{\mu b^4}{16\pi\chi V} \frac{v_D}{\dot{\gamma}} \right) - \frac{kT}{\mu b^3} \tau V. \quad (5.25)$$

Inserting equation 5.25 into equation 5.23, it can be rewritten as

$$\frac{d\rho^-}{dt} = \frac{\mu b^4}{8\pi\chi V} v_D \exp \left[ -A \ln \left( \frac{\mu b^4}{16\pi\chi V} \frac{v_D}{\dot{\gamma}} \right) + \frac{\tau V}{\mu b^3} \right] \rho. \quad (5.26)$$

Referring to equation 5.16, the friction stress  $\tau_f$  for pure FCC metals may be expressed as

$$\tau_f = \beta \mu b \sqrt{\rho} + \tau_d \quad (5.27)$$

where the first term in the right hand side represents the athermal friction stress due to other existing dislocations [49].  $\beta$  is a constant accounting for the interactions between dislocations and  $\mu$  is the shear modulus.  $\tau_d$  is the friction stress due to viscous drag effects, which may be caused by phonon and electron scattering [36][60]. At moderate temperatures, phonon effects dominate over electron effects [60]. The contribution of electron effects can only be seen at very low temperatures (about 10 percent of Debye temperature) [60]. In the current work, such low

temperature deformation is not considered so that electron effects are neglected. Therefore,  $\tau_d$  is taken as [93]

$$\tau_d = \tau_c \left[ 1 - \exp \left( -\frac{\dot{\gamma}}{\dot{\gamma}_0} \right) \right] \quad (5.28)$$

where  $\tau_c$  is a material related constant which can be measured at a very high strain rate. For instance, it is found that  $\tau_c = 140$  MPa for stainless steels [93].  $\dot{\gamma}_0$  represents an effective damping coefficient affecting the dislocation glide ( $\dot{\gamma}_0 = \rho_m b^2 \tau_y / B$  where  $\tau_y$  is the yield stress at high temperature and  $B$  is the phonon drag coefficient [93]). In the present work  $\dot{\gamma}_0$  is a fitting parameter to be chosen according to the experimental data. The physical explanation of  $\tau_d$  is presented in the literature [93]. Therefore, inserting equations 5.26, 5.27 and 5.28 into equation 5.16, substituting  $dt = d\gamma / \dot{\gamma}$ , and approximating  $E = \mu b^2 / 2$  [68], the dislocation evolution equation 5.16 can be rewritten as

$$\frac{d\rho}{d\gamma} = \frac{\tau_c}{\mu b^2} \left[ 1 - \exp \left( -\frac{\dot{\gamma}}{\dot{\gamma}_0} \right) \right] + \frac{\beta}{b} \sqrt{\rho} - \frac{\mu b^4}{8\pi\chi V} v_D \exp \left[ -A \ln \left( \frac{\mu b^4}{16\pi\chi V} \frac{v_D}{\dot{\gamma}} \right) + \frac{\tau V}{\mu b^3} \right] \rho. \quad (5.29)$$

The first term in the right hand side of the evolution equation 5.29 stands for the dislocation generation caused by phonon drag effects; the second term accounts for dislocation generation due to existing dislocations, which serve as obstacles for dislocation glide; the last term incorporates the effects of DRV due to the cross-slip of screw dislocations.

### 5.2.3 Stress-strain behaviour

By solving equation 5.29 and assuming an initial dislocation density  $\rho_0$  before deformation, the average dislocation density can be obtained. Then, the shear stress-strain behaviour can be predicted by utilizing the relationship between the shear flow stress and the average dislocation density [5][73][76]:

$$\tau = \alpha \mu b \sqrt{\rho} \quad (5.30)$$

where  $\alpha$  is a constant describing the interactions between dislocations.

The quasi-static deformation is assumed to be isothermal, while for high strain rate deformation (say strain rates larger than  $10^2 \text{ s}^{-1}$ ) it is assumed to be adiabatic. The temperature increase  $dT$  during the strain interval  $d\gamma$  for adiabatic deformation is related to the dissipative energy  $dW_{diss}$  and is approximated as

$$dT = \frac{dW_{diss}}{m_p C_V} = \frac{\tau d\gamma - E d\rho}{m_p C_V} \quad (5.31)$$

where  $m_\rho$  is the mass density and  $C_V$  is the heat capacity. Here it is assumed that the heat flow in the bulk is fast enough such that no temperature gradients develop in the bulk. The temperature increase will decrease the shear modulus and increase the cross-slip rate.

### 5.3 Application

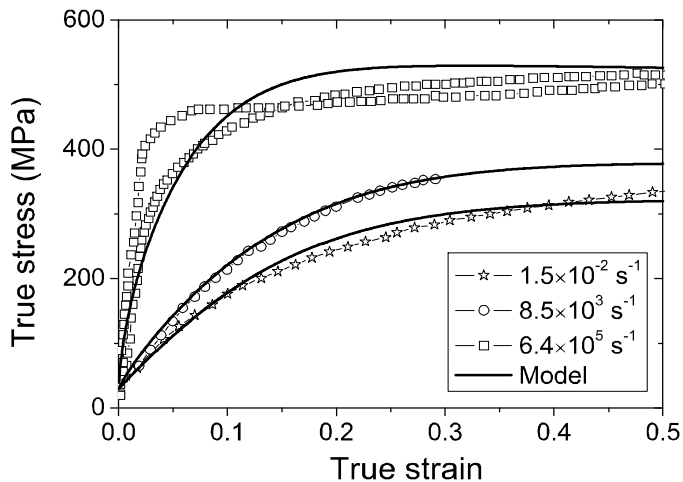


FIGURE 5.2. Model predictions (solid lines) and experimental data (symbols) for pure copper deformed at 295 K and at three strain rates  $1.5 \times 10^{-2}$ ,  $8.5 \times 10^3$  and  $6.4 \times 10^5 \text{ s}^{-1}$  (two experimental data sets for the highest strain rate).

In figure 5.2, the model predictions are compared to the experimental data in oxygen free electronic (OFE) copper (99.99% Cu) with a well annealed equiaxed grain structure and an average grain size of  $40 \mu\text{m}$  deformed at 295 K at different strain rates. The parameters used in the simulation are shown in table 5.1. Figure 5.2 shows that the model predictions are in good agreement with the experimental data of Follansbee and Kocks [35] considering the results cover a wide range of strain rates from  $10^{-2}$  to  $10^5 \text{ s}^{-1}$ . It is worth to note that the axes in figure 5.2 are true normal stress  $\sigma$  ( $\sigma = M\tau$ ) and normal strain  $\varepsilon$  ( $\varepsilon = \gamma/M$ ) where  $M$  is the Taylor factor.

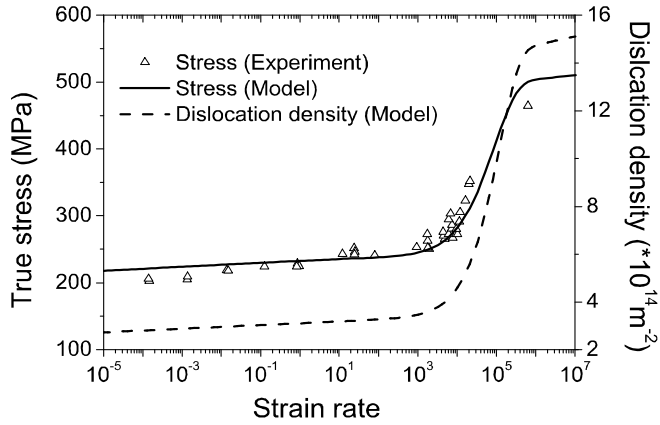


FIGURE 5.3. Flow stress and dislocation density as a function of strain rate at the strain  $\epsilon = 0.15$  for OFE copper deformed at 295 K.

$m_\rho$ (kg/m <sup>3</sup> )	$C_V$ (J/(kg·K))	$\mu$ (GPa)		$b$ (nm)
8940 [89]	386 [89]	$47.7 \times \exp(-3.97 \times 10^{-4}T)$ [84]		0.256 [96]
$\alpha$	$M$	$\rho_0$ (m <sup>-2</sup> )		$V$ (b <sup>3</sup> )
0.4 [67]	3.06 [68]	$5 \times 10^{12}$ [68]		300 [109]
$\beta$	$\chi$ (J·m <sup>-2</sup> )	$\dot{\gamma}_0$	$\tau_c$ (MPa)	$A$
0.024 [73]	$47 \times 10^{-3}$ [96]	$5 \times 10^5$	10	0.98

TABLE 5.1. Parameter values used in the model

Figure 5.3 shows the flow stress and average dislocation density at the strain  $\varepsilon = 0.15$  for wide ranges of strain rates. The strain rate in figure 5.3 is the normal strain rate. It shows that there is a transitional strain rate ( $\sim 10^3 \text{ s}^{-1}$ ) over which the phonon drag effects play a dominant role in dislocation accumulation (equation 5.29) resulting in an important raise in the average dislocation density and flow stress with strain rate.

## 5.4 Discussion

The phonon drag becomes important when the dislocation velocity goes beyond the range  $10^{-3}C_t$  [60], where  $C_t$  is the shear wave velocity. For pure copper  $C_t = 2.9 \times 10^3 \text{ m}\cdot\text{s}^{-1}$  [22]. The velocity at which phonon drag becomes prominent depends on the metallic system. In the present work, a critical dislocation speed of  $10^{-2}C_t$  is assumed. The corresponding strain rate for such dislocation velocity can be calculated from  $\dot{\varepsilon} = \dot{\gamma}/M = \rho_m vb/M = \rho_m(10^{-2}C_t)b/M$ . Assuming a mobile dislocation density  $\rho_m = 5 \times 10^{11} \text{ m}^{-2}$  [36],  $\dot{\varepsilon}$  is found to be  $\sim 10^3 \text{ s}^{-1}$ , confirming that the transitional strain rate for pure copper experimentally observed and used in this work (figure 5.3). Experimental observations confirmed that the dislocation generation at very high strain rates increases significantly in shock-deformed copper [87][90]. This transitional strain rate is also found experimentally in tantalum [70], aluminium alloys [78][79] and Al-6XN stainless steel [93]. For aluminium alloys deformed at strain rates ranging from  $10^3$  to  $6 \times 10^3 \text{ s}^{-1}$ , the average dislocation density measured by TEM was also found to increase rapidly with strain rate [78]. Such increase is comparable to the one predicted by the current model for pure copper (figure 5.3). Three dimensional dislocation dynamics (DD) simulations also reported that the dislocation density increases dramatically at high strain rates for shock compression in copper single crystals [120].

A detailed analysis of the parameters employed in the model (table 5.1) is required. The physical parameters  $m_\rho$ ,  $C_V$ ,  $\mu$ ,  $b$ ,  $\alpha$  and  $M$  and are taken directly from the literature. The initial dislocation density  $\rho_0 = 5 \times 10^{12} \text{ m}^{-2}$  is reasonable for the annealed samples [68]. The activation volume  $V = 300b^3$  is the experimentally measured value for pure Cu [109]. One may argue that the activation volume may slightly change with the progress of deformation. However, as a first order approximation, the present work assumes that the activation volume is constant during deformation. Referring to equation 5.29, the value of  $\beta$  determines the rate of dislocation generation due to existing dislocations. In the present work,  $\beta$  is set as 0.024 which is close to the value used in the Kocks-Mecking model [73].  $\tau_c$  and  $\dot{\gamma}_0$  are the parameters describing the dislocation movement at high strain rates and related to phonon drag effects. Both are fitted to the experimental data in the

current work.  $\tau_c = 10$  MPa is one order magnitude lower than the one employed for stainless steels [93]. Another fitting parameter related to the activation energy is  $A$ , which determines the slope of the curve at low strain rates in figure 5.3.  $\dot{\gamma}_0$  affects the transitional strain rate over which the dislocation density increases dramatically (figure 5.3).  $\tau_c$  determines the magnitude of the dislocation density at the high strain rate regime (figure 5.3). In summary, all parameter values are taken from literature except for  $\tau_c$ ,  $\dot{\gamma}_0$  and  $A$ , which are fitted.

For low stacking fault energy metals such as Cu, twinning may also contribute to the plastic deformation at high strain rate [85][86][105]. However, as a first order approximation, it is assumed here that the dislocation glide is the main mechanism for plastic deformation and the contribution of twinning is neglected.

The current model predicts that the dislocation generation and flow stress saturate when the strain rate is larger than  $\sim 10^6$  s<sup>-1</sup> (figure 5.3). This prediction does not agree with some recent publications. For instance, Meyers and co-workers [87] and Armstrong and co-workers [3] found that the flow stress of pure Cu still increases with strain rate when the strain rate is higher than  $\sim 10^7$  s<sup>-1</sup>. Discrete dislocation dynamics simulations [119] and experiments [87] also show that the dislocation density can still increase even when it is higher than  $10^{17}$  m<sup>-2</sup>. However, in the present model, the dislocation density is almost constant when it reaches a value of about  $1.5 \times 10^{17}$  m<sup>-2</sup>. The origin of this discrepancy is due to the assumption that the friction stress caused by the phonon drag saturates when the strain rate is higher than a critical value (equation 5.28), an assumption which may be relaxed in further research.

In the context of irreversible thermodynamics modelling of plasticity, the current model has introduced a new dislocation generation mechanism: viscous drag effects on high speed movement of dislocations producing new dislocations (equation 5.29). Such mechanism may be related to the energy dissipated by the high speed movement of dislocations. This amount of dissipative energy may be large enough to create new dislocations in the neighbourhood of the moving dislocations. For instance, molecular dynamics simulations have confirmed that new dislocations can be generated around a moving dislocation when its velocity approaches 70% of the velocity of sound [74].

At low strain rates, the first term in the right hand side of equation 5.29 vanishes. Therefore, the current model reduces to an expression similar to the classical Kocks-Mecking model [73] at low strain rates. In other words, the current irreversible thermodynamics model may provide a thermodynamics basis for the Kocks-Mecking model. At high strain rates, it incorporates in a natural manner the influence of phonon drag effects on the accumulation of dislocations. The low and high strain rate regimes are physically integrated into a single formulation.

## 5.5 Conclusions

Based on the theory of irreversible thermodynamics, a physically based constitutive model with a very limited, but yet physically rooted, number of parameters, has been proposed to describe the evolution of the average dislocation density in copper over a wide range of strain rates. It is found that there is a transitional strain rate ( $\sim 10^3 \text{ s}^{-1}$ ) beyond which the phonon drag effects play a dominant role in dislocation generation resulting in a significant raise in the average dislocation density and flow stress. The model reduces to an expression similar to the classical Kocks-Mecking model at low strain rates.

# 6

## Validation of the Irreversible Thermodynamics Model for Steels under Hot Rolling Conditions

### 6.1 Introduction

In order to optimize the hot rolling conditions (e.g. rolling temperature, speed and forces) of various existing steel grades and design new ones, it is essential to understand the physical mechanism controlling the flow behaviour under such deformation conditions [115]. Understanding hot working processes is also useful for controlling and improving mechanical properties such as strength and ductility of the final steel products. For instance, the strength and uniform elongation are related to the grain size of the final products as discussed in Chapter 4. The grain size can be manipulated by optimizing the thermomechanical rolling conditions [8]. Smaller ferrite grain size of the final steel products could be obtained by rolling at lower temperatures in the austenite region [8].

To understand thermomechanical rolling processes, the key is the understanding of the evolution of dislocation density and its distribution. In a conventional hot rolling process, the steel is rolled in the austenite (FCC) region through all rolling passes. As a result, the model developed in Chapter 5 can be applied to these rolling conditions. This chapter discusses the validation of the model for steels deformed in the austenite region under industrial hot rolling conditions. The predictions of the model are also compared to those of an existing model used by the industry.

## 6.2 Model

In Chapter 5, based on the theory of irreversible thermodynamics, it is derived a unified dislocation evolution formulation (equation 5.16) for pure FCC metals deformed at both low and high strain rates. This model is extended in this chapter in order to take into account the effects of solid solution and grain size and is applied to steels under industrial hot rolling conditions (single FCC phase). Under such deformation conditions, the friction stress  $\tau_f$  in equation 5.16 may be expressed as

$$\tau_f = \tau_0 + \tau_b + \beta\mu b\sqrt{\rho} \quad (6.1)$$

where  $\tau_0$  is the friction stress caused by the lattice incorporating the effects of elements dissolved in solid solutions.  $\tau_b$  is the back stress generated by the dislocations located at the grain boundary and is expressed as [122]

$$\tau_b = \frac{\mu b}{D}n \quad (6.2)$$

where  $D$  is the grain size and  $n$  is the number of dislocations per grain located at the grain boundary.  $n$  may change with the progress of deformation and approaches a maximum value. For instance, it is demonstrated, in Chapter 4, that the maximum value of  $n$  for ultrafine grained IF steels deformed at room temperature is 4. However, as a first order approximation, it is assumed here that  $n = 4$  for the entire deformation process. The term  $\beta\mu b\sqrt{\rho}$  is the contribution of existing dislocations. Comparing to equation 5.27, the phonon drag effect is ignored in equation 6.1 since the strain rate considered in this chapter is not higher than  $10^2 \text{ s}^{-1}$ .

Therefore, inserting equations 6.1 and 6.2 into equation 5.16 and approximating  $E = \mu b^2/2$  [68], the dislocation evolution for steels (single FCC phase) deformed at industrial hot rolling conditions is expressed as

$$\frac{d\rho}{dt} = \left( \tau_0 + \frac{\mu b}{D}n + \beta\mu b\sqrt{\rho} \right) \frac{\dot{\gamma}}{\mu b^2} - \frac{d\rho^-}{dt}. \quad (6.3)$$

$d\rho^-/dt$  represents the dislocation annihilation rate which may be caused by DRV and DRX. depending on the deformation temperature and strain rate. For simplicity, the conditions under which DRX occurs are not considered in the current model. The only dislocation annihilation mechanism is assumed to be DRV. It is considered that cross-slip is the main mechanism of DRV for the deformation considered here. Therefore, following the same arguments made in Chapter 5 (equation 5.17), the dislocation annihilation term  $d\rho^-/dt$  is expressed as

$$\frac{d\rho^-}{dt} = N2Lv_{cs}P_{cs} = 2\frac{b}{L}v_D \exp\left(-\frac{\Delta G}{kT}\right)\rho. \quad (6.4)$$

Inserting equation 5.24 and  $V = Ldb$  (see figure 5.1) into equation 6.4, it can be rewritten as

$$\frac{d\rho^-}{dt} = 2\frac{b}{L}v_D \exp\left(-A \ln \frac{c_1 v_D}{\dot{\gamma}} + \frac{\tau L d}{\mu b^2}\right) \rho. \quad (6.5)$$

Inserting equation 6.5 and substituting  $dt = d\gamma/\dot{\gamma}$ , equation 6.3 can be rewritten as

$$\frac{d\rho}{d\gamma} = \frac{\tau_0}{\mu b^2} + \frac{n}{Db} + \frac{\beta}{b}\sqrt{\rho} - 2\frac{b}{L}v_D \exp\left(-A \ln \frac{c_1 v_D}{\dot{\gamma}} + \frac{\tau L d}{\mu b^2}\right) \rho. \quad (6.6)$$

Equation 6.6 describes the evolution of the average dislocation density for the plastic deformation of non-recrystallising single FCC steels at low to modest strain rates.

By solving equation 6.6 with an initial dislocation density  $\rho_0$ , the true stress-strain relation can be obtained from the following equation [5][73][76]:

$$\sigma = M\tau = M\alpha\mu b\sqrt{\rho}. \quad (6.7)$$

### 6.3 Calibration of parameters

The model is applied to three groups of steels: interstitial free steels (4 grades), low carbon steels (5 grades) and medium carbon steels (4 grades). The steel compositions are shown in table 6.1. All experimental data employed in this chapter were supplied by ArcelorMittal and all stress-strain curves in this chapter are true normal stress ( $\sigma = M\tau$ ) and normal strain ( $\epsilon = \gamma/M$ ). The strain rate is the normal strain rate ( $\dot{\epsilon} = \dot{\gamma}/M$ ).

Some parameters used in the model are shown in table 6.2 which are the same for all grades. The friction stress related parameter  $\tau_0$  and the activation energy related parameter  $c_1$  are composition and temperature dependent. They are the only two fitting parameters and are calibrated against the experimental data. For simplicity, the current model does not distinguish the differences between substitutional elements, which implies that  $\tau_0$  and  $c_1$  are taken to depend on the carbon content and the sum of all substitutional elements ( $\sum X$ ).

Figure 6.1 shows the true stress-strain behaviour of 11 steel grades deformed at 900 °C with a strain rate of 10 s<sup>-1</sup>. The experimental data of the other two grades are not available for such temperature and strain rate. For all grades a very good fit to the experimental curves is obtained over all the stress-strain curves. The purpose of the fit in figure 6.1 is to find the chemical composition dependence of  $c_1$  and  $\tau_0$ . These values for each steel grade are indicated in figure 6.1. The dependence of carbon content and  $\sum X$  on  $\tau_0$  and  $c_1$  are demonstrated in figures

	NAME	C	Mn	Si	Cr	Ti	Nb	Al	$\sum X$
IF	DWI	0.002	0.208	0.004	0.017	0.000	0.000	0.010	0.239
	IF Nb	0.002	0.123	0.005	0.019	0.015	0.016	0.027	0.205
	IF HR390	0.004	0.900	0.134	0.019	0.060	0.000	0.024	1.137
	E220BH	0.004	0.195	0.124	0.025	0.002	0.000	0.039	0.385
LC	Soldur 355	0.052	0.627	0.255	0.023	0.068	0.052	0.028	1.053
	DP 450	0.054	1.18	0.125	0.465	0.000	0.000	0.030	1.854
	Soldur 420	0.055	0.362	0.013	0.025	0.001	0.055	0.035	0.491
	Fer Blanc	0.067	0.415	0.010	0.020	0.000	0.000	0.034	0.479
	Soldur 490	0.080	1.480	0.029	0.020	0.002	0.063	0.028	1.622
MC	S355	0.165	1.38	0.008	0.023	0.001	0.001	0.024	1.437
	TRIP800	0.185	1.660	1.605	0.033	0.003	0.001	0.039	3.341
	ST52	0.21	1.440	0.220	0.018	0.001	0.002	0.032	1.713
	C40	0.385	0.673	0.203	0.269	0.001	0.000	0.020	1.166

TABLE 6.1. Steel composition (wt%) of 3 groups of steels: interstitial free steels (IF), low carbon steels (LC) and medium carbon steels (MC).  $\sum X$  represents the sum of all substitutional alloying elements

6.2 and 6.3, respectively.  $\tau_0$  increases with  $\sum X$  and carbon content. While  $c_1$  decreases with carbon content.

The temperature dependence of  $c_1$  is illustrated in figure 6.4:  $c_1$  decreases with temperature. Those values of  $c_1$  plotted in figure 6.4 are obtained by fitting to the experimental stress-strain curves shown in figure 6.5. Using a linear regression method, the parameters  $\tau_0$  (in MPa) and  $c_1$  are fitted as

$$\tau_0 = (0.13 + 32.84 \times \text{C wt\%} + 2.48 \times \sum X) \{ \exp [0.002 (300 - T)] \} \quad (6.8)$$

and

$$c_1 = 1.028 - 0.335 \times \text{C wt\%} - 3.41 \times 10^{-3} \times \sum X - 6 \times 10^{-4} T. \quad (6.9)$$

$\mu$ (MPa)	$\alpha$	$M$	$b$ (nm)	$D$ ( $\mu\text{m}$ )
$85115-34 \times T$	0.25	3.06 [68]	0.258	50
$\beta$	$\rho_0$ ( $\text{m}^{-2}$ )	$A$	$d$ ( $b$ )	$L$ ( $b$ )
0.01 [73]	$10^{12}$ [68]	0.9	1	30

TABLE 6.2. Parameters used in the model

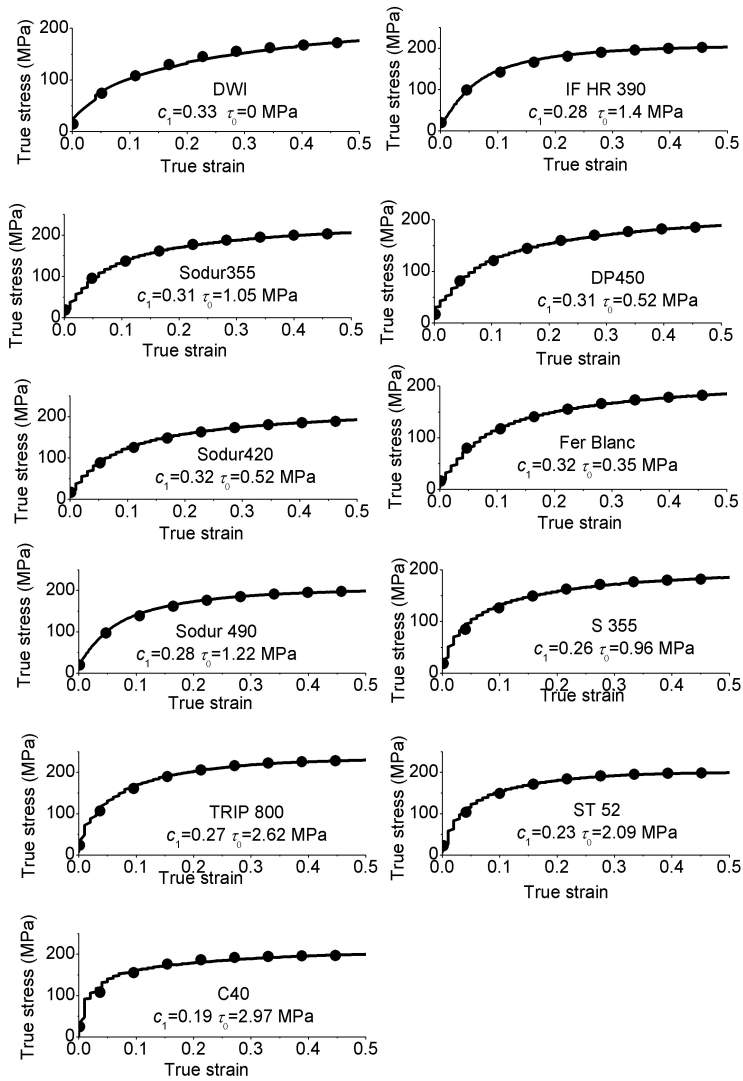


FIGURE 6.1. True stress-strain curves for 11 steel grades at 900 °C and  $10 \text{ s}^{-1}$ . Solid lines are experimental observations and points are model predictions.

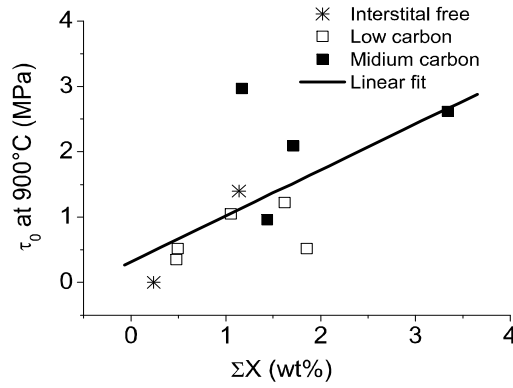


FIGURE 6.2.  $\tau_0$  vs  $\Sigma X$  at 900 °C

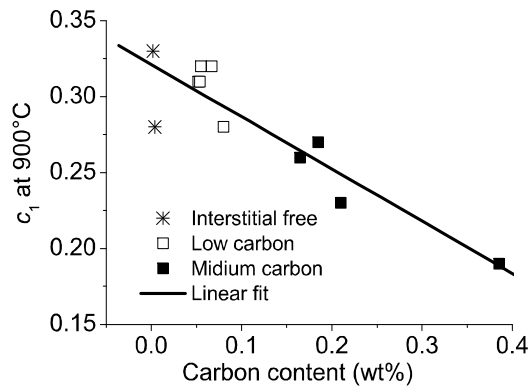


FIGURE 6.3.  $c_1$  vs carbon content at 900 °C

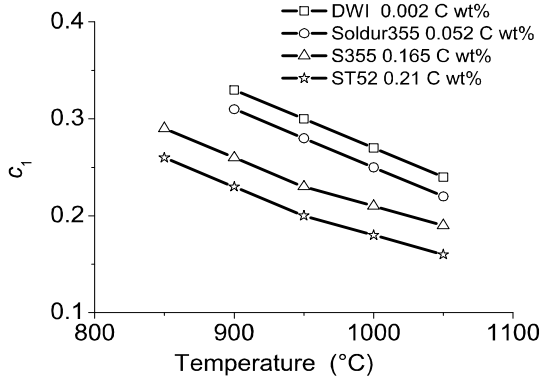


FIGURE 6.4.  $c_1$  vs temperature for 4 steel grades

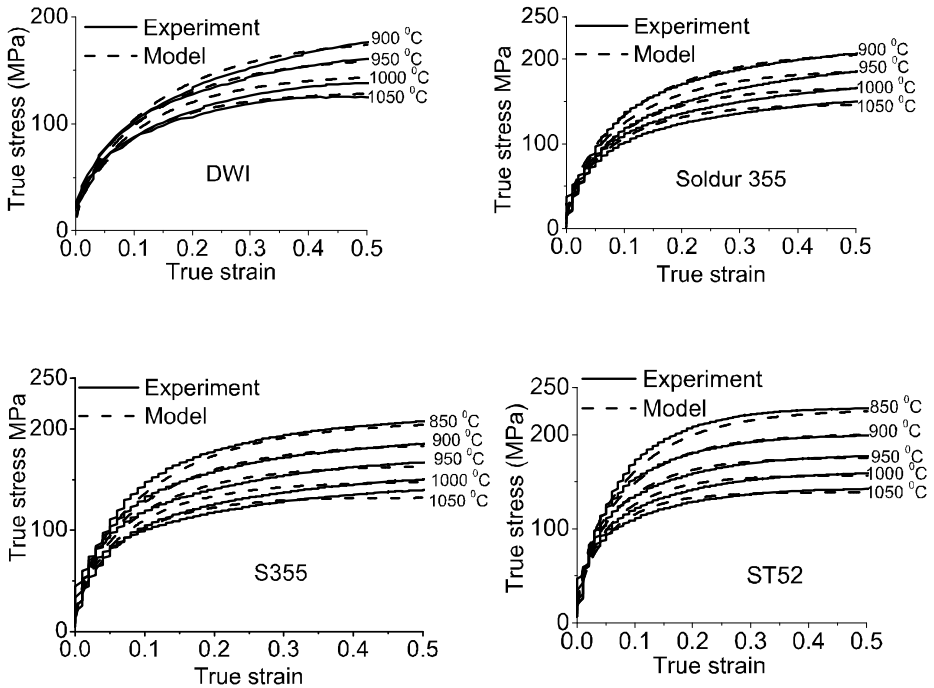


FIGURE 6.5. Stress-strain curves for 4 different steel grades with different carbon content

## 6.4 Comparison of the current model to experimental data and industrial model

### 6.4.1 Comparison with experimental data

Employing the calibrated parameters presented in section 6.3, the model is applied to 13 steel grades (figure 6.6 to figure 6.18). The flow stresses increase with strain rate and decrease with temperature. The temperature effects are shown in the part (a) of the figures and the strain rate effects are illustrated in the part (b).

As shown in these figures, the predictions of the current model are, in general, in good agreement with the experimental observations considering it covers such a wide range of chemical compositions, temperatures and strain rates. However, it is noted that the degree of accuracy for different steel grades may be different since all substitutional elements are assumed to have the same effect on the frictional stress and activation energy ( equations 6.8 and 6.9). For instance, the model has a very high accuracy for Sodur 490 (figure 6.14) but is less accurate for TRIP800 (figure 6.16), DP 450 (figure 6.11) and C40 (figure 6.18). The Si content in TRIP800 is at least one order magnitude higher than all other grades. While the Cr content in DP 450 and C40 are at least one order magnitude higher than all other grades (table 6.1).

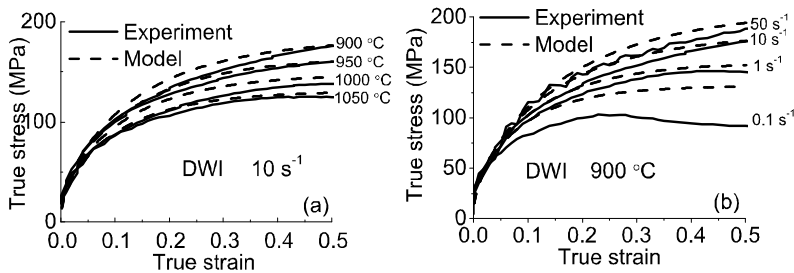


FIGURE 6.6. DWI stress-strain curves: (a) at the strain rate of  $10 \text{ s}^{-1}$  for different temperatures and (b) at  $900 \text{ }^\circ\text{C}$  for 4 strain rates

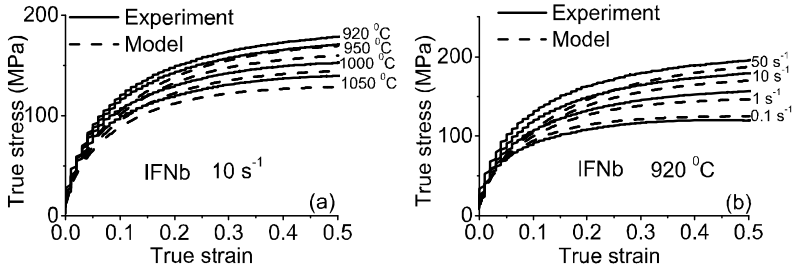


FIGURE 6.7. IFNb stress-strain curves: (a) at the strain rate of  $10 \text{ s}^{-1}$  for different temperatures and (b) at  $920 \text{ }^\circ\text{C}$  for 4 strain rates

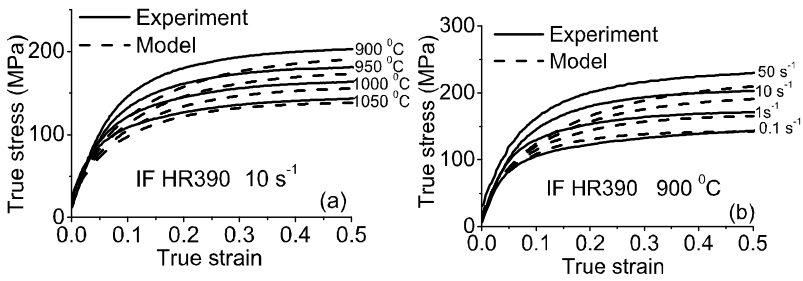


FIGURE 6.8. IFHR390 stress-strain curves: (a) at the strain rate of  $10 \text{ s}^{-1}$  for different temperatures and (b) at  $900 \text{ }^\circ\text{C}$  for 4 strain rates

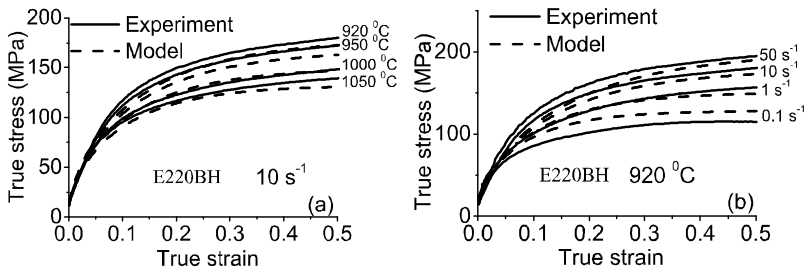


FIGURE 6.9. E220BH stress-strain curves: (a) at the strain rate of  $10 \text{ s}^{-1}$  for different temperatures and (b) at  $920 \text{ }^\circ\text{C}$  for 4 strain rates

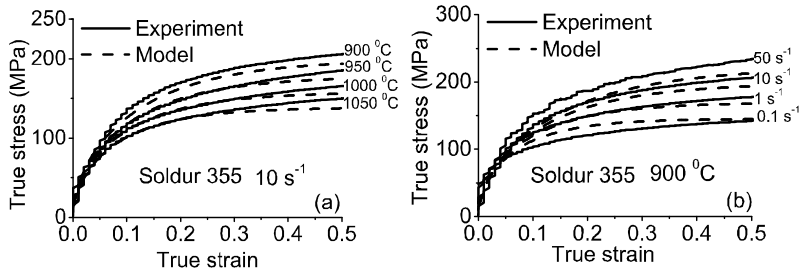


FIGURE 6.10. Soldur355 stress-strain curves: (a) at the strain rate of  $10 \text{ s}^{-1}$  for different temperatures and (b) at  $900 \text{ }^\circ\text{C}$  for 4 strain rates

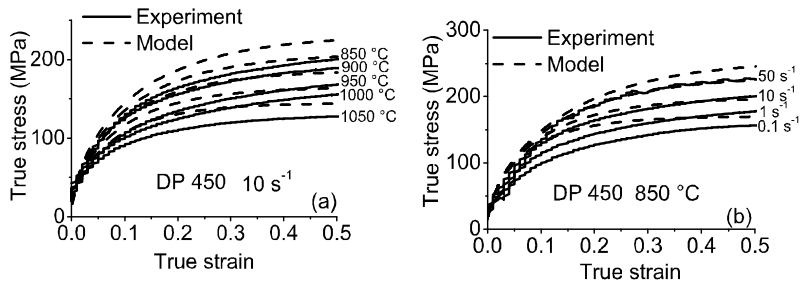


FIGURE 6.11. DP450 stress-strain curves: (a) at the strain rate of  $10 \text{ s}^{-1}$  for different temperatures and (b) at  $850 \text{ }^\circ\text{C}$  for 4 strain rates

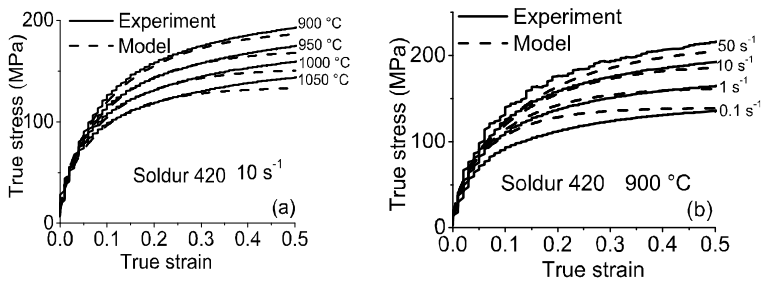


FIGURE 6.12. Soldur420 stress-strain curves: (a) at the strain rate of  $10 \text{ s}^{-1}$  for different temperatures and (b) at  $900 \text{ }^\circ\text{C}$  for 4 strain rates

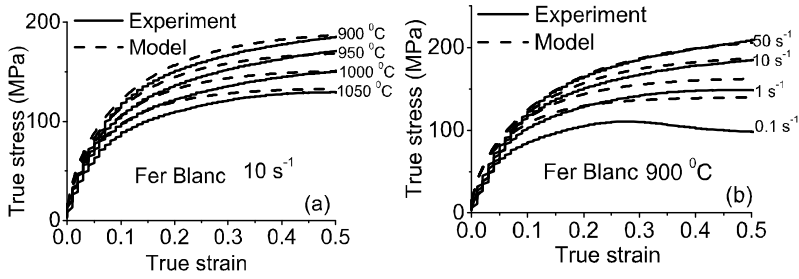


FIGURE 6.13. Fer Blanc stress-strain curves: (a) at the strain rate of  $10 \text{ s}^{-1}$  for different temperatures and (b) at  $900 \text{ }^\circ\text{C}$  for 4 strain rates

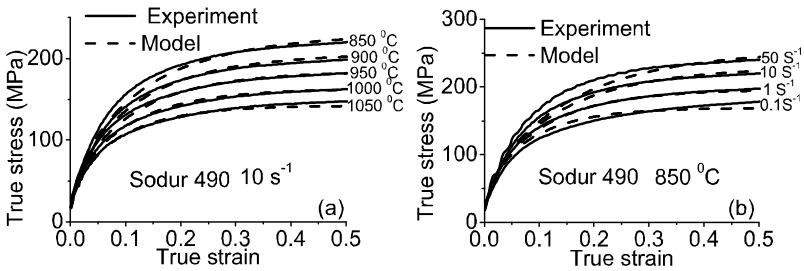


FIGURE 6.14. Soldur490 stress-strain curves: (a) at the strain rate of  $10 \text{ s}^{-1}$  for different temperatures and (b) at  $850 \text{ }^\circ\text{C}$  for 4 strain rates

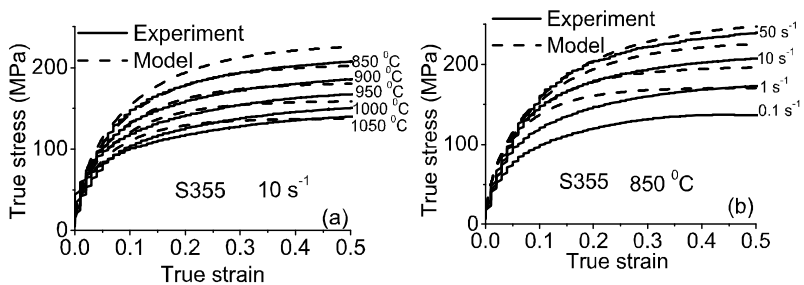


FIGURE 6.15. S355 stress-strain curves: (a) at the strain rate of  $10 \text{ s}^{-1}$  for different temperatures and (b) at  $850 \text{ }^\circ\text{C}$  for 4 strain rates

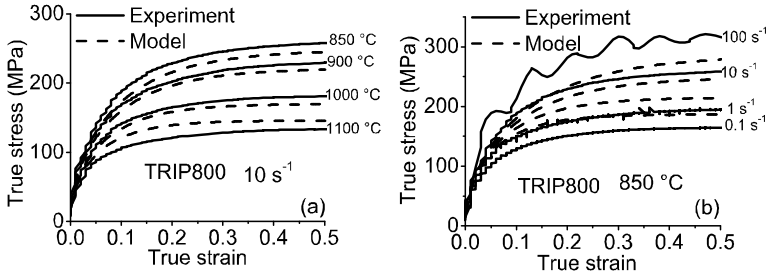


FIGURE 6.16. TRIP800 stress-strain curves: (a) at the strain rate of  $10 \text{ s}^{-1}$  for different temperatures and (b) at  $850 \text{ }^\circ\text{C}$  for 4 strain rates

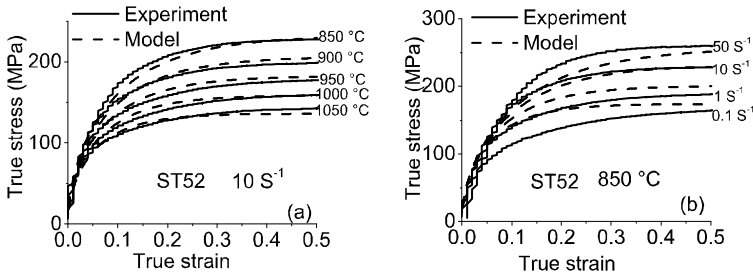


FIGURE 6.17. ST52 stress-strain curves: (a) at the strain rate of  $10 \text{ s}^{-1}$  for different temperatures and (b) at  $850 \text{ }^\circ\text{C}$  for 4 strain rates

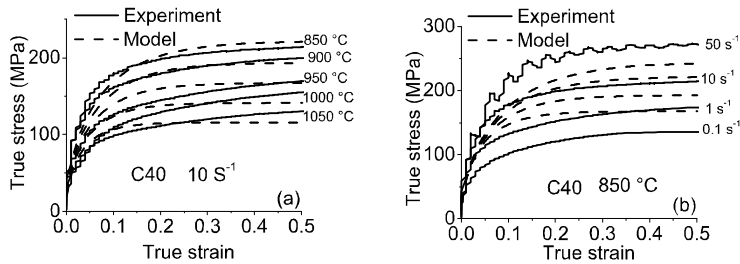


FIGURE 6.18. C40 stress-strain curves: (a) at the strain rate of  $10 \text{ s}^{-1}$  for different temperatures and (b) at  $850 \text{ }^\circ\text{C}$  for 4 strain rates

### 6.4.2 Comparison with the industrial model

This section compares the predictive capability of the current model to the model employed by ArcelorMittal. The ArcelorMittal model employs 7 fitting parameters ( $k_0$ ,  $f_0$ ,  $f_1$ ,  $\sigma_0$ ,  $\tau_{va}$ ,  $\dot{\epsilon}_0$ ,  $Q$ ) as shown in the following equations [11]:

$$\frac{d\rho}{d\epsilon} = M \left[ \frac{1}{bD} + \frac{1}{k_0 b} \sqrt{\rho} - (f_0 - f_1 \sqrt{\rho}) \rho \right] \quad (6.10)$$

and

$$\sigma = (\sigma_0 + M\alpha\mu b\sqrt{\rho}) \left\{ 1 + \frac{kT}{b^3\tau_{va}} \operatorname{arcsinh} \left[ \frac{\dot{\epsilon}}{\dot{\epsilon}_0} \exp \left( \frac{Q}{RT} \right) \right] \right\}. \quad (6.11)$$

The average dislocation density is predicted by equation 6.10 and the flow stress is described by equation 6.11. The fitting parameters of the ArcelorMittal model are fitted to the carbon content and most of the substitutional alloying elements. For instance, the friction stress  $\sigma_0$  is fitted as

$$\sigma_0 = \sigma_0(20^\circ\text{C}) \exp[0.0011(300 - T)] \quad (6.12)$$

where  $\sigma_0(20^\circ\text{C})$  is the friction stress at  $20^\circ\text{C}$  and is fitted to chemical compositions as

$$\sigma_0(20^\circ\text{C}) = \sigma_{00} + \sum_{i=1}^{N_s} \lambda_i X_i \quad (6.13)$$

where  $\sigma_{00}$  is a constant.  $\lambda_i$  is the coefficient for each alloying element.  $N_s$  is the total number of alloying elements in the steels.  $X_i$  is the weight percentage of each alloying element.

Figure 6.19 shows the comparisons of the predictive ability between the current and ArcelorMittal models. The experimental and current model flow stresses shown in figure 6.19(a) are obtained from the part (a) of figures 6.6-6.18 at the strain of 0.3; while the ones in figure 6.19(b) are from the part (b) of figures 6.6-6.18 at the strain of 0.3. Figure 6.19(a) shows the temperature effects and figure 6.19(b) shows the strain rate effects. Though both models are in good agreement with experimental data, the current model is slightly less accurate than ArcelorMittal model. However, the current model only has two fitting parameters which are adjusted to carbon content and the sum of all substitutional alloying elements, while the ArcelorMittal model contains no less than 7 parameters.

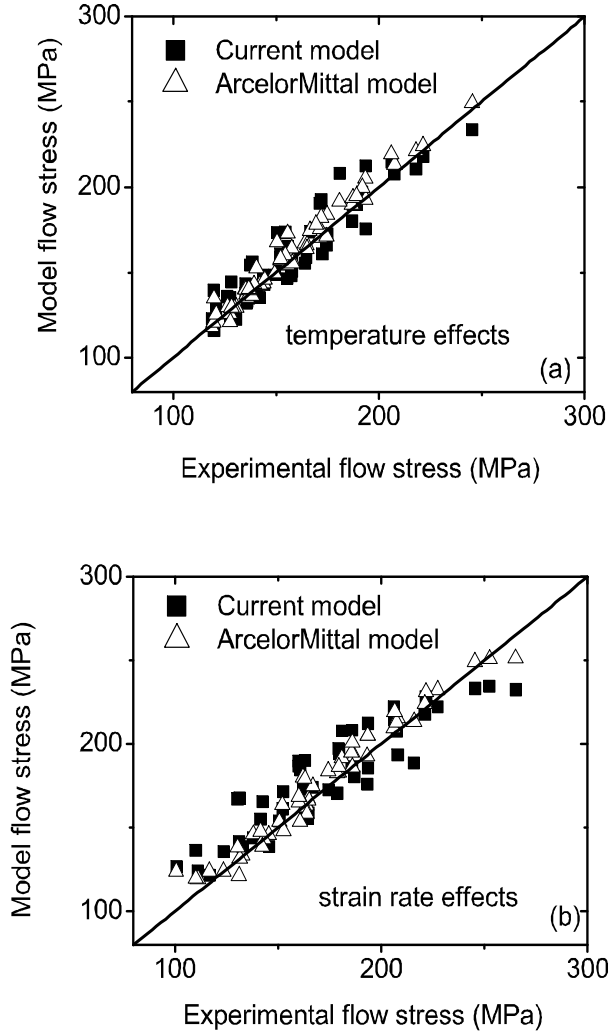


FIGURE 6.19. Comparison between the current model and ArcelorMittal model (a) temperature effects and (b) strain rate effects

## 6.5 Discussion

The core of the model in this chapter is the dislocation evolution formulation (equation 6.6); this shows that the dislocation density may be increased due to elements present in solid solution, grain size reductions and existing dislocations. Compared to the model developed in Chapter 5 (equation 5.29), the current model incorporates two new contributions to the dislocation multiplication rate: solid solution and grain boundary effects, and neglects the phonon drag mechanism due to the modest strain rate deformation conditions. After introducing the two new components, the alloying and grain size effects can be incorporated, which allows the current model to be applied to steels deformed under hot rolling conditions (single FCC phase).

There are only two fitting parameters in the current model ( $\tau_0$  and  $c_1$ ). They are assumed to depend on temperature and chemical composition (carbon content and the sum of substitutional alloying elements). As demonstrated in equation 6.8, the friction stress related parameter  $\tau_0$  increases with carbon content and  $\sum X$ . To contrast, the activation energy related parameter  $c_1$  decreases with carbon content and  $\sum X$  (equation 6.9), which implies that the activation energy for DRV decreases with carbon content and  $\sum X$ . It has been reported in the literature that increasing carbon content decreases the activation energy for DRV in steels due to the increase of the iron diffusivity [108].  $\sum X$  is about one order magnitude less important than carbon in determining  $\tau_0$  and two magnitude less important than carbon in determining  $c_1$  (equations 6.8 and 6.9, respectively). This implies that both carbon and substitutional alloying elements are important in the friction stress, but only carbon plays a dominant role in the activation energy for DRV.

Besides  $\tau_0$  and  $c_1$ , there are also a few constants (see table 6.2) present in the current model, which require further analysis. The stacking fault width  $d$  is related to the stacking fault energy and can be calculated from equation 5.19. The stacking fault energies for the steels considered here at such high temperature are very high [1] resulting a very narrow stacking fault width. Therefore, it is reasonable to set  $d = b$ . The activation length  $L$  is set as  $30b$  which is similar the one for pure Cu in Chapter 5 ( $\sim 50b$  calculated from equation 5.20).  $\alpha$  and  $\beta$  are similar to the values used in the Kocks-Mecking model [73].  $\mu, b$  and  $D$  are obtained from an internal report by ArcelorMittal [11].  $10^{12} \text{ m}^{-2}$  is a reasonable value for the initial dislocation density  $\rho_0$  at such a high temperature.

As shown in figures 6.6-6.19, especially in figure 6.19, the current model predicts the temperature effects better than the strain rate effects. The reason is that the temperature dependent parameter  $c_1$  is fitted to different chemical composition (equation 6.9). But the parameter  $A$  which determines the strain rate dependence of the activation energy (equation 5.24 and also see the discussion in Chapter 5)

is assumed to be the same for all steel grades. Therefore, the model may have a better predictive capability in strain rate effects if the parameter  $A$  changes with chemical composition.

The predictive ability of the current model is compared to the model developed in ArcelorMittal. It shows that both models have similar predictive capability. But the current model is derived from the theory of irreversible thermodynamics, which offers it a solid thermodynamics foundation. Moreover, the current model only has two fitting parameters which are related to the carbon content and the sum of all substitutional alloying elements. The ArcelorMittal model has, however, 7 fitting parameters related to chemical compositions. Moreover, the ArcelorMittal model does not incorporate the strain rate effect on the evolution of the dislocation density, while the current model does via the dislocation annihilation term (equation 6.5).

The model as used here only takes into account the DRV as the softening mechanism and neglects the DRX. Therefore, the flow stresses predicted by the current model should be higher than the experimental observations for the deformation conditions under which DRX occurs. This is clearly shown in figures 6.6(b) ( $0.1 \text{ s}^{-1}$ ) and 6.13(b) ( $0.1 \text{ s}^{-1}$ ).

## 6.6 Conclusions

The model developed in Chapter 5 is extended to incorporate the alloying and grain boundary effects on the dislocation multiplication rate during plastic deformation. The extended model has only two fitting parameters related to the friction stress and activation energy respectively, and is applied to three groups of steels varying from very low carbon content to medium carbon content under industrial hot rolling conditions. Notwithstanding its simplicity, the stress-strain curves predicted by the model show good agreements with experimental stress-strain curves, provided DRX does not occur.

# Summary

The main objective of this thesis is to provide an irreversible thermodynamics framework to describe and predict the work hardening and stress-strain phenomena occurring in single grained and polycrystalline metals. Models to quantitatively describe these are presented. Especial emphasis is placed on the understanding of the evolution of dislocations. The models are applied to pure metals and single phase alloys with FCC or BCC structures over a wide range of temperatures, strain rates and grain sizes.

As described in Chapter 1, the motion of dislocations and their various forms of interactions are considered to constitute the only mechanisms inducing plastic deformation. Other deformation mechanisms such as twinning, grain boundary sliding and TRIP effects are excluded in this thesis.

In Chapter 2 it is argued why and described how irreversible thermodynamics can be employed to model plastic deformation in metals. A comparison between equilibrium and irreversible thermodynamics is made: while the former describes the properties of a system as a state of equilibrium is approached (e.g. phase diagrams), the later is able to describe the properties of a system at non-equilibrium states, and can describe the evolution kinetics of such properties. The plastic deformation of metals, being a non-equilibrium system, can be described by irreversible thermodynamics. The key to employing irreversible thermodynamics is calculating the entropy production, which is described in Chapter 2. Such calculations are performed in terms of an average dislocation density, which can be subdivided in cell

interior and wall sub-densities. Such an approach is contrasted to models describing the spatiotemporal distribution of dislocations employing discrete dislocation dynamics simulations in two and three dimensions.

A first attempt to apply irreversible thermodynamics to plastic deformation is performed by describing the steady state of plastic deformation in Chapter 3. The approach is based on the assumption that the steady state of plastic deformation is a stationary non-equilibrium state in the context of irreversible thermodynamics. The average dislocation density is found to be a function of shear strain rate and a velocity term combining the climb velocity of edge dislocations and the grain boundary velocity. The model is successfully applied to three different metallurgical processes: (1) constant strain rate deformation with dynamic recovery, where it is demonstrated for single crystals of Al, Ag, Cu and Ni that the average dislocation density decreases with the stacking fault energy but increases with the self diffusion energy; (2) creep deformation with dynamic recovery, where the model can reproduce the behaviour of coarse grained polycrystalline Al over a wide range of temperatures without invoking transitions in creep mechanisms from dislocation climb to pipe diffusion, as the empirical power-law model does; (3) constant strain rate deformation with dynamic recovery and dynamic recrystallization. In this case, the effects of dynamic recovery and recrystallization on the average dislocation density at the steady state are naturally incorporated into one single formula. At low temperatures, the model predicts that the dynamic recovery is the dominant softening mechanism, while at high temperatures, dynamic recrystallization plays the major role. The model is validated for coarse grained polycrystalline Cu.

In Chapter 4, the model is extended to predict the evolution of the average dislocation density for single crystals of Al and Cu. A proportionality relationship between the development of entropy and the work hardening rate in a metallic system undergoing plastic deformation is assumed as both depend on the internal disorder of the material. This assumption states that, under quasi-static and isothermal deformation conditions, the entropy of metals undergoing deformation decreases with deformation. This assumption is supported on the basis that the entropy flux (proportional to the heat flux) from the metal to the environment is larger than the entropy production, and that the deformed metal is in a more ordered state than its original form due to the formation of dislocation structures (e.g. cells) and/or the development of texture. Both the entropy flux and the ordering are consistent with a decreasing entropy. This assumption leads to a description of the stress-strain behaviour of single crystals, and the resulting expressions are qualitatively similar to those from the classical semi-phenomenological Kocks-Mecking model. The predicted stress-strain curves for single crystalline Cu and Al

are compared to experimental results over a wide range of temperatures and show good agreement.

The model for single crystals is further extended in Chapter 4 incorporating grain size effects via the back stress. The average dislocation density in the grain interior is predicted as a function of grain size. The model is applied to (ultra)fine grained interstitial free steels and Al alloys. For both systems, it is found that, when the grain size is smaller than  $0.4 \mu\text{m}$ , the dislocation density in the grain interior increases very little during the deformation, which causes a loss in work hardening and thereby very low uniform elongation. For grain sizes in the range of  $0.4$  to  $1 \mu\text{m}$ , the evolution kinetics of the dislocation density in the grain interior increases sharply with grain size, which results in a sharp increase in the work hardening capability and therefore a sharp increase of the uniform elongation with grain size. When the grain size is between  $1$  and  $10 \mu\text{m}$ , the evolution kinetics of the dislocation density in the grain interior increases slowly with grain size and approaches an asymptotic value at the grain size larger than  $10 \mu\text{m}$ . This results in the uniform elongation to increase slowly with grain size and to approach a constant value. The model illustrates that a way to improve the ductility of ultrafine grained alloys is to increase the dislocation density in the grain interior. This can be achieved by increasing the activation energy of dynamic recovery. According to the model predictions, for a grain size of  $0.4 \mu\text{m}$ , the true uniform strain for interstitial free steels can be increased from  $4.3\%$  to  $28.2\%$  when the activation energy increases from  $0.766 \text{ eV}$  to  $0.8 \text{ eV}$ . For AA1100 alloys, it increases from  $2.2\%$  to  $26.3\%$  when the activation energy increases from  $0.748 \text{ eV}$  to  $0.78 \text{ eV}$ . Therefore, finding proper alloying elements to increase the activation energy (which may be related to the melting temperature) could be a solution to improve the ductility of the ultrafine grained alloys, which will enhance their practical engineering applications.

The approach developed in the first chapters is applicable to isothermal (low strain rate) deformation conditions; it assumes that the entropy of the deformed metal decreases with deformation. In Chapter 5 the irreversible thermodynamics model is extended to cover high strain rate conditions. In such case, where the strain rate is typically larger than  $10^2 \text{ s}^{-1}$ , there is not enough time to radiate heat into the environment, and the entropy flux vanishes. The entropy production rate is expressed as the sum of the products of generalised forces and the corresponding fluxes of the irreversible processes. The evolution kinetics of the average dislocation density is thus derived, showing that it increases dramatically when the strain rate exceeds  $10^3 \text{ s}^{-1}$  causing the flow stress to considerably increase. That effect has been experimentally observed in many metallic systems. It is explained by the model that the phonon drag effect on the high speed movement

of dislocations induces a significant raise in the dislocation generation rate. Such dislocation generation mechanism may be related to the energy dissipated by the high speed movement of dislocations. This amount of dissipative energy may be large enough to create new dislocations in the neighbourhood of the moving dislocations. It is shown that at low strain rates, the term accounting for phonon drag effects vanishes and this model reduces to an expression similar to the classical Kocks-Mecking model. The model predictions are in good agreement with the experimental stress-strain curves of polycrystalline Cu at strain rates ranging from  $1.5 \times 10^{-2}$  to  $6.4 \times 10^5 \text{ s}^{-1}$ .

The model developed in Chapter 5 is extended in Chapter 6 to combine the effects of grain size and alloying elements at low to moderate strain rate conditions. The phonon drag effects can be ignored at such deformation conditions. The model is applied to 13 grades of three steel families (interstitial free, low carbon, and medium carbon) under hot working conditions in the single austenitic state. A comparison between the prediction capability of the current model and an industrial model is made, showing their accuracy to be similar. However, the current model requires less fitting parameters while it incorporates strain rate effects on the evolution of dislocation density.

# Samenvatting

Doel van dit proefschrift is de ontwikkeling van een nieuw model voor de beschrijving en voorspelling van het verstevigingsgedrag en de kracht-rek kromme van metallische één-kristallen en poly-kristallijne metalen op basis van concepten afkomstig uit de irreversibele thermodynamica. In deze dissertatie worden enige kwalitatieve modellen gepresenteerd, waarbij de nadruk ligt op het verklaren van de ontwikkeling van de dislocatiedichtheid. De modellen zijn getoetst aan het gedrag van zuivere metalen en dat van één-fase legeringen met een kubisch vlakken gecentreerd (KVG) of kubisch ruimtelijk gecentreerd (KRG) kristalrooster, over een groot temperatuurbereik, voor een breed scala van vervormingssnelheden en als functie van de korrelgrootte.

Zoals beschreven in hoofdstuk 1, worden in dit proefschrift enkel dislocatieverplaatsingen en dislocatieinteracties bepalend gehouden voor het plastisch gedrag. Andere vervormings-mechanismen zoals tweelingvorming, afschuiving langs de korrelgrenzen en “TRIP” effecten zijn buiten beschouwing gelaten.

Hoofdstuk 2 beschrijft waarom en hoe irreversibele thermodynamica toegepast kan worden in het modelleren van plastische deformatie van metalen. Er wordt een vergelijking gemaakt tussen evenwichts- en irreversibele thermodynamica, waarbij de eerstgenoemde een beschrijving geeft van de eigenschappen van een systeem in evenwicht (leidend tot, bijvoorbeeld, de voorspelling van fase diagrammen). Irreversibele thermodynamica maakt het mogelijk de eigenschappen van een systeem in een niet-evenwichtsconditie weer te geven en het verloop van de kinetiek van

de structuurveranderingen te beschrijven. Plastische vervorming van metalen, wat in essentie een successie van niet-evenwichtstoestanden is, kan daarom beschreven worden via irreversibele thermodynamicaconcepten. De sleutel voor het toepassen van irreversibele thermodynamica is het berekenen van de entropieproductie. De berekeningen zijn uitgevoerd als functie van de gemiddelde dislocatiedichtheid, welke onderverdeeld kan worden in de dislocatiedichtheid in het inwendige van een cel en de dislocatiedichtheid in de rand van de cel. Hierbij onderscheidt dit model zich van eerdere modellen die de distributie van de dislocaties in ruimte en tijd beschrijven door het toepassen van discrete dislocatie dynamica simulaties in 2 en 3 dimensies.

Een eerste poging om irreversibele thermodynamica toe te passen op plastische deformatie betreft de beschrijving van de “steady state” conditie van plastische vervorming, welke te vinden is in hoofdstuk 3. De benadering is gebaseerd op de aanname dat de “steady state” van plastische vervorming een stationaire instabiele toestand is binnen de context van de irreversibele thermodynamica. De gemiddelde dislocatiedichtheid is dan een functie van de afschuifsnelheid en een term die een combinatie is van de snelheid waarmee randdislocaties kunnen klimmen en de verplaatsingssnelheid van korrelgrenzen. Het model is succesvol toegepast op drie verschillende metaalkundige processen: (1) voor vervorming met een constante reksnelheid, waarbij dynamisch herstel optreedt, is aangetoond dat voor één-kristallen van Al, Ag, Cu en Ni de gemiddelde dislocatiedichtheid afneemt met de stapelfoutenergie, maar dat deze toeneemt met de activeringsenergie voor zelfdiffusie; (2) voor kruip, waarbij dynamisch herstel optreedt, is aangetoond dat de theorie het gedrag van polykristallijn Al met een grote korrelgrootte over een groot temperatuurinterval goed kan reproduceren, zonder dat hierbij een overgang in het kruipmechanisme van het klimmen van dislocaties naar pijpdiffusie verondersteld moet worden, zoals nu nog het geval is in het proefondervindelijke machts-wet model; (3) voor vervormingen bij een constante snelheid waarbij zowel dynamisch herstel als dynamische rekristallisatie plaatsvinden. In dat geval worden de afzonderlijke effecten van dynamisch herstel en dynamische rekristallisatie op de gemiddelde dislocatiedichtheid tijdens de “steady state” automatisch beschreven binnen een en dezelfde formule. Bij lage temperaturen voorspelt het model dat dynamisch herstel het dominante ontstevigingsmechanisme is, terwijl bij hoge temperaturen dynamische rekristallisatie het belangrijkste proces is. Het model is toegepast op en gevalideerd voor grofkorrelig polykristallijn Cu.

In hoofdstuk 4 volgt een uitbreiding van het model waardoor het mogelijk wordt om de gemiddelde dislocatiedichtheidsontwikkeling in één-kristallen van Al en Cu tijdens de vervorming te voorspellen. Hierbij is aangenomen dat de verandering van de entropie evenredig is met de hoeveelheid versterking in een metallisch sys-

teem, aangezien beide processen op een soortgelijke wijze afhangen van de mate van interne wanorde in het materiaal. Dit houdt in dat, onder quasi-statische en isotherme vervormings-condities, de entropie in een metaal afneemt bij toenevende deformatie. Deze aanname wordt gesteund door het feit dat de entropiestroom (welke evenredig is met de warmtestroom) van het metaal naar de omgeving groter is dan de entropieproductie. Bovendien geldt dat het gedeformeerde metaal, ten gevolge van de vorming van dislocatiestructuren (i.e. deformatiecellen) en/of de vorming van texturen, zich in een meer geordende toestand bevindt dan in de uitgangstoestand. Zowel de entropiestroom als de ordening van de structuur is consistent met een afname van de entropie. Dankzij deze aanname kan het kracht-rek gedrag van één-kristallen kwantitatief beschreven worden. De uiteindelijke vergelijkingen zijn kwalitatief gezien gelijk aan de vergelijkingen uit het klassieke, min-of-meer fenomenologische, Kocks-Mecking model. De voorspelde kracht-rek krommes voor éénkristallijn Cu en Al komen over een uitgebreid temperatuurgebied goed overeen met de experimentele resultaten.

Het model van hoofdstuk 4 is vervolgens verder uitgebreid om de effecten van korrelgrootte te beschrijven, gebruikmakend van het “back stress” concept. De gemiddelde dislocatiedichtheid in het inwendige van de korrel kan nu voorspeld worden als functie de deformatie en als functie van de korrelgrootte. Het model is toegepast op ultra-fijnkorrelige IF (interstitieel vrije) staalsoorten en Aluminium legeringen. Voor beide systemen is waargenomen dat bij korrelgroottes kleiner dan  $0.4 \mu\text{m}$  de dislocatiedichtheid in het inwendige van de korrel marginaal toeneemt tijdens de deformatie, hetgeen resulteert in een verdwijnen van de versterking en als geval daarvan in een zeer kleine homogene verlenging. Voor korrelgroottes tussen  $0.4$  en  $1 \mu\text{m}$ , neemt het verloop van de dislocatiedichtheid in het inwendige van de korrel sterk toe met toenemende korrelgrootte, hetgeen resulteert in een sterke toename van de uniforme verlenging met toenemende korrelgrootte. Bij korrelgroottes tussen de  $1$  en  $10 \mu\text{m}$  neemt de ontwikkeling van de dislocatiedichtheid langzaam met de korrelgrootte toe, om te convergeren naar een asymptotische waarde voor korrelgroottes groter dan  $10 \mu\text{m}$ . Hierdoor neemt de homogene verlenging eerst langzaam toe om daarna te stabiliseren op een constante waarde. Het model laat zien dat een mogelijke aanpak voor het verbeteren van de vervormbaarheid van ultra-fijnkorrelige legeringen gevonden kan worden door de maximale dislocatiedichtheid in het inwendige van de korrels te laten stijgen. Dit kan bereikt worden door de activeringsenergie voor dynamisch herstel te laten toenemen. Op basis van de voorspellingen van dit model en uitgaande van een korrelgrootte van  $0.4 \mu\text{m}$ , kan de “ware” uniforme rek van IF staalsoorten stijgen van  $4.3\%$  naar  $28.2\%$  indien de activeringsenergie voor herstel stijgt van  $0.766 \text{ eV}$  naar  $0.8 \text{ eV}$ . Voor aluminium AA1100 legeringen neemt de uniforme rek toe van  $2.2\%$  naar  $26.3\%$

bij een toename van de activeringsenergie van 0.748 eV naar 0.78 eV. Legerings-elementen welke resulteren in een verhoging van de activeringsenergie (welke zelf mogelijk gerelateerd is aan de smelttemperatuur) bieden derhalve in potentie een mogelijkheid voor het verbeteren van de vervormbaarheid van ultra-fijnkorrelige legeringen resulterend in een verbeterde toepasbaarheid in technische applicaties.

De in de eerdere hoofdstukken ontwikkelde aanpak is toepasbaar voor deformaties bij lage reksnelheden en onder isotherme condities. In hoofdstuk 5 is het irreversibele thermodynamica model verder uitgebreid naar hoge reksnelheden. Onder deze condities, waarbij de reksnelheden hoger zijn dan  $10^2 \text{ s}^{-1}$ , is er te weinig tijd om warmte kwijt te raken aan de omgeving, waardoor er niet langer een warmtestroom optreedt. De snelheid van entropieproductie wordt nu beschreven in de som van producten van gegeneraliseerde krachten en bijbehorende debieten van de irreversibele processen. Het verloop van de kinetiek van de gemiddelde dislocatiedichtheid is onderzocht en deze laat een drastische toename zien bij reksnelheden boven de  $10^3 \text{ s}^{-1}$  resulterend in aanzienlijke toename van de vloeispanning. Een dergelijk gedrag is voor diverse verschillende metallische systemen experimenteel waargenomen. Met behulp van het model kan verklaard worden dat fononinteractie effecten bij hoge dislocatiesnelheden zorgen voor een significante verhoging van de dislocatievermenigvuldigingssnelheid. Dit vermenigvuldigingsmechanisme is mogelijk gerelateerd aan de energiedissipatie tijdens hoge snelheidsverplaatsingen van dislocaties. De hoeveelheid gedissipeerde energie is mogelijk groot genoeg voor de vorming van nieuwe dislocaties in de nabijheid van de bewegende dislocatie. Het is bewezen dat de bijdrage van de fononinteractieterm bij lage reksnelheden verdwijnt, en dat het model vereenvoudigt tot een vergelijking die lijkt op die van het klassieke Kocks-Mecking model. De voorspellingen van het model komen overeen met experimenteel bepaalde kracht-rek krommes voor polykristallijn Cu over het reksnelheidsbereik van  $1.5 \times 10^{-2}$  tot  $6.4 \times 10^5 \text{ s}^{-1}$ .

Het model uit hoofdstuk 5 is verder uitgebreid in hoofdstuk 6 om de effecten van korrelgrootte en legeringselementen bij lage tot middelmatige reksnelheden te combineren. Onder deze deformatiecondities kunnen de fononinteractie-effecten verwaarloosd worden. Het model is toegepast op de warmvervorming in de austenitische toestand van 13 verschillende staalsoorten uit drie staalklassen (IF, LC en MC). Een vergelijking tussen de kwaliteit van de voorspellingen van het nieuwe model en een model dat nu in de industrie gebruikt wordt, laat zien dat beide modellen een zelfde nauwkeurigheid bereiken. Het nieuwe model maakt echter gebruik van minder fitting parameters maar is wel in staat om rekening te houden met de effecten van de reksnelheid en is tevens in staat om het verloop van de dislocatiedichtheid tijdens de vervorming te beschrijven.

# Appendix A

## A Statistical Mechanics Model for Grain Deformation

### A.1 Introduction

The main contents of this thesis deal with plastic deformation in metals by employing irreversible thermodynamics at a mesoscale level. Down to the atomic level, Rivera Díaz del Castillo and Van der Zwaag [18] recently proposed a two dimensional single grain model for describing the plastic deformation in metals based on the equilibrium thermodynamics and statistical mechanics. The energetically most favourable atomic configuration after the plastic deformation is quantified in the model distinguishing atoms in the grain interior and at the grain boundary. The details of the model are introduced next and some of its potential applications are discussed. The limitations of the model are also demonstrated.

### A.2 Model

Consider a two dimensional hexagonal grain (one  $\{111\}$  atomic plane of FCC metals) isolated from its neighbouring microstructure (figure A.1). The plastic deformation process is described in terms of the displacement of rows of atoms. As demonstrated in figure A.1, when a stress  $\sigma_a$  is applied to the grain, the atoms in rows 1, 2, ...,  $m/2 - 1$  will be displaced successively towards the edges of the grain, and/or redistributed into the bulk.

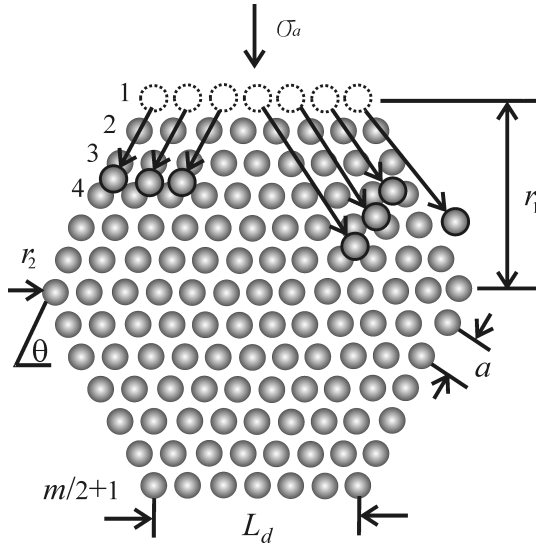


FIGURE A.1. Schematic representation of the deformed grain. One atom row is displaced by two mechanisms: (1) bond breaking atoms displaced to the edge of the grain and (2) dislocation atoms redistributed into the grain bulk. There are  $m/2 + 1$  atom rows in this grain. In this representation, 1 bond breaking atom and 6 dislocation atoms forming two dislocations are shown.

### A.2.1 Bond breaking or dislocation production atoms

During the displacement of one atomic row consisting  $n_r$  atoms (figure A.1),  $n_b$  atoms (defined as *bond breaking atoms*) will be displaced towards the edges of the grain and  $n_\perp$  atoms (defined as *dislocation atoms*) will be redistributed into the bulk ( $n_r = n_b + n_\perp$ ). If all  $n_\perp$  atoms are displaced in one line in the bulk, it is said that one “*dislocation*” is formed. If  $n_\perp$  atoms are divided into  $n_d$  lines, it is said that  $n_d$  “*dislocation*” are formed (e.g. 2 dislocations are schematically shown in figure A.1). In this ideal two dimensional model, the definition of dislocation has to be redefined. It is not the same definition as the one used in real three dimensional case in literature [60].

The first step towards a quantitative description of the possible atom arrangements by deformation of the grain requires the calculation of the number of combinations  $\Omega_1$  by which  $n_\perp$  atoms can be selected from a set of  $n_r$  available atoms composing the grain considered:

$$\Omega_1 = \frac{n_r!}{n_\perp!(n_r - n_\perp)!} = \frac{n_r!}{n_\perp!(n_r - n_\perp)!} \quad (\text{A.1})$$

### A.2.2 Bond breaking and dislocation atom arrangements

The bond breaking atoms can be ordered by arranging them on the available sites on the grain free interface. Say  $m/2 + 1$  atom rows can be counted across the direction where the grain is deformed (figure A.1). After deformation of one atom row there are  $m/2$  rows and  $m$  positions ( $m/2$  per side) where the atoms can be arranged (figure A.1). The arrangement of  $n_b$  atoms in  $m$  positions is isomorphic to the calculation of the number of ways of ordering  $n_b$  distinguishable objects in  $m$  distinguishable positions:

$$\Omega_2 = n_b!m! \quad (\text{A.2})$$

Similarly, each of the  $n_{\perp}$  distinguishable atoms that form dislocations can be ordered by a number of ways given by

$$\Omega_3 = n_{\perp}! \quad (\text{A.3})$$

### A.2.3 Dislocation line arrangements in the grain interface and bulk

Say the  $n_{\perp}$  dislocation atoms are decomposed into  $n_d$  dislocations. The number of possible dislocation line arrangements can be quantified by calculating the number of ways of placing  $n_d$  dislocation lines end in  $P_d$  interface points. The possible number of such arrangements is given by

$$\Omega_4 = n_d + P_d - 1 \quad (\text{A.4})$$

A dislocation can start in the bulk and end at the grain interface, having in between a number of kinks present. This situation is shown schematically in figure A.2a, where the vectors  $d_1$ ,  $d_2$ ,  $d_3$ , and  $d_4$  account for kinks of the dislocation line, and produce  $c = 3$  changes of direction. Thus the possibility of dislocation line direction changes imposes another way of atom arrangement to be quantified. This is introduced by defining the *envelope* of a dislocation line as shown in figure A.2b. The envelope is characterised by an area termed “area of the envelope” ( $A_E$ ), whereas the dislocation line will be able to extend itself only within the dashed area shown in figure A.2b and termed “area of interest” ( $A_I$ ).

Assuming that the dislocation finishes not on a grain boundary point (figure A.2a) but at any point within the grain, for  $c$  direction changes in an FCC structure at the referred orientation, the possibilities for direction change are 6 between the dislocation end and the first change, 4 for the second change and so on until reaching the start of the dislocation. Thus counting  $6 \times 4^{c-1}$  possibilities. However, these are constrained by the area of interest of the dislocations, and the number of ways a dislocation ending in point  $P_e$  shown in figure A.2b can change direction

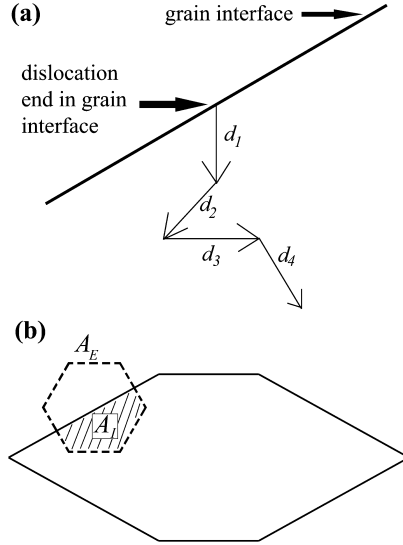


FIGURE A.2. To describe how dislocation can be arranged by (a) dislocation direction changes, which extend across (b) an area of interest termed  $A_I$

is approximated as

$$\Omega_5 = \sum_{i=1}^{n_d} \frac{A_{Ii}}{A_E} \times 6 \times 4^{c-1} = \frac{6 \times 4^{c-1}}{A_E} \sum_{i=1}^{n_d} A_{Ii} \quad (\text{A.5})$$

It is noted that  $A_{Ii}$  changes with the interface point  $i$  where the dislocation is assumed to end.

#### A.2.4 Entropy production

The number of ways the system can be ordered to produce one atom row deformation is equal to the number of ways of ordering the bond breaking atoms plus the number of ways of ordering the dislocation atoms. Thus the entropy increase due to this deformation process is given by

$$S = k \ln(\Omega_1 \Omega_2 + \Omega_1 \Omega_3 \Omega_4 \Omega_5) \quad (\text{A.6})$$

where  $k$  is the Boltzmann constant.

### A.2.5 Deformation energy

Along with an expression for entropy, the stored energy  $U$  of the system is to be quantified. This is an addition of the contributions of two elements: (1) the bond breaking atoms (2) the dislocations induced in the microstructure. This can be expressed as [18]

$$U = \underbrace{E_b n_b}_i + \underbrace{\frac{\sqrt{3}}{2} a \mu b^2 n_d \left( \frac{1}{2} + 2c \right)}_{ii} \quad (\text{A.7})$$

where  $E_b$  is the average atomic bond energy,  $a$  is the lattice constant and  $\mu$  is the shear modulus. Term  $i$  accounts for the contribution of bond breaking energy and term  $ii$  is the contribution of the dislocations.

### A.2.6 Geometrical simplifications

So far an equation for the system entropy and energy which depends on a great number of geometrical variables have been presented. The problem is highly simplified by acknowledging the relationships existing between them. In equation A.2, the number of planes  $m$  is given by equating the number of planes per side with the number of planes counted in an FCC structure aligned in the [111] direction and characterised by a lattice parameter  $a$ :

$$\frac{m}{2} = \frac{2r_1}{a\sqrt{\frac{3}{8}}} \Rightarrow m = 8\sqrt{\frac{2}{3}} \frac{r_1}{a} \quad (\text{A.8})$$

Similarly, the total number of one row of atoms  $n_r$  is given by

$$n_r = \sqrt{2} \frac{L_d}{a} \quad (\text{A.9})$$

By counting the number of atoms in the interface, it can be seen that  $P_d$  in equation A.4 can be expressed as

$$P_d = \frac{2\sqrt{2}L_d}{a} + \frac{\sqrt{2}}{a} \sqrt{4r_1^2 + (2r_2 - L_d)^2} \quad (\text{A.10})$$

The angle of deformation  $\theta$  in figure A.1 is expressed as

$$\theta = \tan^{-1} \left( \frac{2r_1}{2r_2 - L} \right) \quad (\text{A.11})$$

Note that this angle has not been used so far in the previous formulae, but will be included in the forthcoming theory.

Finally, it is seen that the volume of the grain remains unchanged throughout deformation. Therefore there is an additional relationship between the variables that describe the grain shape through the known area  $A$  the grain:

$$A = (L + 2r_2) r_1 \quad (\text{A.12})$$

In summary, the number of  $m$  planes and  $n_r$  atoms can be calculated in terms of the lattice parameter  $a$  and one of the geometrical parameters that describe the grain.

Given that the original size of the grain is assumed to be known,  $A$  and the degree of deformation  $r_1 - \Delta r_1$  are known; therefore, the geometrical parameters that describe the grain  $(r_1, r_2, L_d, \theta)$  are reduced to only one by employing equations A.10 to A.12.

### A.2.7 Thermodynamical equations

In addition to the equations A.6 and A.7 for the system energy and the entropy, respectively, the thermodynamical stability of the deformation process requires energy conservation and the maximisation of entropy.

The energy conservation consideration comes from considering the nature of the deformation process occurring. The energy spent on the deformation of a single atomic row is given by

$$dU = \frac{3}{16} \sigma_a L_d a dr_1 \quad (\text{A.13})$$

where  $\sigma_a$  is the stress required to deform a grain.

Finally, during displacing one row of atoms, stability of the deformation process requires

$$dS = 0 \quad (\text{A.14})$$

### A.2.8 Solution of the system

Four thermodynamic equations have been presented: A.6, A.7 A.13 and A.14. The variables are  $n_\perp$ ,  $n_d$ ,  $U$ ,  $S$ ,  $\theta$ ,  $c$ . Thus, apparently the system has multiple solutions; however, the theory developed so far is for a single-grain scenario, a non-physical situation. When the grains are assembled in a microstructure, an additional geometrical parameter may be obtained through simultaneous solution of the equations describing each grain, this will enable to determine  $\theta$ . For the forthcoming calculations, a value of  $\theta = 60^\circ$  will be assumed to remain constant as deformation proceeds.

During displacing one row of atoms, the differential changes of energy is expressed as

$$\begin{aligned} dU &= E_b(dn_r - dn_{\perp}) + \frac{\sqrt{3}}{2}a\mu b^2 \left(\frac{1}{2} + 2c\right) dn_d + \frac{\sqrt{3}}{2}a\mu b^2 2n_d dc \\ &= -E_b dn_{\perp} + \frac{\sqrt{3}}{2}a\mu b^2 \left(\frac{1}{2} + 2c\right) dn_d + \frac{\sqrt{3}}{2}a\mu b^2 2n_d dc \end{aligned} \quad (\text{A.15})$$

by using equation A.7 and  $n_b = n_r - n_{\perp}$  and acknowledging  $n_r$  is a constant. Equations A.13 and A.15 are equal, which offers

$$S_r = -E_r dn_{\perp} + \left(\frac{1}{2} + 2c\right) dn_d + 2n_d dc \quad (\text{A.16})$$

where

$$S_r = \frac{\sqrt{3}}{8} \frac{\sigma L_d a}{a\mu b^2} dr_1 \quad (\text{A.17})$$

$$E_r = \frac{2}{\sqrt{3}} \frac{E_b}{a\mu b^2} \quad (\text{A.18})$$

are the ratios of the strain energy and dislocation energy, and the bond breaking energy and dislocation energy, respectively.

Substituting equation A.6 in equation A.14 offers

$$dS = 0 = \ln(n_r - n_{\perp}) dn_{\perp} + \ln(n_d + P_d - 1) dn_d + \ln 4 \quad (\text{A.19})$$

Equations A.16 and A.19 may be rearranged as a pair of simultaneous equations as

$$-E_r dn_{\perp} + \left(\frac{1}{2} + 2c\right) dn_d = S_r - 2n_d dc \quad (\text{A.20})$$

$$\ln(n_r - n_{\perp}) dn_{\perp} + \ln(n_d + P_d - 1) dn_d = -\ln 4 \quad (\text{A.21})$$

where the dislocation disorder  $dc$  is assumed to be a parameter dependent upon the conditions under which the deformation is carried out, rendering thus just two variables for the system:  $dn_{\perp}$  and  $dn_d$ . The solution of the system is given by

$$dn_{\perp} = \frac{1}{d_E} [(-\ln(4)dc)(1/2 + 2c) - (S_r - 2n_d dc) \ln(n_d P_d - 1)] \quad (\text{A.22})$$

$$dn_d = \frac{1}{d_E} [\ln(n_r - n_{\perp})(S_r - 2n_d dc) - E_r \ln(4)dc] \quad (\text{A.23})$$

where

$$d_E = \ln(n_r - n_{\perp})(1/2 + 2c) - E_r \ln(n_d + P_d - 1) \quad (\text{A.24})$$

### A.3 Application of the model

The model was applied to the hot deformation of steel in the austenitic condition (single FCC phase). Thus, typical steel properties were employed as input:  $a = b = 2 \times 10^{-10}$  m,  $\sigma = 400$  MPa,  $E_r = 0.5$ ,  $\mu = 83$  GPa.

Equations A.22 and A.23 describe the evolution of the deformation process in terms of the increase in the number of atoms going to dislocations and the number of dislocations. Since the thermodynamic equations describe the most energetically favourable changes in the thermodynamic variables, it is necessary to describe the initial state of deformation in terms of: (1) the initial number of atoms in the deformation process that contribute to the dislocation formation or bond breaking processes, this parameter was normalised as  $n_{\perp}/n_r$  and will be referred as the dislocation atom fraction, in which an initial value of 1 indicates that the deformation starts by the formation of dislocations only; (2) the initial dislocation density in the grain; (3) the number of direction changes per dislocation  $c$  prior to deformation. Additionally, it is required to set a value for  $dc$ .

The model is first applied to a grain assumed to have an initial hexagonal shape, and an initial dislocation density  $\rho_0 = 5 \times 10^{12}$  m<sup>-2</sup>. The dislocation density is defined as  $n_d/A$ . It is noted that the initial aspect ratio for such a grain is approximately 1.15 due to the shape assumption.

Perhaps some of the most interesting predictions of this model are those shown in figure A.3, which displays the variation of the dislocation density with grain aspect ratio, and indicates that small grain sizes of  $10^{-7}$  m are characterised by a dislocation density of three orders of magnitude larger than large grains of the order of  $10^{-4}$  m. Furthermore, this dislocation density approaches an asymptotic value almost immediately after the deformation process starts with large grains of  $10^{-5}$  and  $10^{-4}$  m, whereas the  $10^{-7}$  m grain keeps forming dislocations even at a grain aspect ratio of 10, which implies a very big strain. Figure A.3 shows also that as the  $dc$  value is increased from 0.005 to 0.1, the asymptotic value for the selected grain sizes is lowered by about one order of magnitude, and is reached at a faster pace with the increase of  $dc$ .

### A.4 Limitations of the model

The objective of the proposed model is to describe the plastic deformation of bulk FCC metals. However, the model is based on one atomic plane. In such two dimensional model, the deformation may be induced by displacing one row of atoms as described in the model. In contrast the plastic deformation in the

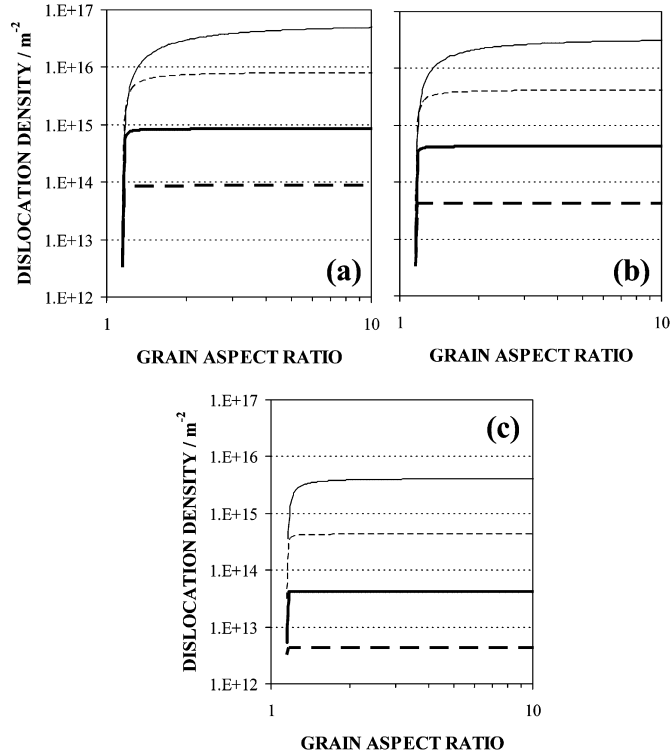


FIGURE A.3. Dislocation density variation with grain aspect ratio for selected grain sizes and  $dc =$  (a) 0.005, (b) 0.01, (c) 0.1. Value of grain size of  $10^{-7}$ ,  $10^{-6}$ ,  $10^{-5}$ , and  $10^{-4}$  m are represented by the thin solid and dotted lines, and the thick solid and dotted lines, respectively.

real bulk metals is induced by the glide of linear defects (dislocations). These two mechanisms are substantially different.

One “dislocation” in the model is defined as one extra row of atoms in the interior of one atomic plane (figure A.1). ignoring the change of the direction of such extra row of atoms, the strain energy of such “dislocation” is approximately  $\sqrt{3}a\mu b^2/4$ . In this strain energy term, the number of atoms in the extra row is not relevant. However, one would expect that more atoms in the extra row will cause more distortion in the lattice, which will induce higher strain energy. For instance, if the extra row contains 2 atoms, it could be seen as two point defects. If it has 10 atoms, it corresponds to 10 point defects. The strain energy of the 10 atoms should be higher than the 2 atoms considered here.

Furthermore, the model assumes that the entropy of the system is constant during the deformation ( $dS = 0$ ). However, if some “dislocation” are presented, the entropy of the system changes due to the change of arrangement of the atoms.

In conclusion, the model proposed in this appendix might provide a new approach to describe the plastic deformation of FCC metals, but it requires further development.

# Bibliography

- [1] Allain, S., Chateau, J.P., Bouaziz, O., Migot, S., Guelton, N.: Correlations between the calculated stacking fault energy and the plasticity mechanisms in fe-mn-c alloys. *Materials Science and Engineering A* **387-389**, 158–162 (2004)
- [2] Argon, A.S., Moffatt, W.C.: Climb of extended edge dislocations. *Acta Metallurgica* **29**(2), 293–299 (1981)
- [3] Armstrong, R.W., Arnold, W., Zerilli, F.J.: Dislocation mechanics of shock-induced plasticity. *Metallurgical and Materials Transactions A* **38**(11), 2605–2610 (2007)
- [4] Ashby, M.F.: The deformation of plastically non-homogeneous materials. *Philosophical Magazine* **21**, 399–424 (1970)
- [5] Bailey, J.E., Hirsch, P.B.: The dislocation distribution, flow stress, and stored energy in cold-worked polycrystalline silver. *Philosophical Magazine* **5**, 485–497 (1960)
- [6] Bay, B., Hansen, N., Hughes, D.A., Kuhlmann-Wilsdorf, D.: Overview no. 96 evolution of f.c.c. deformation structures in polyslip. *Acta Metallurgica et Materialia* **40**(2), 205–219 (1992)

- [7] Bhadeshia, H.K.D.H., Honeycombe, R.W.K.: *Steels Microstructure and Properties*, third edn. Elsevier, Oxford (2006)
- [8] Bodin, A.: *Intercritical deformation of low-alloy steels*. Ph.D. thesis, Delft University of Technology (2002)
- [9] Bonneville, J., Escaig, B.: Cross-slipping process and the stress-orientation dependence in pure copper. *Acta Metallurgica* **27**(9), 1477–1486 (1979)
- [10] Bouaziz, O., Dirras, G.: Effet de la taille de grain sur les écrouissages isotrope et cinématique dans la gamme 0.35 à 75  $\mu\text{m}$ . In: *MATERIAUX 2006*. Dijon, France (2006)
- [11] Bouaziz, O., Feuillu, D., Quidort, D.: *Prévision du comportement des aciers à l'état austénitique*. Internal report, ArcelorMittal (2001)
- [12] Bouaziz, O., Guelton, N.: Modelling of twip effect on work-hardening. *Materials Science and Engineering A* **319-321**, 246–249 (2001)
- [13] Bouaziz, O., Iung, T., Kandel, M., Lecomte, C.: Physical modelling of microstructure and mechanical properties of dual-phase steel. *Journal de Physique IV* **11**, 223–231 (2001)
- [14] Bréchet, Y.J.M., Canova, G.R., Kubin, L.P.: Static versus propagative plastic strain localisations. *Scripta Metallurgica et Materialia* **29**(9), 1165–1170 (1993)
- [15] Bridgman, P.: *The Nature of Thermodynamics*. Harper & Row, New York (1961)
- [16] Brown, A.M., Ashby, M.F.: Correlations for diffusion constants. *Acta Metallurgica* **28**(8), 1085–1101 (1980)
- [17] Callen, H.: *Thermodynamics and an introduction to thermostatistics*, second edition edn. John Wiley & Sons, Inc., New York (1985)
- [18] Rivera Díaz del Castillo, P.E.J., van der Zwaag, S.: A statistical mechanics theory of grain deformation and its prediction of dynamical recovery and recrystallization. *Materials Science Forum* **467-470**, 87–92 (2004)
- [19] Cizek, P.: Characteristics of the equiaxed cell block structure formed within cube-textured grains during tensile deformation of aluminium. *Scripta Materialia* **45**(7), 815–822 (2001)
- [20] Coble, R.L.: A model for boundary diffusion controlled creep in polycrystalline materials. *Journal of Applied Physics* **34**(6), 1679–1682 (1963)

- [21] De Hosson, J.T.M., Boom, G., Schlagowski, U., Kanert, O.: Solution hardening in al—zn alloys mean jump distance and activation length of moving dislocations. *Acta Metallurgica* **34**(8), 1571 (1986)
- [22] De Hosson, J.T.M., Roos, A., Metselaar, E.D.: Temperature rise due to fast-moving dislocations. *Philosophical Magazine A* **81**(5), 1099–1120 (2001)
- [23] De Hosson, J.T.M., Huis in't Veld, A., Tamler, H., Kanert, O.: Dislocation dynamics in al-li alloys. mean jump distance and activation length of moving dislocations. *Acta Metallurgica* **32**(8), 1205–1215 (1984)
- [24] DeHoff, R.T.: *Thermodynamics in Materials Science*. McGraw-Hill, Inc., New York (1993)
- [25] Delince, M., Bréchet, Y., Embury, J.D., Geers, M.G.D., Jacques, P.J., Pardoen, T.: Structure-property optimization of ultrafine-grained dual-phase steels using a microstructure-based strain hardening model. *Acta Materialia* **55**(7), 2337–2350 (2007)
- [26] Devincere, B., Hoc, T., Kubin, L.: Dislocation mean free paths and strain hardening of crystals. *Science* **320**, 1745–1748 (2008)
- [27] Dieter, G.: *Mechanical metallurgy*. McGraw-Hill, New York (1986)
- [28] Doherty, R.D., Hughes, D.A., Humphreys, F.J., Jonas, J.J., Jensen, D.J., Kassner, M.E., King, W.E., McNelley, T.R., McQueen, H.J., Rollett, A.D.: Current issues in recrystallization: a review. *Materials Science and Engineering A* **238**(2), 219–274 (1997)
- [29] El-Azab, A.: Statistical mechanics treatment of the evolution of dislocation distributions in single crystals. *Physical Review B* **61**(18), 11,956 (2000)
- [30] El-Azab, A.: The statistical mechanics of strain-hardened metals. *Science* **320**, 1729–1730 (2008)
- [31] Estrin, Y., Mecking, H.: A unified phenomenological description of work hardening and creep based on one-parameter models. *Acta Metallurgica* **32**(1), 57–70 (1984)
- [32] Estrin, Y., Tóth, L.S., Molinari, A., Bréchet, Y.: A dislocation-based model for all hardening stages in large strain deformation. *Acta Materialia* **46**(15), 5509–5522 (1998)

- [33] Fischer, F.D., Svoboda, J.: Void growth due to vacancy supersaturation - a non-equilibrium thermodynamics study. *Scripta Materialia* **58**(2), 93–95 (2008)
- [34] Fischer, F.D., Svoboda, J., Fratzl, P.: A thermodynamic approach to grain growth and coarsening. *Philosophical Magazine* **83**(9), 1075 – 1093 (2003)
- [35] Follansbee, P.S., Kocks, U.F.: A constitutive description of the deformation of copper based on the use of the mechanical threshold stress as an internal state variable. *Acta Metallurgica* **36**(1), 81–93 (1988)
- [36] Follansbee, P.S., Weertman, J.: On the question of flow stress at high strain rates controlled by dislocation viscous flow. *Mechanics of Materials* **1**(4), 345–350 (1982)
- [37] Forland, K., Forland, T., Ratkje, S.: *Irreversible Thermodynamics: Theory and Application*. John Wiley & Sons, New York (1988)
- [38] Fournet, R., Salazar, J.M.: Formation of dislocation patterns: Computer simulations. *Physical Review B* **53**(10), 6283–6290 (1996). Copyright (C) 2007 The American Physical Society Please report any problems to prola@aps.org PRB
- [39] Gao, W., Belyakov, A., Miura, H., Sakai, T.: Dynamic recrystallization of copper polycrystals with different purities. *Materials Science and Engineering A* **265**(1-2), 233–239 (1999)
- [40] Gaskell, D.R.: *Introduction to the Thermodynamics of Materials*, fifth edn. Taylor & Francis, New York (2008)
- [41] van der Giessen, E., Needleman, A.: Discrete dislocation plasticity: a simple planar model. *Modelling and Simulation in Materials Science and Engineering* **3**, 689–735 (1995)
- [42] Gottstein, G.: *Physical Foundations of Materials Science*. Springer, Berlin (2004)
- [43] Gottstein, G., Argon, A.S.: Dislocation theory of steady state deformation and its approach in creep and dynamic tests. *Acta Metallurgica* **35**(6), 1261–1271 (1987)
- [44] Gottstein, G., Bewerunge, J., Mecking, H., Wollenberger, H.: Stored energy of 78 k tensile deformed copper crystals. *Acta Metallurgica* **23**(5), 641–652 (1975)

- [45] Gottstein, G., Kocks, U.F.: Dynamic recrystallization and dynamic recovery in  $\langle 111 \rangle$  single crystals of nickel and copper. *Acta Metallurgica* **31**(1), 175–188 (1983)
- [46] Gottstein, G., Lee, T., Schmidt, U.: Deformation temperature and recrystallization. *Materials Science and Engineering A* **114**, 21–28 (1989)
- [47] Groma, I.: Link between the microscopic and mesoscopic length-scale description of the collective behavior of dislocations. *Physical Review B* **56**(10), 5807 (1997)
- [48] Groma, I., Pawley, G.S.: Role of the secondary slip system in a computer simulation model of the plastic behaviour of single crystals. *Materials Science and Engineering A* **164**(1-2), 306–311 (1993)
- [49] Haasen, P.: *Physical Metallurgy*, third edn. Cambridge University Press, Cambridge (1996)
- [50] Hähner, P.: A theory of dislocation cell formation based on stochastic dislocation dynamics. *Acta Materialia* **44**(6), 2345–2352 (1996)
- [51] Hähner, P., Bay, K., Zaiser, M.: Fractal dislocation patterning during plastic deformation. *Physical Review Letters* **81**(12), 2470–2473 (1998)
- [52] Hansen, N.: The effect of grain size and strain on the tensile flow stress of aluminium at room temperature. *Acta Metallurgica* **25**(8), 863–869 (1977)
- [53] Hansen, N.: Boundary strengthening in undeformed and deformed polycrystals. *Materials Science and Engineering: A* **409**(1-2), 39–45 (2005)
- [54] Hansen, N., Kuhlmann-Wilsdorf, D.: Low energy dislocation structures due to unidirectional deformation at low temperatures. *Materials Science and Engineering* **81**, 141–161 (1986)
- [55] Hart, E.W.: A phenomenological theory for plastic deformation of polycrystalline metals. *Acta Metallurgica* **18**(6), 599–610 (1970)
- [56] Herring, C.: Diffusional viscosity of a polycrystalline solid. *Journal of Applied Physics* **21**(5), 437–445 (1950)
- [57] Hillert, M., Agren, J.: Extremum principles for irreversible processes. *Acta Materialia* **54**(8), 2063 (2006)

- [58] Hirsch, E., Plešek, J.: A theoretical analysis of experimental results of shock wave loading of copper relating the observed internal structure to the deformation mechanism. *International Journal of Impact Engineering* **32**(1), 1339–1356 (2006)
- [59] Hirsch, P., Cockayne, D., Spence, J., Whelan, M.: 50 years of theory of dislocations: Past, present and future. *Philosophical Magazine* **86**(29), 4519–4528 (2006)
- [60] Hirth, J.P., Lothe, J.: *Theory of Dislocations*. John Wiley & Sons, New York (1982)
- [61] Hirth, J.P., Zbib, H.M., Lothe, J.: Forces on high velocity dislocations. *Modelling and Simulation in Materials Science and Engineering* **6**(2), 165–169 (1998)
- [62] Holt, D.L.: Dislocation cell formation in metals. *Journal of Applied Physics* **41**(8), 3197–3201 (1970)
- [63] Hosford, W.F., Fleischer, R.L., Backofen, W.A.: Tensile deformation of aluminum single crystals at low temperatures. *Acta Metallurgica* **8**(3), 187–199 (1960)
- [64] Huang, M., Rivera Díaz del Castillo, P.E.J., Bouaziz, O., van der Zwaag, S.: Irreversible thermodynamics modelling of plastic deformation of metals. *Materials Science and Technology* **24**(4), 495–500 (2008)
- [65] Huang, M., Rivera Díaz del Castillo, P.E.J., Bouaziz, O., van der Zwaag, S.: Modelling strength and ductility of ultrafine grained bcc and fcc alloys using irreversible thermodynamics. *Materials Science and Technology* (accepted)
- [66] Huang, M., Rivera Díaz del Castillo, P.E.J., van der Zwaag, S.: Modelling dynamic recovery and recrystallization of metals by a new non-equilibrium thermodynamics approach. *Materials Science Forum* **558-559**, 517–522 (2007)
- [67] Huang, M., Rivera Díaz del Castillo, P.E.J., van der Zwaag, S.: Modelling steady state deformation of fcc metals by non-equilibrium thermodynamics. *Materials Science and Technology* **23**(9), 1105–1108 (2007)
- [68] Humphreys, F., Hatherly, M.: *Recrystallization and Related Annealing Phenomena*. Elsevier, Oxford (2004)
- [69] Jakobsen, B., Poulsen, H.F., Lienert, U., Almer, J., Shastri, S.D., Sørensen, H.O., Pantleon, C.G.W.: Formation and subdivision of deformation structures during plastic deformation. *Science* **312**, 889–892 (2006)

- [70] Kapoor, R., Nemat-Nasser, S.: Comparison between high and low strain-rate deformation of tantalum. *Metallurgical and Materials Transactions A* **31**(3), 815–823 (2000)
- [71] Kassner, M.E., Perez-Prado, M.T.: Five-power-law creep in single phase metals and alloys. *Progress in Materials Science* **45**(1), 1 (2000)
- [72] Kjelstrup, S., Bedeaux, D.: *Non-equilibrium Thermodynamics of Heterogeneous Systems*. World Scientific Publishing Co. Pte. Ltd, Singapore (2008)
- [73] Kocks, U.F., Mecking, H.: Physics and phenomenology of strain hardening: the fcc case. *Progress in Materials Science* **48**(3), 171–273 (2003)
- [74] Koizumi, H., Kirchner, H.O.K., Suzuki, T.: Lattice wave emission from a moving dislocation. *Physical Review B* **65**(21), 214,104 (2002)
- [75] Kubin, L.P., Canova, G.: The modelling of dislocation patterns. *Scripta Metallurgica et Materialia* **27**(8), 957–962 (1992)
- [76] Kuhlmann-Wilsdorf, D.: The theory of dislocation-based crystal plasticity. *Philosophical Magazine A* **79**, 955–1008 (1999)
- [77] Kuiken, G.: *Thermodynamics for Irreversible Processes*. Wiley, Chichester (1994)
- [78] Lee, W.S., Chen, T.H.: Rate-dependent deformation and dislocation substructure of al-sc alloy. *Scripta Materialia* **54**(8), 1463–1468 (2006)
- [79] Lee, W.S., Shyu, J.C., Chiou, S.T.: Effect of strain rate on impact response and dislocation substructure of 6061-t6 aluminum alloy. *Scripta Materialia* **42**(1), 51–56 (2000)
- [80] Li, J.C.M.: Petch relation and grain boundary sources,. *Transactions of the Metallurgical Society of AIME* **227** (1963)
- [81] Livingston, J.D.: The density and distribution of dislocations in deformed copper crystals. *Acta Metallurgica* **10**(3), 229–239 (1962)
- [82] Marthinsen, K., Nes, E.: Modelling strain hardening and steady state deformation of al-mg alloys. *Materials Science and Technology* **17**, 376 (2001)
- [83] Mecking, H., Kocks, U.F.: Kinetics of flow and strain-hardening. *Acta Metallurgica* **29**(11), 1865–1875 (1981)
- [84] Mecking, H., Nicklas, B., Zarubova, N., Kocks, U.F.: A universal temperature scale for plastic flow. *Acta Metallurgica* **34**(3), 527–535 (1986)

- [85] Meyers, M.A., Andrade, U.R., Chokshi, A.H.: The effect of grain size on the high-strain, high-strain-rate behavior of copper. *Metallurgical and Materials Transactions A* **26**(11), 1543–1940 (1995)
- [86] Meyers, M.A., Benson, D.J., Vöhringer, O., Kad, B.K., Xue, Q., Fu, H.H.: Constitutive description of dynamic deformation: physically-based mechanisms. *Materials Science and Engineering A* **322**(1-2), 194–216 (2002)
- [87] Meyers, M.A., Gregori, F., Kad, B.K., Schneider, M.S., Kalantar, D.H., Remington, B.A., Ravichandran, G., Boehly, T., Wark, J.S.: Laser-induced shock compression of monocrystalline copper: characterization and analysis. *Acta Materialia* **51**(5), 1211–1228 (2003)
- [88] Mishin, Y., Herzig, C.: Grain boundary diffusion: recent progress and future research. *Materials Science and Engineering A* **260**(1-2), 55–71 (1999)
- [89] Molinari, A., Ravichandran, G.: Constitutive modeling of high-strain-rate deformation in metals based on the evolution of an effective microstructural length. *Mechanics of Materials* **37**(7), 737–752 (2005)
- [90] Murr, L.: Residual microstructure-mechanical property relationships in shock-loaded metals and alloys. In: M.A. Meyers, L.E. Murr (eds.) *Shock-Wave and High-Strain-Rate Phenomena in Metals*, p. 607. Plenum Press, New York (1981)
- [91] Nabarro, F.R.N.: Work hardening and dynamical recovery of f.c.c. metals in multiple glide. *Acta Metallurgica* **37**(6), 1521–1546 (1989)
- [92] Narutani, T., Takamura, J.: Grain-size strengthening in terms of dislocation density measured by resistivity. *Acta Metallurgica et Materialia* **39**(8), 2037–2049 (1991)
- [93] Nemat-Nasser, S., Guo, W.G., Kihl, D.P.: Thermomechanical response of al-6xn stainless steel over a wide range of strain rates and temperatures. *Journal of the Mechanics and Physics of Solids* **49**(8), 1823–1846 (2001)
- [94] Nemat-Nasser, S., Yulong, L.: Flow stress of f.c.c. polycrystals with application to ofhc cu. *Acta Materialia* **46**(2), 565–577 (1998)
- [95] Nes, E.: Constitutive laws for steady state deformation of metals, a microstructural model. *Scripta Metallurgica et Materialia* **33**(2), 225 (1995)
- [96] Nes, E.: Modelling of work hardening and stress saturation in fcc metals. *Progress in Materials Science* **41**(3), 129–193 (1997)

- [97] Nes, E., Marthinsen, K.: Modeling the evolution in microstructure and properties during plastic deformation of f.c.c.-metals and alloys - an approach towards a unified model. *Materials Science and Engineering A* **322**(1-2), 176–193 (2002)
- [98] Nix, W., Gibeling, J., Hughes, D.A.: Time-dependent deformation of metals. *Metallurgical Transactions A* **16**, 2215–2226 (1985)
- [99] Onsager, L.: Reciprocal relations in irreversible processes. i. *Physical Review* **37**(4), 405 (1931)
- [100] Onsager, L.: Reciprocal relations in irreversible processes. ii. *Physical Review* **38**(12), 2265 (1931)
- [101] Oster, G., Silver, I., Tobias, C. (eds.): *Irreversible Thermodynamics and the Origin of Life*. Gordon and Breach, Science Publishers, Inc., New York (1974)
- [102] Pao, Y., Gilat, A.: Modeling 1100-0 aluminum over a wide range of temperatures and strain rates. *International Journal of Plasticity* **5**, 183–196 (1989)
- [103] Parhami, F., McMeeking, R.M., Cocks, A.C.F., Suo, Z.: A model for the sintering and coarsening of rows of spherical particles. *Mechanics of Materials* **31**(1), 43–61 (1999)
- [104] Park, K.T., Han, S.Y., Shin, D.H., Lee, Y.K., Lee, K.J., Lee, K.S.: Effect of heat treatment on microstructures and tensile properties of ultrafine grained c-mn steel containing 0.34 mass% v. *ISIJ International* **44**(6), 1057–1062 (2004)
- [105] Petit, J., Dequiedt, J.L.: Constitutive relations for copper under shock wave loading: Twinning activation. *Mechanics of Materials* **38**(3), 173–185 (2006)
- [106] Poliak, E.I., Jonas, J.J.: A one-parameter approach to determining the critical conditions for the initiation of dynamic recrystallization. *Acta Materialia* **44**(1), 127–136 (1996)
- [107] Prigogine, I.: *Introduction to Thermodynamics of Irreversible Process*. John Wiley and Sons, New York (1961)
- [108] Puchi-Cabrera, E.S.: Constitutive description of plain carbon steels deformed at high temperatures: effect of carbon content. *Materials Science and Technology* **21**, 757–770 (2005)

- [109] Puschl, W.: Models for dislocation cross-slip in close-packed crystal structures: a critical review. *Progress in Materials Science* **47**(4), 415–461 (2002)
- [110] Rios, P.R.: Irreversible thermodynamics, parabolic law and self-similar state in grain growth. *Acta Materialia* **52**(1), 249–256 (2004)
- [111] Rios, P.R., Gottstein, G., Shvindlerman, L.S.: Application of the thermodynamic theory of irreversible processes to normal grain growth. *Scripta Materialia* **44**(6), 893–897 (2001)
- [112] Rocca, R., Bever, M.B.: Thermoelastic effect in iron and nickel (as a function of temperature). *Trans. AIME* **188**, 327–333 (1950)
- [113] Roters, F., Raabe, D., Gottstein, G.: Work hardening in heterogeneous alloys—a microstructural approach based on three internal state variables. *Acta Materialia* **48**(17), 4181–4189 (2000)
- [114] Roucoules, C., Pietrzyk, M., Hodgson, P.D.: Analysis of work hardening and recrystallization during the hot working of steel using a statistically based internal variable model. *Materials Science and Engineering A* **339**(1-2), 1–9 (2003)
- [115] Sakui, S., Sakai, T., Takeishi, K.: Hot deformation of austenite in a plain carbon steel. *Transactions ISIJ* **17**, 718–725 (1977)
- [116] Sandstrom, R., Lagneborg, R.: A controlling factor for dynamic recrystallisation. *Scripta Metallurgica* **9**(1), 59–65 (1975)
- [117] Sandstrom, R., Lagneborg, R.: A model for hot working occurring by recrystallization. *Acta Metallurgica* **23**(3), 387–398 (1975)
- [118] Shan, Z., Stach, E.A., Wiezorek, J.M.K., Knapp, J.A., Follstaedt, D.M., Mao, S.X.: Grain boundary-mediated plasticity in nanocrystalline nickel. *Science* **305**(5684), 654 – 657 (2004)
- [119] Shehadeh, M.A., Bringa, E.M., Zbib, H.M., McNaney, J.M., Remington, B.A.: Simulation of shock-induced plasticity including homogeneous and heterogeneous dislocation nucleations. *Applied Physics Letters* **89**(17), 171,918–3 (2006)
- [120] Shehadeh, M.A., Zbib, H.M., Diaz de la Rubia, T.: Multiscale dislocation dynamics simulations of shock compression in copper single crystal. *International Journal of Plasticity* **21**(12), 2369–2390 (2005)

- [121] Sherby, O.D., Burke, P.M.: Mechanical behavior of crystalline solids at elevated temperature. *Progress in Materials Science* **13**, 323–390 (1968)
- [122] Sinclair, C.W., Poole, W.J., Bréchet, Y.: A model for the grain size dependent work hardening of copper. *Scripta Materialia* **55**(8), 739–742 (2006)
- [123] Soliman, M.S.: Creep of pure metals at intermediate temperatures: Effect of stacking fault energy. *Scripta Metallurgica et Materialia* **29**(7), 987 (1993)
- [124] Song, R., Ponge, D., Raabe, D., Speer, J.G., Matlock, D.K.: Overview of processing, microstructure and mechanical properties of ultrafine grained bcc steels. *Materials Science and Engineering: A* **441**(1-2), 1–17 (2006)
- [125] Swygenhoven, H.V., Derlet, P.M.: Grain-boundary sliding in nanocrystalline fcc metals. *Physical Review B* **64**(22), 224,105 (2001)
- [126] Taylor, G.I.: The mechanism of plastic deformation of crystals. *Proceedings of the Royal Society A* **145**, 362–415 (1934)
- [127] Tsuji, N., Ito, Y., Saito, Y., Minamino, Y.: Strength and ductility of ultrafine grained aluminum and iron produced by arb and annealing. *Scripta Materialia* **47**(12), 893–899 (2002)
- [128] Tsuji, N., Ueji, R., Minamino, Y.: Nanoscale crystallographic analysis of ultrafine grained if steel fabricated by arb process. *Scripta Materialia* **47**(2), 69–76 (2002)
- [129] Valiev, R.Z., Ivanisenko, Y.V., Rauch, E.F., Baudalet, B.: Structure and deformaton behaviour of armco iron subjected to severe plastic deformation. *Acta Materialia* **44**(12), 4705–4712 (1996)
- [130] Walgraef, D.: Rate equation approach to dislocation dynamics and plastic deformation. *Materials Science and Engineering A* **322**(1-2), 167–175 (2002)
- [131] Walgraef, D., Aifantis, E.: On the formation and stability of dislocation patterns i: One-dimensional considerations. *International Journal of Engineering Science* **23**, 1351–1358 (1985)
- [132] Walgraef, D., Aifantis, E.: On the formation and stability of dislocation patterns ii: Two-dimensional considerations. *International Journal of Engineering Science* **23**, 1359–1364 (1985)
- [133] Walgraef, D., Aifantis, E.: On the formation and stability of dislocation patterns iii: Three-dimensional considerations. *International Journal of Engineering Science* **23**, 1365–1372 (1985)

- [134] Zaiser, M., Bay, K., Hähner, P.: Fractal analysis of deformation-induced dislocation patterns. *Acta Materialia* **47**(8), 2463–2476 (1999)
- [135] Zehetbauer, M.: Cold work hardening in stages iv and v of f.c.c. metals—ii. model fits and physical results. *Acta Metallurgica et Materialia* **41**(2), 589–599 (1993)
- [136] Zehetbauer, M., Seumer, V.: Cold work hardening in stages iv and v of f.c.c. metals—i. experiments and interpretation. *Acta Metallurgica et Materialia* **41**(2), 577 (1993)
- [137] Zerilli, F.J., Armstrong, R.W.: Dislocation-mechanics-based constitutive relations for material dynamics calculations. *Journal of Applied Physics* **61**(5), 1816–1825 (1987)
- [138] Zurob, H.S., Hutchinson, C.R., Bréchet, Y., Purdy, G.: Modeling recrystallization of microalloyed austenite: effect of coupling recovery, precipitation and recrystallization. *Acta Materialia* **50**(12), 3075–3092 (2002)

# Acknowledgements

This thesis is the summary of the four-year research work carried out at the group of Fundamentals of Advanced Materials, Faculty of Aerospace Engineering, Delft University of Technology. This thesis would not have been possible without the support and help of many people to whom I would like to express my sincere acknowledgements.

First of all, I would like to gratefully thank my supervisor Prof. dr. ir. Sybrand van der Zwaag for offering me the opportunity to come to Delft to pursue my Ph.D. degree and for his excellent guidance, tremendous support, and enthusiastic encouragements in my research and my personal life. He is an outstanding example of how a supervisor should be. I very much appreciate that he left me sufficient research freedom, which I believe is a key element for a Ph.D. student to grow into an independent researcher. Moreover, whenever I encountered a research problem he was always around me and offered me inspiring discussions and guidance. Another special thank to him is for the fact that he has been always supporting my requests for attending international conferences, which are important for Ph.D. students to show their research works to the rest of the world and to build up professional networks for their future career.

Another very important person to whom I am especially grateful is my daily supervisor Dr. Pedro E.J. Rivera Díaz del Castillo. I thank him for his enormous efforts and very long hours he has spent on my Ph.D. project. Especially, the intensive daily stimulating discussions and his effective suggestions in the first year

were particularly essential to the development of the main concept of this thesis. I would also like to thank him for his great help in improving my written and spoken English, especially for his very detailed revision of the scientific publications. Furthermore, I am particularly grateful to him for being more than simply a supervisor: I have learned a lot from our non-scientific talks and his words in the beer time and dinner time. Thanks a lot Pedro!

I would also like to express my gratitude to Prof. Yves Bréchet (Grenoble Institute of Technology), Prof. Ekkes H. Brüeck (TU Delft), Prof. Jeff Th. M. De Hosson (University of Groningen) and Prof. Leo A. I. Kestens (TU Delft) for being the members of the doctoral committee.

From ArcelorMittal Maizières, I am particularly grateful to Dr. Olivier Bouaziz for his contributions to Chapter 4 (suggesting the back stress model to account for the grain size effects), for his help during my one week visit at ArcelorMittal Maizières, the stimulating discussions in the regular progress meetings hold at ArcelorMittal Maizières, and for his recommendation of my employment at ArcelorMittal Maizières, to Dr. Astrid Perlade for providing the experimental data of Chapter 6 and her valuable comments on Chapters 5 and 6, to Dr. Philippe Maugis for interesting discussions, to Dr. Thierry Jung and Dr. Kangying Zhu for their hospitalities and interesting discussions during my visit at Maizières. I am also grateful to ArcelorMittal Maizières for the financial support.

My warm acknowledgements also go to the friends and (former) colleagues at the FAM group. For Alwin Knijnenberg (my nice officemate for almost 4 years and my paranymp), I thank him for creating a very pleasant office atmosphere, for teaching me Dutch culture and habits, and for translating the summary from English to Dutch. I also acknowledge the good friendship provided by him and his partner Ivette Meester. For Wei Xu, I would like thank him for both the daily scientific and non-scientific discussions. I also like to thank him and his wife Xi Wu for the good friendship, for sharing lots of activities outside the office, and for the very nice barbecue in their garden. For Steven Mookhoek, I would like to thank him for sharing the daily coffee breaks which relaxed me very much, for teaching me Dutch culture, for translating the propositions from English to Dutch. The good friendship provided by him and his partner Renée Maenhout is also appreciated. For Sanna Heinonen, I like to thank her for being my paranymp and the nice daily talks. For Dr. David San Martin (former FAMily), I thank him for providing the EBSD images for the cover of this thesis, for being the tour guide when my wife and I visited Madrid, and for the interesting scientific discussions about steels. I would also like to thank other members of FAMily like Laura Chant, Geeta van der Zaken and Pim Quist for helping me to sort out many administrative issues; Suresh Neelakantan for interesting discussions about science and Indian

culture and for helping to order the nice Indian lunch; Mazhar Iqbal for offering the nice Pakistan dinner; Rahul Thorat for the discussions about India and China; Dr. Doty Risanti for interesting discussions and explaining me some experimental techniques; Meijie Yin for interesting scientific and non-scientific discussions in Chinese; Dr. Christiaan de Ruijter (former FAMily) and Arkadiusz Kotlewski for the nice talks and sharing the daily coffee breaks; Dr. Fabrizio Micciche (former FAMily) for sharing the job interview experiences; Dr. Theo Dingemans, Dr. Hartmut Fischer, Dr. Natalia Sitnikova, Dr. Tien Dung Bui, Dr. Yanmin Jia, Maruti Hegde, Jie Yang, Dr. Guiming Song (former FAMily), and Sang Woo Choi (former FAMily) for the interesting discussions and talks. Although I may have forgotten to mention someone, it does not mean that I am not grateful.

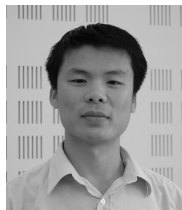
I would also like to express my gratitude to my former supervisor Prof. Zhonghua Li (Shanghai Jiao Tong University) who brought me into the research field of dislocations, which offered me the knowledge about dislocations that has been one of the requirements for carrying out this Ph.D. project.

Concerning the non-academic side of my time in Delft, I would like to thank all the friends here (too many to mention one by one) that have been around me for these years. Thanks for the fun, the help, the dinners, playing basketball, badminton, tennis, skiing, travelling together. Your friendship will be a significant part of my life forever.

I would like to thank my parents, elder sister, younger brother and grandparents for their love, encouragement and support, without them I would not have made it this far. Last but not least, a very special thank goes to Xiao Liang, my dear wife, not only for her unwavering love and support, but also for the patience and understanding she had in these years. Especially in the first and last year of my Ph.D. that were very difficult, she never said any word of complaining for I worked very late almost every day and even on the weekends.



# Curriculum Vitae



Mingxin HUANG

born on 24 May 1979  
in Lingshui, Hainan Province, China

**Sept. 1998 - Jul. 2002**

Bachelor of Science in Engineering Mechanics at Shanghai Jiao Tong University, Shanghai, China.

**Sept. 2002 - Jul. 2004**

Master of Science in Solid Mechanics at Shanghai Jiao Tong University, Shanghai, China. Thesis under supervision of Prof. Zhonghua Li: “The Interaction between Dislocations and Cracks”.

**Aug. 2004 - Oct. 2008**

Ph.D. candidate in Physical Metallurgy at the group of Fundamentals of Advanced Materials, Faculty of Aerospace Engineering, Delft University of Technology, Delft, The Netherlands, under supervision of Prof.dr.ir. Sybrand van der Zwaag and Dr. Pedro E.J. Rivera Díaz del Castillo.

**Oct. 2008 - Present**

Researcher, ArcelorMittal, Maizières-lès-Metz, France

## List of Publications

### 2008

- **Huang, M.**, Rivera Díaz del Castillo, P.E.J., Bouaziz, O., van der Zwaag, S.: *Modelling Dynamic Recovery and Dynamic Recrystallization at the Steady State: An Irreversible Thermodynamics Approach*. Acta Materialia, to be submitted.
- **Huang, M.**, Rivera Díaz del Castillo, P.E.J., Bouaziz, O., van der Zwaag, S.: *Predicting the Stress-Strain Behaviour of Interstitial Free, Low and Medium Carbon Steels under Hot Working Conditions*. ISIJ International, to be submitted.
- **Huang, M.**, Rivera Díaz del Castillo, P.E.J., Bouaziz, O., van der Zwaag, S.: *A Constitutive Model for High-strain-rate Deformation in FCC Metals Based on Irreversible Thermodynamics*. Mechanics of Materials, submitted.
- **Huang, M.**, Rivera Díaz del Castillo, P.E.J., Bouaziz, O., van der Zwaag, S.: *Modelling Strength and Ductility of Ultrafine Grained BCC and FCC Alloys Using Irreversible Thermodynamics*, Materials Science and Technology, accepted for publication.
- **Huang, M.**, Rivera Díaz del Castillo, P.E.J., Bouaziz, O., van der Zwaag, S.: *Irreversible Thermodynamics Modelling of Plastic Deformation of Metals*. Materials Science and Technology **24**(4), 495-500 (2008).
- **Huang, M.**, Rivera Díaz del Castillo, P.E.J., Bouaziz, O., van der Zwaag, S.: *Predicting the Strength and Ductility of Ultrafine Grained Interstitial Free Steels Using Irreversible Thermodynamics*, New Developments on Metallurgy and Applications of High Strength Steels, Buenos Aires, Argentina, 26-28 May, 2008, CDRom.

### 2007

- **Huang, M.**, Rivera Díaz del Castillo, P.E.J., van der Zwaag, S.: *Modelling Steady State Deformation of FCC Metals by Non-Equilibrium Thermodynamics*. Materials Science and Technology **23**(9), 1105-1108 (2007).
- **Huang, M.**, Rivera Díaz del Castillo, P.E.J., van der Zwaag, S.: *Modelling Dynamic Recovery and Recrystallization of Metals by a New Non-Equilibrium Thermodynamics Approach*, Materials Science Forum **558-559**, 517-522 (2007).

- **Huang, M.**, Rivera Díaz del Castillo, P.E.J., van der Zwaag, S.: *Modelling Deformation Structures in Metals Based on an Entropic Analysis*. Materials Science Forum **550**, 571-576 (2007).

## 2006

- **Huang, M.**, Rivera Díaz del Castillo, P.E.J., Li, Z.: *Edge Dislocation Dipole Emission from a Blunt Crack Tip and its Morphological Effects*. Scripta Materialia **54**(4) 649-653 (2006).
- **Huang, M.**, Rivera Díaz del Castillo, P.E.J., van der Zwaag, S.: *Modelling Steady State Deformation in Metals by a Novel Thermostatistical Approach*, Proceedings of Materials Science and Technology 2006 Conference and Exhibition **1**, 373-382 (2006).
- Rivera Díaz del Castillo, P.E.J., **Huang, M.**, van der Zwaag, S.: *A Thermostatistical Model for Cell Formation in Two Dimensions*. TMS Letters **1**, 13-14 (2006).

## 2005

- **Huang, M.**, Rivera Díaz del Castillo, P.E.J., van der Zwaag, S.: *Modelling the Deformation of Ultrafine Grained Metals Using Statistical Mechanics Concepts*. Iron and Steel **40** Supplement, 60-65 (2005).
- Rivera Díaz del Castillo, P.E.J., **Huang, M.**, van der Zwaag, S.: *Statistical Mechanics Prediction of Solid-Solid Transformations Induced by Plastic Deformation*, Proceedings of the International Conference on Solid-Solid Phase Transformations In Inorganic Materials (PTM 2005), Arizona **1** 621-628 (2005).

## 2004

- **Huang, M.**, Li, Z.: *Dislocation Emission Criterion From a Blunt Crack Tip*. Journal of the Mechanics and Physics of Solids **52**(9), 1991-2003 (2004).
- **Huang, M.**, Li, Z.: *The Ductile versus Brittle Fracture Behavior Assessed by the Competition between Dislocation Emission and Cleavage at Blunt Crack Tip*. Key Engineering Materials **274-276**, 135-140 (2004).